Title
Towards understanding the environmental durability and corrosion behavior of protected silver mirrors

Author
Folgner, Kelsey Anne

Publication Date
2019

Peer reviewed|Thesis/dissertation

UNIVERSITY OF CALIFORNIA

Los Angeles

Towards understanding the environmental durability and corrosion behavior of protected silver mirrors

A dissertation submitted in partial satisfaction of the requirements for the degree Doctor of Philosophy in Materials Science and Engineering

by

Kelsey Anne Folgner

2019

ABSTRACT OF THE DISSERTATION

Towards understanding the environmental durability and

corrosion behavior of protected silver mirrors

by

Kelsey Anne Folgner

Doctor of Philosophy in Materials Science and Engineering

University of California, Los Angeles, 2019

Professor Jenn-Ming Yang, Co-Chair

Professor Bruce Dunn, Co-Chair

High-reflectivity silver mirrors are widely used in optical applications. However, silver tarnishes and corrodes in air, which degrades its reflectivity and optical performance. While various layer schemes have been developed to protect thin film silver mirrors from corrosion and degradation, the mechanisms by which these protective layers improve durability are not fully understood. Accelerated environmental exposure was utilized to investigate the effects of layer composition and nanostructure on the environmental durability and corrosion behavior of Gemini-style protected silver mirrors prepared by plasma beam sputtering. Mixed flowing gas exposures of mirrors with various NiCr- and Cr- based layers revealed that the mechanisms of corrosion and degradation depend largely on the composition of the layers adjacent to the silver.

The corrosion process originates at defects in the dielectric protection layer and proceeds into the coating structure, laterally along various layer interfaces, only sometimes resulting in substantial silver corrosion. Mirrors with one Cr-based layer adjacent to the silver develop characteristic circular corrosion regions along the Ag-Cr interfaces, influenced by oxidation and chloridation of Ag and Cr, reduced adhesion due to dissolution, and stress-induced delamination. Mirrors with NiCr-based layers on either side of the silver develop characteristic corrosion nodules as the interfacial attack is limited but corrosive attack of nickel and silver is locally disruptive to the layered structure. Single flowing gas exposures showed that low concentrations of chlorine significantly influence the extent of corrosion. Investigations on reduced stress in the mirror layers revealed that while stress affects the corrosion kinetics, the composition of the layers has a larger influence on corrosion feature development and growth.

The electrochemical behavior of the layers adjacent to the silver also substantially influences the corrosion process as moisture transports corrosive species into the coating. NiCr, $NiCrN_x$, and freshly-deposited Cr are available to cathodically protect Ag, whereas CrN_x is not. However, these materials may be easily passivated, making them less available to provide protection. The oxidation and chloridation of nickel in the NiCr-based layers affects the silver dissolution and redistribution process. A novel application of coulometric reduction showed that optical degradation in these mirrors requires very little corrosion product.

The dissertation of Kelsey Anne Folgner is approved.

Pei-Yu Chiou

Aaswath Raman

Bruce Dunn, Committee Co-Chair

Jenn-Ming Yang, Committee Co-Chair

University of California, Los Angeles

2019

Table of Contents

List of Figures

List of Tables

Acknowledgements

I would like to express my immense gratitude to everyone who made this possible and to sincerely thank you all for supporting me.

To Dr. Jim Barrie, it's been a pleasure to work for you all these years. You have been a wonderful advisor and role model. Thank you for your confidence in me and for making me do all the things I did not want to; I'm better because of it.

To my thin films group, your endless support was invaluable. Dr. Chung-Tse Chu, thank you for the numerous discussions and for always helping me in the lab. Diana Alaan, thank you for being so careful and detailed. Chris Panetta, thank you for always being willing and able to help with anything. Dr. Pete Fuqua, thank you for always looking at things in a new way.

To my EPL colleagues, Scott Sitzman, Dr. Sean Stuart, Dr. Zach Lingley, Miles Brodie, Dr. Brendan Foran, and Dr. Billy Hubbard, thank you for your SEM, TEM, FIB, and ToF-SIMS magic. Your images and data are beautiful and amazing.

To Professor Robert Kelly from UVA, thank you for sharing your corrosion expertise, for the hours of discussions, and for putting up with us thin film people. Your enthusiasm and support were refreshing and very much appreciated.

To all the others at Aerospace who supported and helped me, especially Paul Adams and Dr. Hyun Kim, thank you for sharing your expertise and for making my work better. Our interns, Kat Nelms and Nicolas Liang, thank you for a very productive summer. Geena Ferrelli and Tait McLouth, thank you for commiserating, and for making this whole thing way more fun.

To my Aerospace management, Dr. Shant Kenderian, Dr. Jim Nokes, Dr. Tim Graves, and Dr. Chuck Gustafson, thank you for the incredible support and flexibility. Dr. Sherrie Zacharius, thank you also for fighting for us when we needed it.

I would also like to acknowledge the support and funding from the Aerospace Corporate Fellowship Program, which was foundational to this work. Thank you also to iLab; funding for this research was provided by the Aerospace Technical Investment Program.

Thank you to everyone at UCLA who made this possible. My advisor, Professor Jenn-Ming Yang, thank you for supporting us Aerospace Fellows. My committee co-chair, Professor Bruce Dunn, thank you for making this a better product. Thank you also to Professor Pei-Yu Chiou and Professor Aaswath Raman for serving on my doctoral committee.

To my family, thank you for supporting me through everything and for your love always. You have always been there for me and I truly appreciate it. Thank you also for putting up with my grumpiness.

Finally, thank you to my best friend, Dr. Rafael Zaldivar. You are incredible and inspiring. Thank you for always believing in me and for making me a better person. I would have never done any of this without you.

Portions of Chapter 3 are derived from the published work: K.A Folgner, C.-T. Chu, Z. L. Lingley, H. I. Kim, J.-M. Yang, and J. D. Barrie, "Environmental durability of protected silver mirrors prepared by plasma beam sputtering" *Applied Optics* 56, C75-C86 (2017). (doi: 10.1364/AO.56.000C75). The TEM was performed by Z. L. Lingley and the XPS by H. I. Kim; C.-T. Chu oversaw MFG testing; and J.-M. Yang and J. D. Barrie served as principal investigators.

Chapter 4 is a modified version of: K.A Folgner, C.-T. Chu, S. D. Sitzman, S. C. Stuart, Z. L. Lingley, and J. D. Barrie, "Development and growth of corrosion features on protected silver mirrors during accelerated environmental exposure," which has been submitted for publication. TEM and SEM were performed by Z. L. Lingley and S. D. Sitzman; ToF-SIMS by S. C. Stuart; C.-T. Chu oversaw MFG testing; and J. D. Barrie was the principal investigator.

Vita

2003 – 2006	*Undergraduate Technical Support, Intern*
	The Aerospace Corporation, El Segundo, California
2005	*Bachelor of Science in Aerospace Engineering, Summa Cum Laude*
	University of California, Los Angeles
2006 – 2008	*Laboratory Associate*
	The Aerospace Corporation, El Segundo, California
2008 – 2011	*Research Associate*
	The Aerospace Corporation, El Segundo, California
2011 – 2014	*Senior Research Associate*
	The Aerospace Corporation, El Segundo, California
2014 – 2016	The Aerospace Corporation Master of Science Corporate Fellowship
2014 – present	*Advanced Degree Fellow, MTS*
	The Aerospace Corporation, El Segundo, California
2016	*Master of Science in Materials Science and Engineering*
	University of California, Los Angeles
2016 – 2019	The Aerospace Corporation PhD Corporate Fellowship

Selected Publications and Presentations

1. K. A. Folgner, J. D. Barrie, and P. D. Chaffee, "Design and fabrication of a thin-film deposition system using a high-density plasma beam," El Segundo, California: Aerospace Corporation, 2010.

2. J. D. Barrie, P. D. Fuqua, K. A. Folgner, and C.-T. Chu, "Control of stress in protected silver mirrors prepared by plasma beam sputtering," *Applied Optics* 50, C135-C140 (2011).

3. K. A. Folgner, C.-Y. Tang, M. J. O'Brien, and P. D. Fuqua, "Investigating Stress in Hybrid Electronic Packages Using White Light Surface Profilometry," *International Symposium on Microelectronics*, Vol. 2011, No. 1, pp. 000719-000728 (2011).

4. K. A. Folgner, "Environmental durability of silver mirrors with nanostructured protective coatings," M.S. thesis, University of California, 2016.

5. K. A. Folgner, C.-T. Chu, Z. R. Lingley, H. I. Kim, J.-M. Yang, and J. D. Barrie, "Environmental durability of protected silver mirrors prepared by plasma beam sputtering," *Applied Optics* 56, C75-C86 (2017).

6. K. A. Folgner, C.-T. Chu, S. D. Sitzman, S. C. Stuart, Z. R. Lingley, and J. D. Barrie, "Effects of adhesion layer composition on the environmental durability of protected silver mirrors," *Proceedings SPIE 10691, Advances in Optical Thin Films VI*, 106910X (2018).

7. K. A. Folgner, C.-T Chu, S. D. Sitzman, S. C. Stuart, and J. D. Barrie, "Investigations of corrosion feature development on protected silver mirrors during accelerated environmental exposure," in *Optical Interference Coatings (OIC) 2019*, OSA Technical Digest Series (Optical Society of America, 2019), paper MB.3.

8. K. A. Folgner, C.-T. Chu, S. D. Sitzman, Z. R. Lingley, P. M. Adams, and J. D. Barrie, "Effects of sputtering gas environment on the nucleation and growth, optical properties, and durability of thin film silver mirrors," presented at *Plathinium 2019*, paper DEPO1-O2-025.

9. C.-T. Chu, D. R. Alaan, K. A. Folgner, J. D. Barrie, and P. D. Fuqua, "Correlation of long-duration and accelerated testing of protected silver mirrors," submitted for publication, 2019.

10. K. A. Folgner, C.-T. Chu, S. D. Sitzman, S. C. Stuart, Z. R. Lingley, and J. D. Barrie, "Development and growth of corrosion features on protected silver mirrors during accelerated environmental exposure," submitted for publication, 2019.

Chapter 1. Introduction

Silver is the material of choice for the most demanding visible and infrared mirror applications [1 – 4]. A lustrous noble metal, silver possesses the highest broadband reflectivity, the corresponding lowest emissivity, and the lowest polarization splitting of all metals [1 – 6]. These outstanding properties make thin film silver mirrors desirable as broadband reflectors in optical applications such as space-based sensors and large astronomical telescopes, especially when compared to other metals often used, such as gold and aluminum [1, 2, 7]. The theoretical reflectivity of silver is 98% at 500 nm and improves to better than 99% at longer wavelengths, as shown in Figure 1.

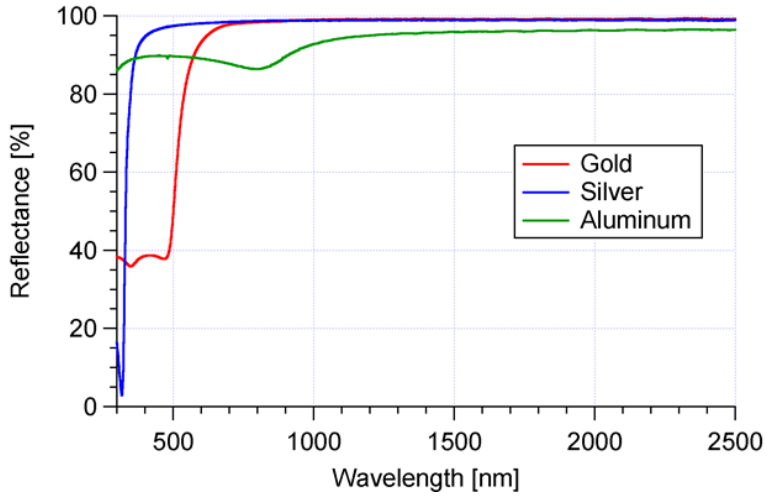

Figure 1. Reflectance spectra of common mirror materials deposited as thin film metallic reflectors.

While gold has comparably high reflectivity and low emissivity in the infrared (IR) spectrum, it exhibits substantial absorption at visible wavelengths. Aluminum maintains moderately high reflectivity across both the visible and IR, though it is substantially lower than silver at all wavelengths. The theoretical reflectivity of aluminum is only 89% at 600 nm. This difference has a dramatic effect in a multiple mirror optical system, where each reflection reduces

the overall throughput of light. For a theoretical three mirror system, the overall throughput is equal to the reflectance to the third power, R^3. For silver-coated mirrors in this system, the throughput would be approximately 94% at 600 nm, while aluminum mirrors would manage only 71%.

Though silver exhibits excellent optical properties, it is far more susceptible to atmospheric corrosion than either gold or aluminum [6, 7, 8]. Gold naturally resists corrosion well, while aluminum develops a protective oxide coating that inhibits corrosion without impacting its optical properties. Silver, however, is known to tarnish and corrode in air, which degrades its reflectivity and optical performance [6 – 10]. This is a substantial problem for astronomical telescopes that operate in air for years as well as for space mirrors prior to launch during terrestrial storage, spacecraft integration, and testing.

1.1 Silver Corrosion

Silver is readily tarnished and corroded by trace amounts of common atmospheric pollutants in the environment [6, 8 – 13]. Specifically, silver is very sensitive to sulfur and halogen compounds, such as hydrogen sulfide (H_2S) and chlorine (Cl_2). Oxidizing species such as ozone (O_3) and nitrogen dioxide (NO_2) as well as ultraviolet (UV) radiation have been shown to enhance tarnish formation on silver surfaces. In addition, the presence of moisture in the environment can significantly impact silver corrosion. Atmospheric corrosion generally increases with relative humidity, as the amount of moisture adsorbed on a surface is a function of relative humidity [6, 8, 12]. Eliminating moisture through low relative humidity is believed to be more effective in preventing silver corrosion than trying to reduce the small amount of trace pollutants in the environment [8, 10, 14]. Additionally, silver corrosion is affected by the deposition of airborne

particles, air flow conditions, and temperature [12, 13, 15]. There is believed to be a synergistic effect from multiple pollutants that accelerates silver corrosion [8, 16].

Atmospheric corrosion of silver results in the formation of silver sulfide (Ag_2S), silver chloride (AgCl), silver oxide (Ag_2O or AgO), and silver sulfate (Ag_2SO_4) tarnish films on the surface [6, 8, 11, 17]. Silver sulfide, a highly absorbing compound, is the most common tarnish observed on silver surfaces, often developing as dark brown markings that significantly degrade silver's outstanding optical properties [5, 6, 9, 10, 14, 18, 19]. Tarnish and corrosion on silver surfaces degrade reflectivity and increase scatter, vastly reducing the optical performance.

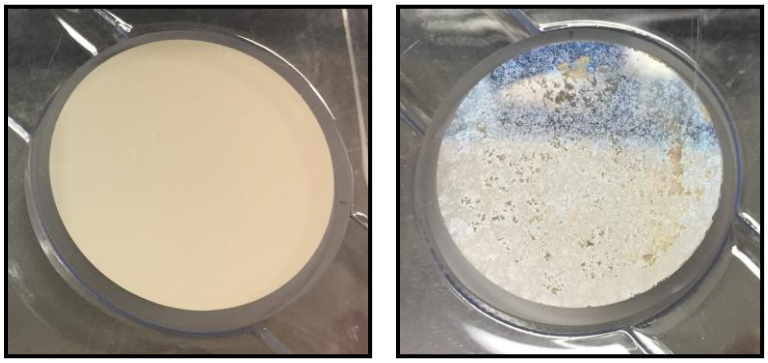

Figure 2. Freshly-deposited silver mirror (left) is smooth and reflective, compared to a degraded mirror (right) that is tarnished and corroded.

1.2 Protection Layer Schemes

Various coating layer schemes have been developed to protect thin film silver mirrors from corrosion and degradation [1, 2, 7, 9, 10, 20 – 24]. These layer schemes generally include a base layer underneath the silver for adhesion to the substrate, one or more dielectric layers over the silver to protect it, and frequently a thin adhesion interlayer that keeps the protection layers well-adhered to the silver and increases their effectiveness (Figure 3). The base layer is necessary as silver does not adhere well to typical substrate materials such as glass. The protective dielectric

layers prevent corrosive species from reaching the silver and protect it from abrasion and mechanical damage, as silver is very soft. While these additional layers substantially improve mirror durability, they do not provide complete protection to the silver. Moreover, although significant work has been done to develop these protection layer schemes, the mechanisms by which these layers improve mirror durability are not fully understood.

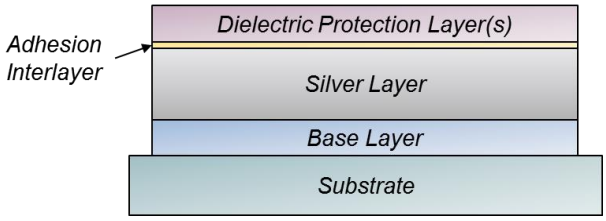

Figure 3. Schematic of protected silver mirror layers.

Numerous materials have been utilized for the adhesion and protection layers in various protection layer schemes. The protection layer materials must be transparent with low scatter to minimize their impact on the mirror's reflectance [2, 7, 9, 10]. In addition, they should be deposited with a minimum of defects and pinholes to prevent corrosive species from reaching the silver [2, 5, 9, 10, 25, 26]. Finally, materials with low diffusion rates for silver are preferred because silver is known to be highly mobile [9]. Various metal oxides, nitrides, and fluorides such as SiO_2, SiO, Al_2O_3, TiO_2, Ta_2O_5, HfO_2, ZrO_2, Si_3N_4, AlON, MgF_2, YbF_3, and YF_3 have been utilized as protection layers [2, 4, 7, 9, 10, 21, 27 – 30].

The adhesion and base layer materials are thought to improve adhesion at the interfaces by bonding well to the materials on either side, which is considered important for durability [1, 2, 20, 24, 26, 31, 32]. Chromium, nickel-chromium, and their nitrides, CrN_x and $NiCrN_x$, are common adhesion and base layer materials, as are copper and various other metal nitrides and oxides such as TiN, AlN, NiO, Al_2O_3, and Y_2O_3 [2, 4, 20 – 22, 24, 26, 27, 30 – 32]. The stoichiometry of the

nitride layers is not usually known due to the nature of the reactive deposition process. Generally, the adhesion layers are very thin, on the order of 10Å or less. Thin layers are required to minimize impact on mirror reflectance, as the materials used generally have substantial absorption in the blue wavelengths [20, 33]. This reduces silver's reflectance, which is already decreasing in the ultraviolet (UV) spectrum, dropping to near zero at 320 nm due to surface plasmon resonance [20, 34 – 38].

To offset these losses, alternating layers of dielectric materials with high and low refractive indices can be used together to enhance mirror reflectance at specific wavelengths by means of interference effects [9, 20, 39]. When used in these combinations, multiple dielectric protection layers may also provide better protection to the silver [40, 41]. However, these extra layers do have some penalty in emittance and reflectance at wavelengths where their interference effect is destructive [5, 9]. Therefore, the choice of protection layer and adhesion layer materials for each application must be optimized for both optical performance and durability.

1.3 Protected Silver Mirrors

One such protection layer scheme that has been used with reasonable success consists of two very thin adhesion layers of nickel chromium nitride ($NiCrN_x$) on either side of the silver, followed by a protective overcoat of silicon nitride (SiN_x) on top of the tri-layer [1, 21, 27, 31, 32, 39, 42, 43]. While this protection layer scheme substantially improves mirror durability, it also significantly reduces mirror reflectance, particularly in the blue and UV (Figure 4 and Figure 5). During coating development, Wolfe et al. [32] found that $NiCrN_x$ provided the optimal balance between durability and optical performance when compared to the other materials tested. To achieve this, the $NiCrN_x$ adhesion layer must be as thin as 8Å to balance the improved durability

it provides with the loss in reflectance it imposes. This protection layer scheme is utilized on multiple mirrors of the twin Gemini astronomical telescopes and, in some instances, has managed up to 12 years in operation without significant degradation [42]. However, most of the Gemini mirrors degrade far more quickly and require re-coating much more often, on average every 2 to 5 years.

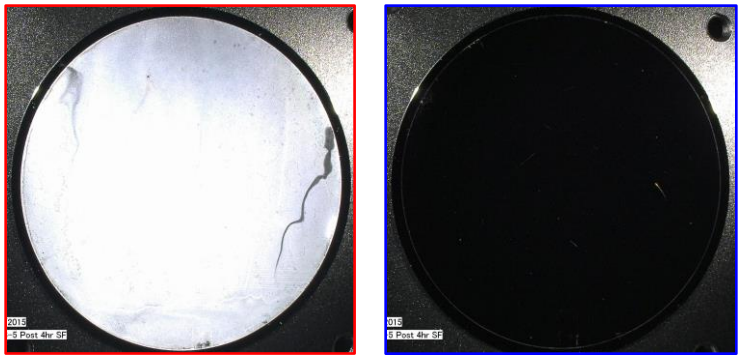

Figure 4. A bare silver mirror (left) exhibits substantial scatter and degradation after accelerated environmental exposure, while a Gemini-style protected silver mirror (right) maintains its smooth, reflective surface.

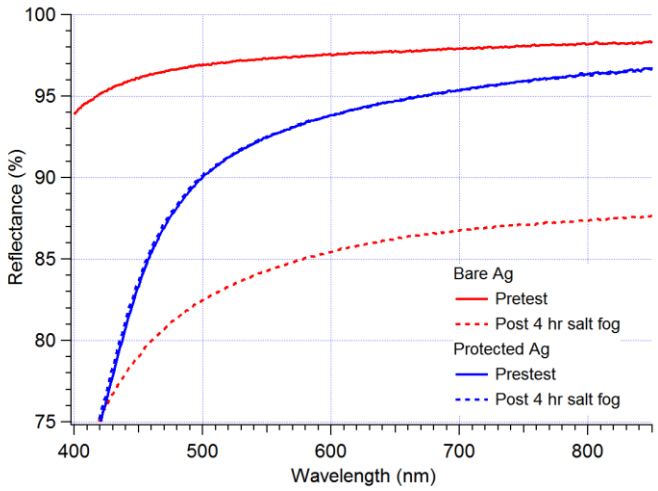

Figure 5. Reflectance of the two mirrors in Figure 4; note the initial reduced reflectance of the protected mirror, but the far more severe degradation of the bare silver after accelerated environmental exposure.

Wolfe et al. [32] reported that $NiCrN_x$ is an effective adhesion layer because it improves adhesion at the silver-dielectric interface by depositing as an ad-mixture of Ni and CrN_x [20]. A metal-to-metal bond is believed to form between the Ag and Ni, as neither is expected to form a nitride under these conditions; while a chemical bond is believed to form between the CrN_x and SiN_x. They reported that mirrors with Cr-based adhesion layers were not as durable as mirrors with Ni-based or NiCr-based adhesion layers [39]. As the higher nickel content was directly related to durability, they suggested that $NiCrN_x$ is a more effective adhesion layer because the nickel and silver alloy at the interface [32, 39]. However, it is unclear whether this behavior is truly related to interface adhesion, or whether chemical or electrochemical effects are the reason for the improved durability.

Additionally, Wolfe et al. [32] reported that $NiCrN_x$ is not an effective barrier to corrosion on its own; the SiN_x overcoat is also required [1, 44, 45]. Their data suggested this was because the $NiCrN_x$ was not a continuous layer, but rather, deposited as islands [46].

Fuqua and Barrie [47] and later Chu et al. [31] reported that $NiCrN_x$ provides nucleation sites for the growth of a dense and, therefore, effective SiN_x protection layer. Their work with accelerated environmental exposure and electrochemical impedance spectroscopy (EIS) showed that the $NiCrN_x$ affords protection to the silver by reducing porosity in the SiN_x layer, thereby reducing its permeability to corrosive species that could penetrate through and react with the silver. They speculated that a delaminated zone between the dielectric and silver layers develops when corrosive species penetrate through a porous SiN_x layer, leading to further corrosion [31, 47]. Additional EIS studies by Ben Amor et al. [48] further support this mechanism.

The $NiCrN_x$, therefore, is believed to serve two purposes: (1) reducing porosity in the dielectric protection layer and (2) improving adhesion at the silver-dielectric interface. While

reduced porosity and improved adhesion are generally considered necessary for durable coatings, the mechanisms by which the $NiCrN_x$ affords protection to the silver are not fully understood. Moreover, as the Gemini-style protection layer scheme requires balancing improved durability with reduced reflectance, the quest for more reflective and durable protection layer schemes continues.

1.4 Silver Mirror Durability

Research on silver mirror durability extends back into the 1960s [2, 6, 7, 9, 10] and continues to be an active area of research today [25, 27, 30, 34, 49, 50]. Yet despite years of experience, long-term exposure of silver mirrors in air continues to be a significant problem for the optical coating community. The mechanisms by which the protection layer schemes improve mirror durability are not fully understood.

1.4.1 Porosity and Defects in the Protection Layers

Multiple researchers have reported that corrosion and degradation in silver mirrors occur at defect sites, while large areas of the mirror coatings remain intact and unaffected [5, 10, 15, 25]. Pellicori [10] and Hass et al. [5] were among the first to document the existence of numerous small localized corrosion sites on various protected silver mirrors due to exposure to atmospheric pollutants. These corrosion sites reduced the optical performance of the mirrors by increasing scatter and are thought to occur due to localized dissolution and attack of the coatings [15].

Localized corrosion has also been widely reported to result from small disruptions in the smooth coating layers. Particles on the substrate prior to coating result in pinholes and pores in the coating that allow ingress of corrosive species (Figure 6) [1, 5, 41, 51]. Limam et al. [25, 52]

has recently shown that defects in the substrate prior to coating resulted in defects in the coating layers as they were deposited. These coating defects enabled the local initiation of tarnishing of the silver layer by allowing corrosive species to reach the bare silver. Surface preparation to remove the substrate defects reduced the coating defects and improved durability. Proper surface preparation and clean conditions during coating deposition are critical to long-term durability.

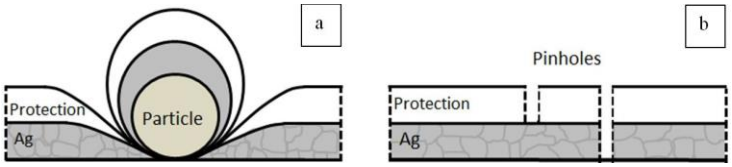

Figure 6. Disruptions in film growth lead to defect sites that enable corrosion [51]. Reprinted with permission. S. Schwinde, et al., "Protected and enhanced silver for mirrors: damage mechanisms and how to prevent them," in *Proc. SPIE 9627*, 96271R, 2015.

Recent work on Al_2O_3 protection layers deposited by atomic layer deposition (ALD) further indicates that reducing porosity in the protection layers is important for improving durability. ALD can produce conformal, pinhole-free, amorphous films, properties generally considered to improve protection and barrier layer schemes. Phillips et al. [21] and Fryauf et al. [22, 41] showed significantly better durability for Al_2O_3 protection layers deposited by ALD compared to identical coatings deposited by physical vapor deposition (PVD) techniques. The PVD-deposited coatings are believed to have more defects and therefore allow corrosive species to more easily reach the silver. However, Schwinde et al. [23] did not find a significant difference in the durability of Al_2O_3 protection layers deposited by ALD compared to PVD. This may be due to the cleaner environment in which these coatings were deposited, resulting in fewer particles on the surface prior to coating. Reducing defects in the protection layers, regardless of how that is achieved, is critical for improving long-term durability.

1.4.2 Particle Induced Degradation

Clean and dry conditions during long-term use or storage of silver mirrors is also extremely important for preserving optical performance. Long term exposure of various protected silver mirrors in both laboratory and telescope observatory environments indicates that particles on the mirror surface degrade mirror durability [1, 19, 28, 42]. Phillips et al. [28] has shown that upward facing mirrors, which receive more deposited particles on their surfaces due to gravity, suffer more extensive corrosion than downward facing mirrors. Similarly, mirrors at the Gemini North telescope, in Hawaii, degrade less than mirrors at Gemini South, in Chile, due to increased dust settling on the mirror surfaces at the southern location [19, 42]. In addition, Boccas et al. [1] reported that downward-facing mirrors and upward-facing mirrors that were washed regularly to remove particles corroded less than upward-facing mirrors that were not washed. Washing removes particles from the surface and improves long-term durability; it also has the added benefit of recovering degraded reflectance.

Schwinde et al. [15] reported extensively on a particle induced mechanism of degradation whereby hygroscopic airborne particles adsorb on the surface of the protected silver coatings [15, 40, 51]. These particles attract moisture from the environment, leading to the formation of droplets on the surface and the dissolution of sulfur and chlorine species from the particles into the surface water layer (Figure 7). Theses resulting salt solutions weaken the protective coating, permeate through it, and attack and damage the silver below. Protective coatings with low water absorption and low porosity are critical to resisting this dissolution and attack [2, 7, 23, 29, 40, 49]. Dense, impermeable, defect-free protection layers, as well as clean and dry environments, are necessary, though not sufficient, for long-term durability.

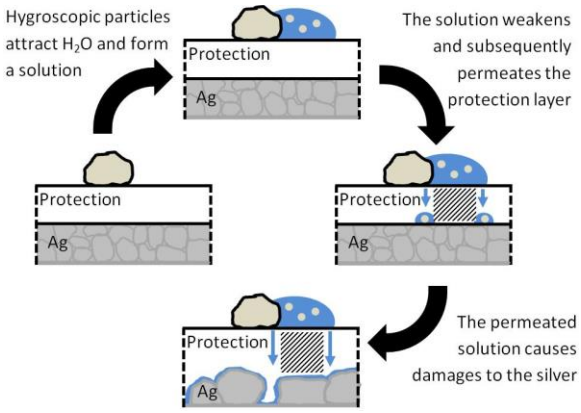

Figure 7. Particle induced damage mechanism in protected silver mirror coatings [51]. Reprinted with permission. S. Schwinde, et al., "Protected and enhanced silver for mirrors: damage mechanisms and how to prevent them," *Proc. SPIE 9627*, 96271R, 2015.

1.4.3 Adhesion at the Silver – Dielectric Interface

While good adhesion is generally considered necessary for durable coatings, there are limited techniques to quantify adhesion in multilayer coatings [53, 54]. Moreover, the structure of the protected silver mirror coatings is not conducive to the indentation tests most commonly used to quantify adhesion in single or bi-layer coatings. The soft silver layer cannot withstand the loads required to indent the hard, dielectric protection layer; the silver squeezes out of the coating under load. Tape pull tests, eraser rub tests, or cheesecloth tests are therefore used to test the adhesion and mechanical integrity of protected silver mirror coatings [29, 43, 55]. The tape pull test [56, 57] is most commonly used to assess good adhesion in multilayer structures, though it can only qualitatively test the weakest interface in the coating. Even with this limitation, tape pull testing is often used as a predictor for long-term durability [29, 32, 43]. Barrie et al. [24] reported that silver mirrors with no adhesion layer between the silver and the dielectric layers fail the tape pull test, with the dielectric separating from the silver below; these mirrors also did not pass

durability testing. Whereas, mirrors with adhesion layers passed both adhesion tape pull testing and durability screening.

During development of what is now known as the Gemini coating design, Wolfe et al. [32, 39] suggested that $NiCrN_x$ is an effective adhesion layer because the Ni and Ag alloy at the interface to improve adhesion, and therefore durability. They reported that mirrors with Cr-based adhesion layers were not as durable as mirrors with Ni-based or NiCr-based adhesion layers, and that the higher Ni content was directly related to durability. It is unclear whether this behavior is only related to interface adhesion, or whether chemical or electrochemical effects also contribute to the improved durability.

1.4.4 Stress and Durability

Large stresses can develop in thin film coatings during the energetic, nonequilibrium deposition processes. These stresses can affect the stability of the thin films [58] and may influence the long-term durability of protected silver mirrors [21, 23, 24, 46, 49, 59, 60]. Phillips et al. [21] investigated a variety of oxide, nitride, and fluoride protection layers on silver mirrors; they reported that the most durable mirrors had relatively low stress protection layers, whereas mirrors with high stress protection layers showed poor durability. However, Barrie et al. [24], working with yet another protected silver mirror design, reported that, within the range of film stresses studied, the net stress state of the mirror did not impact overall durability. They noted that the mirror design, specifically the inclusion of the thin adhesion layer between the silver and the protective dielectric layers, was more important for ensuring long-term durability.

Multiple researchers have suggested various mechanisms whereby stress may influence the long-term durability of protected silver mirrors. Wolfe et al. [46] suggested a stress-corrosion

cracking mechanism in which the combined action of stress and corrosive species leads to time-dependent crack growth [20]. This may reduce adhesion at the layer interfaces and allow chemical pathways for attack of the silver below. Schwinde et al. [23] showed that a silver mirror design with lower stress protective layers reduced the expansion of corrosion sites. They suggest that buckling of highly-compressive protective layers at the corrosion sites leads to more extensive corrosion. This is likely associated with reduced adhesion at the interfaces resulting from corrosion of the silver layer. Finally, Lalo et al. [60] reported that voiding in the silver layer increased as external stress and heat were applied to silver mirrors, and that similar voiding was observed in long-term aging experiments. Therefore, they suggest that a stress-induced voiding mechanism impacts long-term aging behavior as stress may influence the kinetics associated with silver transport and corrosion.

Stress in the mirror coatings has been shown to influence the corrosion processes that occur, even if the mechanisms by which it does so are not fully understood. Stress may play a role in failure of the dielectric protection layers or loss of adhesion at layer interfaces. Once the silver is exposed directly to corrosive species, stress may also influence the kinetics of silver dissolution.

1.4.5 Electrochemical Behavior

It has been suggested that the protection layer schemes provide electrochemical protection to the silver to reduce corrosion and degradation. Pellicori et al. [10] suggested that electrochemical reactions may occur between the silver and base layers materials, spurred by water and dissolved sulfur species entering the coating. Song et al. [2] reported that a base layer of copper below the silver reduced corrosion of the silver and preserved reflectance of the mirrors. The copper performed better than other base layer materials, even with no protective dielectric

layer above the silver. They suggested that the copper provides cathodic protection to the silver, which, along with good adhesion between the two layers, was critical to the improved durability. They also observed copper on the surface of the silver after corrosion, which suggests it participated in the corrosion reactions that occurred.

During development of the Gemini-style coating, it was suggested that the $NiCrN_x$ adhesion layer acts as a passivation layer to reduce silver corrosion [18, 39, 61]; it was also suggested that corrosion between silver and an underlayer of aluminum occurs by means of galvanic effects [61, 62]. Phillips et al. [28, 61] further reported that protected silver mirrors with copper base layers were more durable than those with aluminum base layers; similarly, mirrors with titanium or NiCr base layers were most durable of all. They suggested that materials closer together on the galvanic series would result in more durable mirrors, in part due to the importance of water in the corrosion process. While galvanic interactions are believed play a role in the corrosion behavior, as dissimilar metals are in intimate contact at the interfaces, there have been limited quantifiable studies to understand the electrochemical processes that occur in protected silver mirrors.

Electrochemical characterization of these mirror systems to date has largely focused on electrochemical impedance spectroscopy (EIS). As mentioned previously, Fuqua and Barrie [47] and later Chu et al. [31] used EIS to determine that reduced porosity in the dielectric protection layer reduced its permeability to corrosive species that could penetrate through and react with the silver. They showed that a $NiCrN_x$ adhesion layer affords protection to the silver by reducing porosity in the SiN_x protection layer, whereas mirrors with no adhesion layers had more porous SiN_x layers and were more susceptible to degradation. More recent work by Ben Amor et al. [48]

with a different silver coating design and electrolyte chemistry further supports their conclusions that porosity leads to further corrosion.

Ultimately, while the protection layer schemes are necessary to reduce corrosion and degradation in silver mirrors, the mechanisms by which the adhesion and protection layers improve mirror durability are not fully understood. Layer porosity, interface adhesion, coating stress, and electrochemical interactions have been suggested as contributing factors to the corrosion behavior in protected silver mirrors, though the interplay and importance of each of these factors is not clear. A better understanding of the underlying causes of corrosion and degradation is crucial to developing more durable mirrors.

Chapter 2. Motivation & Objectives

Despite decades of experience, prolonged exposure to air is still a significant problem for silver mirrors. Moreover, the mechanisms by which the protection layer schemes improve mirror durability are not fully understood. Understanding the underlying causes of corrosion and degradation is crucial to selecting appropriate materials for the adhesion and protection layers. Traditionally, choosing new materials has largely been done experimentally: materials with improved optical properties or promising corrosion resistance are tested to determine their durability in the layered mirror structure. Recent research has focused primarily on the mechanisms and functions of the dielectric protection layers. Far less research has been performed on the functions of the adhesion layer materials, even though numerous materials have been screened through durability testing. The Gemini-style coating of $NiCrN_x$-SiN_x is widely considered the most durable protection layer scheme; however, it is still not understood how the adhesion layer improves durability. There is a need to understand the chemical and electrochemical effects of the adhesion layers on the corrosion mechanisms in these silver mirrors.

It is the purpose of this dissertation to investigate the effects of layer composition and nanostructure on the environmental durability and corrosion behavior of Gemini-style protected silver mirrors. Our approach is to deposit SiN_x-protected silver mirrors with various NiCr- and Cr- based adhesion and base layers and investigate how the resultant layer structure impacts mirror durability through accelerated environmental exposure. The specific objectives of this research are as follows:

1. Gain a deeper understanding of the mechanisms of corrosion in protected silver mirrors by investigating the effects of the adhesion layer materials on mirror durability.

2. Relate the layer composition and nanostructure of the mirror coatings to the final mirror properties, specifically how the layered nanostructure impacts durability.

3. Investigate the chemical and electrochemical effects of the layers during silver mirror corrosion. Develop specialized electrochemical techniques to assess the controlling factors in the silver mirror corrosion processes, including the active corrosion mechanisms, and the relative importance of the environmental variables.

Chapter 3. Effects of Adhesion Layer Composition on Environmental Durability

3.1 Introduction

While the $NiCrN_x$-SiN_x Gemini-style coatings are widely considered the most durable protection layer scheme available for silver mirrors, it is still not understood how these layers improve durability. Wolfe et al. [32] suggested that a chemical bond forms between the CrN_x and SiN_x and that the nickel and the silver alloy at the interface; together this improves adhesion and, therefore, durability. They reported that mirrors with Cr-based adhesion layers were not as durable as mirrors with Ni-based or NiCr-based adhesion layers; the higher nickel content was directly related to durability. Wolfe et al. [39] also suggested that the $NiCrN_x$ adhesion layer may act as a passivation layer to reduce silver corrosion [18, 61]. It is unclear whether the durability behavior is only related to interface adhesion, or whether chemical or electrochemical effects contribute to the improved durability. It's also unclear the extent to which CrN_x compared to $NiCrN_x$ affects the degradation behavior mechanisms, and how important the nickel is in improving durability. Understanding the underlying causes of corrosion and degradation in these protected silver mirrors is crucial to developing more durable mirrors.

In this chapter, the effects of the adhesion layer material on the environmental durability of Gemini-style protected silver mirrors were investigated. Several identical mirror coatings were deposited, differing only in the composition of the very thin adhesion layer between the silver and the protective dielectric: a mirror with no adhesion layer, a mirror with a 5Å CrN_x adhesion layer, and a mirror with a 5Å $NiCrN_x$ adhesion layer. Accelerated environmental exposure was used to investigate how the composition of the very thin adhesion layer changes the environmental durability and the mechanisms of corrosion feature development and growth in these mirrors.

3.2 Experimental Methods

3.2.1 Deposition Processes

Thin film silver mirrors were prepared by a relatively new sputtering technique known as plasma beam sputtering, in which an external, high-density, radio frequency (RF) plasma source is used to produce high-quality thin films [24, 63]. The sputter deposition process begins with the bombardment of a solid target material by energetic ions generated by a plasma [64, 65]. The ions have sufficient energy to eject, or sputter, atoms from the target surface through momentum transfer. The sputtered atoms condense on the substrate surface, producing the thin film. Typically, an inert sputtering gas such as argon is used to enable and sustain the plasma. The creation and maintenance of a high-density plasma during the sputtering process produces higher-quality coatings [63]. In magnetron sputtering, magnets can be used to confine and control the plasma near the target; this increases the ionization efficiency and yields higher deposition rates [64].

The plasma beam sputtering process and chamber have been described in detail previously [24, 63]. The high-density, inductively-coupled, radio frequency (RF) plasma is generated external to the deposition chamber. The remotely-generated plasma is then magnetically steered and electrically accelerated towards the target for sputtering. Exciting the plasma externally from the sputtering environment enables the independent control of process variables that cannot be separated in conventional magnetron sputtering processes. Ion density and ion energy are decoupled in plasma beam sputtering, allowing the structure and properties of the film to be tailored in novel ways [63].

The custom 0.9 m deposition chamber contains the plasma source, the water-cooled, electrically-biased target holder for four 6-inch diameter targets, and the continuously-rotating

sample holder for various substrates, usually 2-inch diameter polished silicon wafers (Figure 8). The deposition process is fully automated, including the RF source power, the DC target bias, and the steering electromagnet current. The chamber is pumped to a base pressure of 3×10^{-7} Torr. For deposition, it is backfilled with argon gas at 40 SCCM (cubic centimeters per minute at standard temperature and pressure) and controlled via throttling valve on the cryopump to a pressure of 2.0 mTorr. During reactive deposition of the nitride layers, additional N_2 gas flows at 13 SCCM although the total pressure is kept constant.

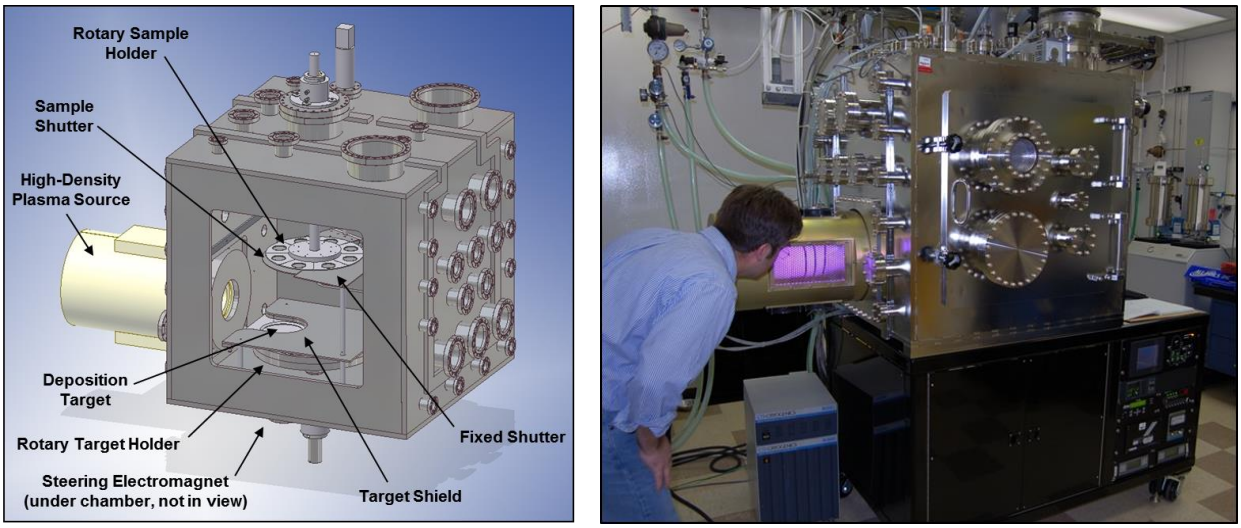

Figure 8. Custom plasma beam sputtering system schematic (left) and during operation in the laboratory (right).

The silver mirror design consists of four layers deposited on polished Si substrates: (1) a thin metal (Cr or NiCr) base layer for adhesion of the silver to the substrate, (2) a thick reflective silver layer, (3) a very thin metal nitride (CrN_x or $NiCrN_x$) interlayer for adhesion of the protective dielectric layer to the silver, and (4) a single protective overcoat layer of silicon nitride (SiN_x). Additionally, mirrors without adhesion layers (3) were deposited. The specifics of the deposition conditions for each layer material are described in Table 1. The nichrome target has a composition of 80 wt. % Ni and 20 wt. % Cr. The purity of each target material is better than 99.95%. For

each mirror, the full coating stack is nominally 150 nm thick. Layer thickness is controlled by quartz crystal monitors (QCM). QCM calibration factors were determined by ellipsometry, using a J.A. Woollam Variable Angle Spectroscopic Ellipsometer (VASE), or profilometry, using a Keyence VK-X200 3D laser scanning confocal microscope. For the very thin layers, the calibration factors were determined for thicker films and do not account for issues, such as the time of shutter actuation, that are no longer negligible during very short depositions. Ellipsometry was also used to measure the optical properties of the dielectric layers.

Table 1. Deposition Conditions for Silver Mirror Layers

Material	**Layer Type**	**Nominal Thickness (Å)**	**Rate (Å/min)**	**Target**	**RF Power (W)**	**Target Bias (W)**
NiCr	Base Layer (1)	200	72	Nichrome	1000	1000
Cr	Base Layer (1)	200	60	Chromium	1000	1000
Ag	Reflective Layer (2)	1200	174	Silver	1000	1000
CrN_x	Adhesion Layer (3)	5	48	Chromium	1000	1000
$NiCrN_x$	Adhesion Layer (3)	5	78	Nichrome	1000	1000
SiN_x	Protective Layer (4)	100	24	Silicon	1300	1000

3.2.2 Silver Mirror Designs

The three protected silver mirror designs deposited for this study are shown in Figure 9. The mirror coatings differed only in the composition of the very thin adhesion layer between the silver and the protective dielectric layer and were otherwise identical. Each mirror had a NiCr base layer, an Ag reflective layer, and a SiN_x protective layer. The no adhesion layer mirror had no adhesion layer; the CrN_x adhesion layer mirror had a 5Å CrN_x adhesion layer; and the $NiCrN_x$ adhesion layer mirror had a 5Å $NiCrN_x$ adhesion layer.

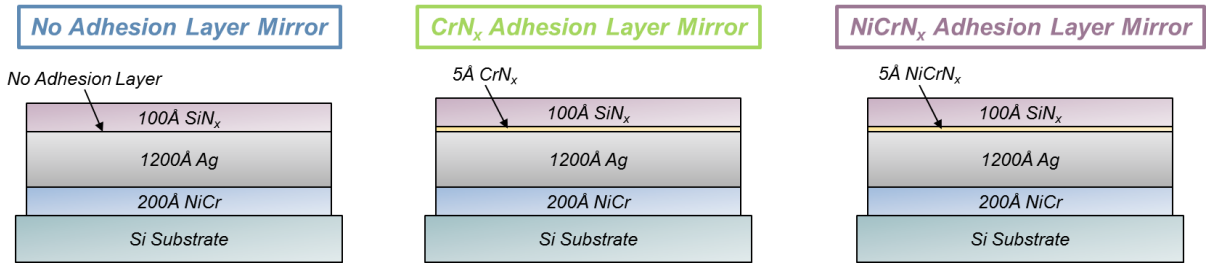

Figure 9. Protected silver mirrors with various adhesion layers deposited for this study.

3.2.3 Accelerated Environmental Exposure

Accelerated environmental exposure tests are designed to evaluate the long-term behavior of materials in a shortened time frame and are intended to assess the corrosion resistance of the materials. Various accelerated environments have been used to evaluate protected silver mirrors, including humidity exposure, acid-vapor exposure, H_2S fog exposure, salt fog exposure, and high-temperature high-humidity exposure [1, 2, 15, 20, 24, 29, 31 – 33, 43, 45]. While salt fog and humidity exposures have been de facto standards for assessing mirror durability, these environments may not accurately represent the corrosion mechanisms that occur in long-term use or storage [20, 66 – 70]. Mixed flowing gas (MFG) exposure has recently been shown to be a more realistic assessment of long-term behavior [67 – 70].

MFG exposure was developed in the 1980s to assess the reliability of electronic components [16, 71, 72]. It is intended to evaluate the behavior of materials in an accelerated time frame by utilizing the synergistic effects of multiple atmospheric pollutants in the presence of humidity to accelerate silver corrosion [8, 16]. The MFG environment is designed to simulate the kinetics and degradation mechanisms of real-world corrosion.

Durability and corrosion resistance of the protected silver mirrors were therefore evaluated by MFG exposure. The MFG exposure test and custom system have been described previously [67 – 70]. Testing was conducted in a custom 3.75 ft^3 acrylic test chamber under ambient

laboratory lighting. Three known air pollutants, H_2S, Cl_2, and NO_2, were utilized at specific concentrations by diluting with purified air produced by a Parker Balston 76-98-N100 zero air generator. The conditions followed the Battelle Laboratory MFG Test Method Class II environment for testing electronic components: 10 ppb hydrogen sulfide (H_2S), 10 ppb chlorine (Cl_2), and 200 ppb nitrogen dioxide (NO_2), in purified air at 70% relative humidity and 30°C [16, 71, 72]. These conditions are designed to simulate an indoor environment such as a laboratory or office that does not have continuous or effective environmental control. A bubbler was used to introduce moisture into the gas flow and control the relative humidity in the test chamber. The gases were supplied in certified gas cylinders. H_2S (10 ppm in N_2) and NO_2 (100 ppm in N_2) were supplied by Scott-Marrin, Inc. and Cl_2 (20 ppm in N_2) was supplied by Matheson Tri-Gas, Inc. The H_2S and NO_2 concentrations were monitored continuously with Teledyne-API gas analyzers, models T101 and T500U, respectively. Cl_2 was monitored separately with a Particle Measuring Systems AirSentry II Chlorine Analyzer. The mirror samples were tested for a total of 10 days, in increments of two, three, or five days at a time. Chu et al. [67, 70] has shown that bare silver mirrors, as well as those without adhesion layers, degrade significantly under these conditions.

3.2.4 Characterization Techniques

Before, during, and after MFG exposure, the mirrors were characterized to observe changes in optical properties and coating morphology. Reflectance was measured at the center of each mirror from 200 to 2500 nm with a Perkin-Elmer Lambda 950 spectrometer with an absolute reflectance accessory (URA). Scatter was measured with a Schmitt Measurement Systems (SMS) μ-scan scatterometer at 670 nm. This instrument measures the bidirectional reflectance distribution function (BRDF) at two angles to calculate an equivalent surface roughness. Optical

microscopy was utilized to image the mirror surfaces to observe changes in film morphology. Degradation on the entire mirror surface was characterized by a Keyence VHX-600 digital microscope under dark field conditions. Specific corrosion features were imaged at higher magnification using a Nikon Eclipse LV100 optical microscope under differential interference contrast (DIC) mode. The as-deposited mirrors were pre-characterized to document coating defects that could potentially affect mirror durability.

After MFG exposure, specific corrosion features were cross-sectioned for detailed observation and elemental analyses of the layered structure. Specimens were prepared by the focused ion beam (FIB) lift-out method [73] on an FEI Strata 400 DualBeam with in-situ platinum deposition and an in-situ sample manipulation probe. Imaging was performed on a JEOL 3100F transmission electron microscope at 300kV in scanning transmission mode (S/TEM). Elemental analyses in the TEM were performed with an Oxford Instruments INCA-TEM energy dispersive x-ray spectroscopy (EDS) system with a 30 mm^2 Oxford silicon-lithium detector. High angle annular dark field mode (HAADF) was used to collect Z-contrast images, where higher-Z material appears brighter. Annular dark field mode (ADF) was used to collect images that include crystallographic orientation contrast.

The corrosion features were also imaged and analyzed from a conventional top-down perspective using an FEI Helios NanoLab 600 scanning electron microscope (SEM) equipped with an Oxford Instruments Aztec EDS system. Imaging and EDS analyses were performed at various imaging modes, accelerating voltages (2 – 30 kV), sample geometries, and total collection times to reveal subtle chemical and structural information within the coating stacks at targeted depths.

X-ray photoelectron spectroscopy (XPS) was also utilized to investigate the elemental composition of the as-deposited mirrors using a Physical Electronics, Inc. VersaProbe II Scanning

XPS Microprobe. To investigate the layers of the mirror coatings, XPS depth profiles were obtained by combining a sequence of ion sputter etch cycles interleaved with XPS elemental compositional analyses. The mirror surface was etched by rastering a 1 keV Ar ion beam over a 2 mm × 2 mm area. The etch rate was 0.55 nm/min. After each sputter cycle, elemental compositional analysis was performed on the center of the sputtered area. A 200 μm diameter X-ray beam was used to generate photoelectrons from the surface, which were then collected and analyzed with a hemispherical analyzer. The generated photoelectron spectrum consists of the number of photoelectrons collected at specific binding energies. The measured photoelectron binding energy represents the energy to remove electrons from atoms and is used for elemental identification. Using the relative photoelectron count at each binding energy as well as tabulated photoelectron yields, the composition of the surface can be calculated in terms of relative atomic percent. For this study, the analyzer pass energy was 46.95 eV and the XPS analysis chamber was ion pumped to a base pressure of 1×10^{-10} Torr.

3.3 Results & Discussion

3.3.1 As-deposited Coatings

Prior to MFG exposure, the as-deposited mirror coatings exhibit excellent optical properties, including high broadband reflectance and low scatter. The no adhesion layer mirror exhibits greater than 95% reflectance at 500 nm (Figure 10), while the addition of the $NiCrN_x$ or CrN_x adhesion layer reduces the reflectance to approximately 90% at 500 nm due to the small quantity of absorptive nickel and chromium on top of the silver. This initial loss is considerable and very undesirable for high-reflectivity mirrors. The reflectance of the mirrors drops rapidly below 450 nm due to surface plasmon resonance [20, 34 – 38]. All three mirrors had initial BRDF

levels below 5×10^{-5}/sr, which is typical for these types of sputter-deposited protected silver mirrors. The surfaces of the mirror coatings are smooth and reflective, as shown in Figure 10 of a typical mirror prior to MFG exposure; this image was taken under dark field conditions, which highlights any degradation on the mirror surface [10]. The layered structure of a typical as-deposited coating is shown in Figure 11. The polished Si substrate is uniformly coated with the smooth NiCr layer, followed by the thick silver layer, which develops moderate roughness. The adhesion layer, if present, and the SiN_x layer follow the undulations at the top of the silver layer. The roughness at the top of the silver prevents direct visualization of the adhesion layer.

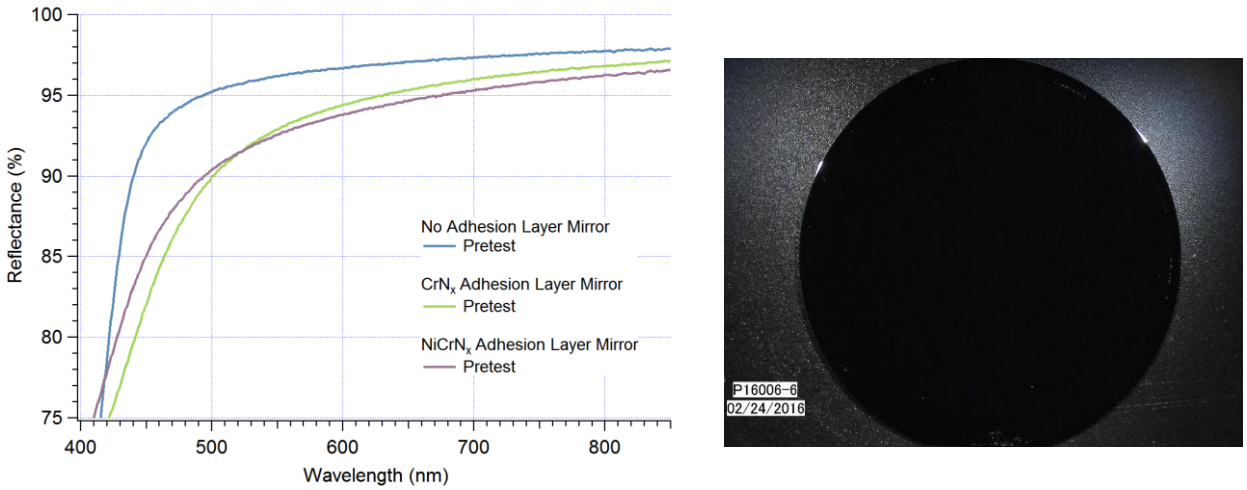

Figure 10. Prior to MFG exposure, reflectance spectra (left) and representative 2" mirror surface under dark field conditions (right).

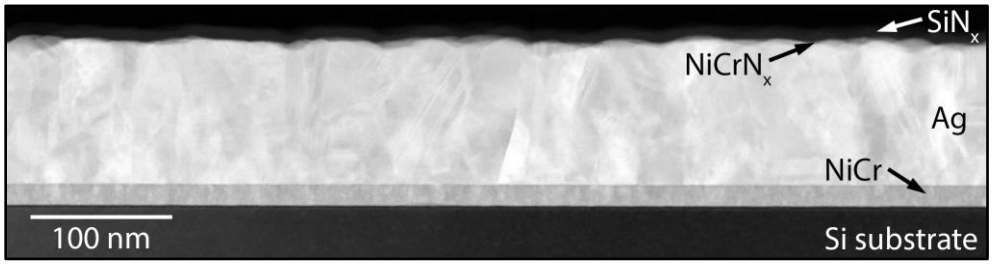

Figure 11. TEM cross-section of an as-deposited mirror coating prior to MFG exposure.

XPS depth profiles were also obtained on the as-deposited mirror coatings to analyze the elemental composition of the layered structure in the region of the adhesion layer (Figure 12). The vertical lines mark the time corresponding to the location of the adhesion layer. The asymmetry of the chromium signal (pink) in the CrN_x adhesion layer mirror compared to that of the nickel signal (teal) in the $NiCrN_x$ adhesion layer mirror suggests that the Cr and Ni behave differently. The nickel signal increases more abruptly as the depth profile progresses, and then decreases much more slowly, extending further into the silver than either the silicon (green) or nitrogen (orange) signals. A similar penetration of the chromium signal in the CrN_x adhesion layer mirror is not observed. The exact nature of the nickel-silver interaction is not clear from these data; however, it is possible that the nickel has implanted in or diffused into the silver to some degree. This could serve to promote better adhesion and interface stability, possibly improving durability.

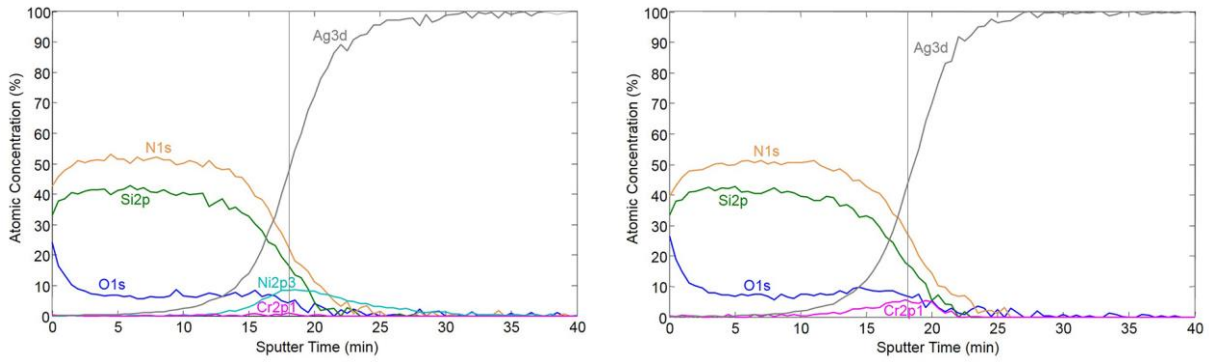

Figure 12. XPS depth profiles of the as-deposited CrN_x adhesion layer mirror (left) and $NiCrN_x$ adhesion layer mirror (right).

3.3.2 Mixed Flowing Gas Exposure

After 10 days of MFG exposure, all three mirrors showed good durability. At the center of each mirror, no loss in reflectance was observed, and only small increases in scatter were measured (Figure 13). In comparison, many commercial mirrors experience significant reductions in optical properties under these MFG conditions [67].

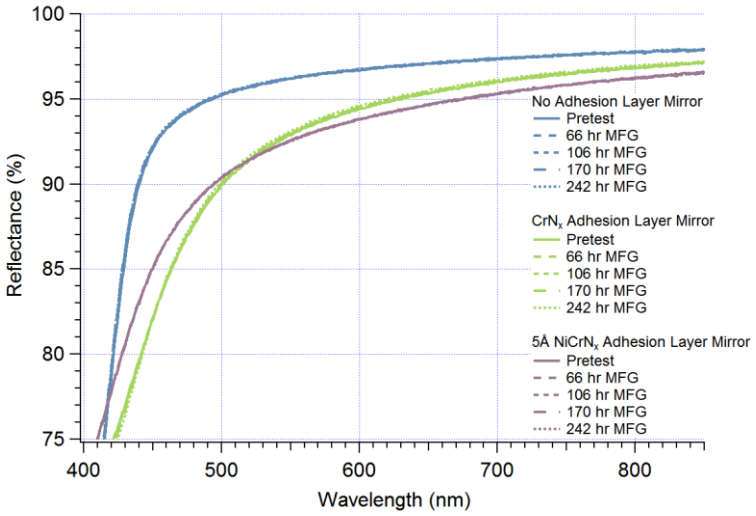

No Adhesion Layer Mirror		
	Before	After
BRDF (0,0)°, ×10^{-5}	4.5	6.3
BRDF (50,180)°, ×10^{-5}	2.3	2.8
Surface Roughness (Å)	4.5	5.5

CrN_x Adhesion Layer Mirror		
	Before	After
BRDF (0,0)°, ×10^{-5}	4.8	7.1
BRDF (50,180)°, ×10^{-5}	2.3	3.5
Surface Roughness (Å)	4.7	5.8

$NiCrN_x$ Adhesion Layer Mirror		
	Before	After
BRDF (0,0)°, ×10^{-5}	3.8	11.8
BRDF (50,180)°, ×10^{-5}	2.1	3.5
Surface Roughness (Å)	4.3	7.9

Figure 13. Reflectance and scatter throughout MFG exposure.

Varying levels of degradation are apparent in dark field images of the mirror surfaces (Figure 14). All three mirrors show scattered corrosion features across their surfaces. These features contribute to the measured increases in scatter but are not disruptive enough to cause losses in reflectance. However, the no adhesion layer mirror shows significant degradation around the edge. The layers of the coating structure are exposed to the environment at the edge, allowing ingress of corrosive species and attack of the unprotected mirror layers. The CrN_x adhesion layer mirror shows significantly less degradation around the edge; the thin 5Å adhesion layer is preventing corrosive species from attacking the coating. The $NiCrN_x$ adhesion layer mirror shows even less degradation around the edge. The only difference in these three mirrors is the composition of the thin adhesion layer at the silver-dielectric interface. This suggests that the silver-dielectric interface in the no adhesion layer mirror is particularly susceptible to corrosive attack, whereas the adhesion layers in the other mirrors reduce this type of degradation. Therefore, attack of the silver layer itself may not be the only mechanism of degradation in these protected silver mirrors.

Figure 14. Dark field images after 10 days of MFG exposure of the no adhesion layer mirror (left), CrN_x adhesion layer mirror (center), and $NiCrN_x$ adhesion layer mirror (right).

Figure 15 shows optical micrographs of the corrosion features on each of the three mirrors. The no adhesion layer mirror exhibits many large circular corrosion regions that contain scattered blisters at their centers. The circular corrosion regions develop from central defects and grow radially in size with time during MFG exposure as the corrosion reaction penetrates laterally within the coating [25, 52, 74]. The low contrast of the circular corrosion regions suggests that the layered structure of the coating is largely preserved, maintaining the mirror's optical performance. The CrN_x adhesion layer mirror exhibits similar large circular corrosion regions that also grow radially in size with time from a central defect. However, no blisters are apparent in the circular corrosion regions; rather small eruptions sometimes appear at the centers. The low contrast of the circular corrosion regions again suggests that the layered structure is largely intact, thus maintaining the optical performance of this mirror. In contrast, the $NiCrN_x$ adhesion layer mirror exhibits very different corrosion features. They are significantly smaller in size and appear as nodules rather than large circular corrosion regions. Their higher contrast suggests that they are more disruptive to the layered structure of the coating, corresponding to the slightly larger increase in scatter observed with this mirror. The composition of the thin 5Å adhesion layer dramatically changes the corrosion feature structure in these mirrors.

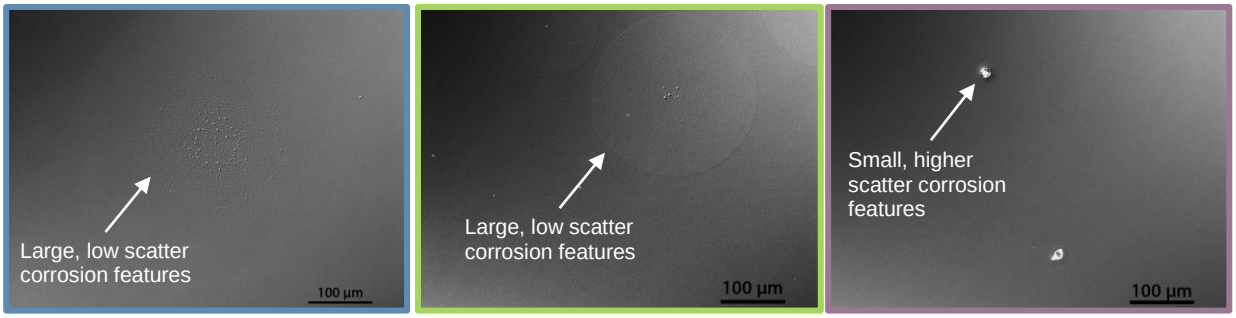

Figure 15. Optical micrographs of corrosion features after 10 days of MFG exposure on the no adhesion layer mirror (left), CrN_x adhesion layer mirror (center), and $NiCrN_x$ adhesion layer mirror (right).

3.3.3 No Adhesion Layer Mirror

Figure 16 shows plan-view SEM micrographs of corrosion features on the no adhesion layer mirror, while Figure 17 and Figure 18 show cross-sectional TEM micrographs. The large radial extent of the circular corrosion region as well as the blisters near the center are apparent. The TEM cross-section was taken through one of the blisters to show that the blisters are created due to delamination at the silver-dielectric interface, as previous researchers have suggested [31, 47]. The layers themselves are largely intact. Besides the central defect, there are no apparent breaks in the SiN_x layer, and the silver and NiCr layers appear uniform and unchanged. The corrosion process is believed to originate at small defects in the protective dielectric layer as corrosive species enter the coating layers and proceed laterally along the silver-dielectric interface, creating the large circular corrosion regions. Without an adhesion layer, the silver-dielectric interface appears more susceptible to corrosive attack than the silver layer itself. As the corrosion reaction proceeds along the interface, the SiN_x layer likely loses adhesion to the silver and the stress in the layer causes it to delaminate [23, 46, 75 – 77]. Further MFG exposure can lead to extensive delamination and eventually complete removal of the protective dielectric layer, exposing the silver directly to the corrosive species.

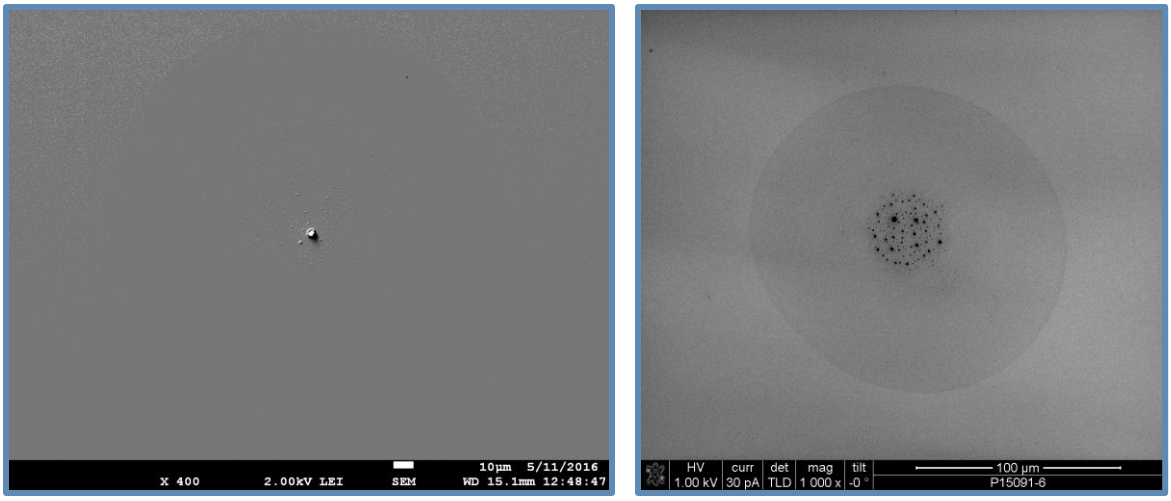

Figure 16. Plan-view SEM micrographs of corrosion features on the no adhesion layer mirror.

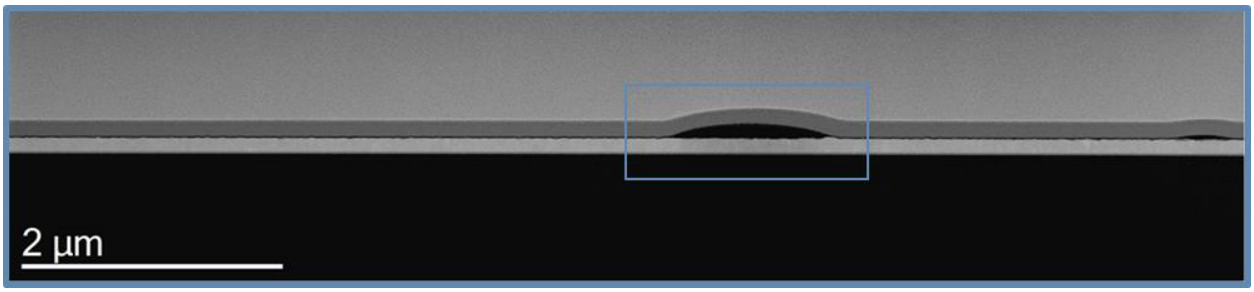

Figure 17. Cross-sectional TEM micrograph of a corrosion feature on the no adhesion layer mirror.

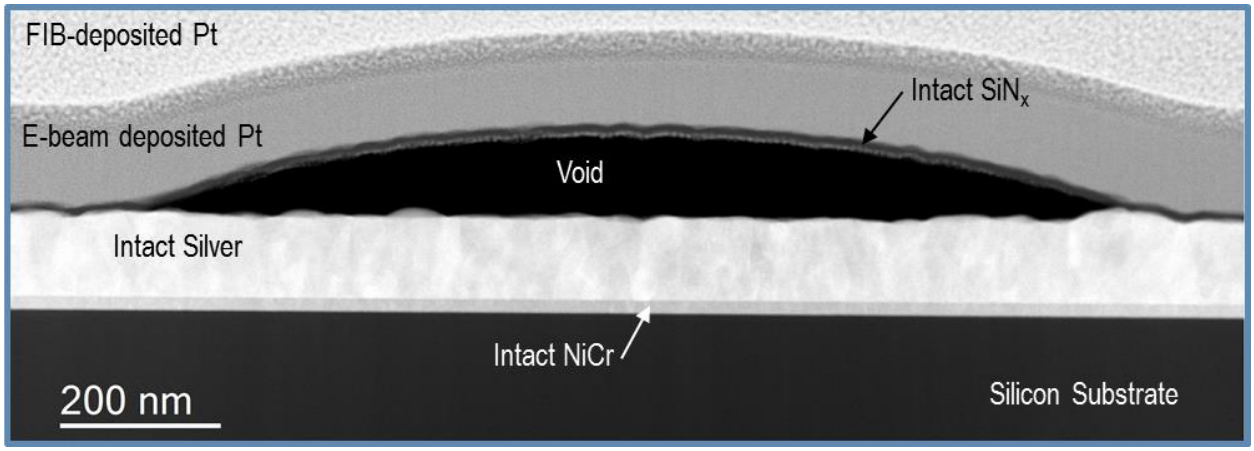

Figure 18. Cross-sectional TEM micrograph of a corrosion feature on the no adhesion layer mirror, corresponding to the area marked in Figure 17.

As the layered structure of the silver in the no adhesion layer mirror is largely preserved, SEM- and TEM-based EDS were inconclusive on detecting trace levels of corrosion products or compositional changes in these corrosion features. The limited data suggest that a small amount of subsurface silver voiding and agglomeration has occurred, indicating that the corrosive species did begin to attack the silver layer at some locations. Nonetheless, the primary mechanism of corrosion in this mirror appears to be interfacial attack at the silver-dielectric interface. This corroborates the extensive corrosion observed around the edge of the no adhesion layer mirror in Figure 14. As corrosive species penetrate the coating layers from the edge, the absence of an adhesion layer allows the reaction to proceed readily along the silver-dielectric interface.

3.3.4 CrN_x Adhesion Layer Mirror

Figure 19 shows plan-view SEM and cross-sectional TEM micrographs of a corrosion feature on the CrN_x adhesion layer mirror. The corrosion process in the CrN_x adhesion layer mirror appears analogous to the corrosion process observed in the no adhesion layer mirror. Corrosive species enter the coating through small defects in the protective dielectric layer and proceed laterally along the silver-dielectric interface, i.e. the Ag-CrN_x-SiN_x interface, creating the large circular corrosion regions. This is evidenced by the voiding at the top of the silver layer. However, there are no blisters on this mirror, as delamination of the SiN_x layer does not occur. The interfacial attack is changed by the addition of the CrN_x adhesion layer. There is limited disruption to the layered structure of the coating in the circular corrosion regions, which preserves the optical properties of this mirror after MFG exposure. However, the small amount of voiding at the top of the silver layer indicates that some attack of the silver has begun, and that lateral transport of this silver is occurring, though it is not entirely clear what drives this process. The low spatial

resolution and poor signal to noise of both SEM- and TEM-based EDS were inconclusive on the quantity, composition, and distribution of trace corrosion products within the circular corrosion regions.

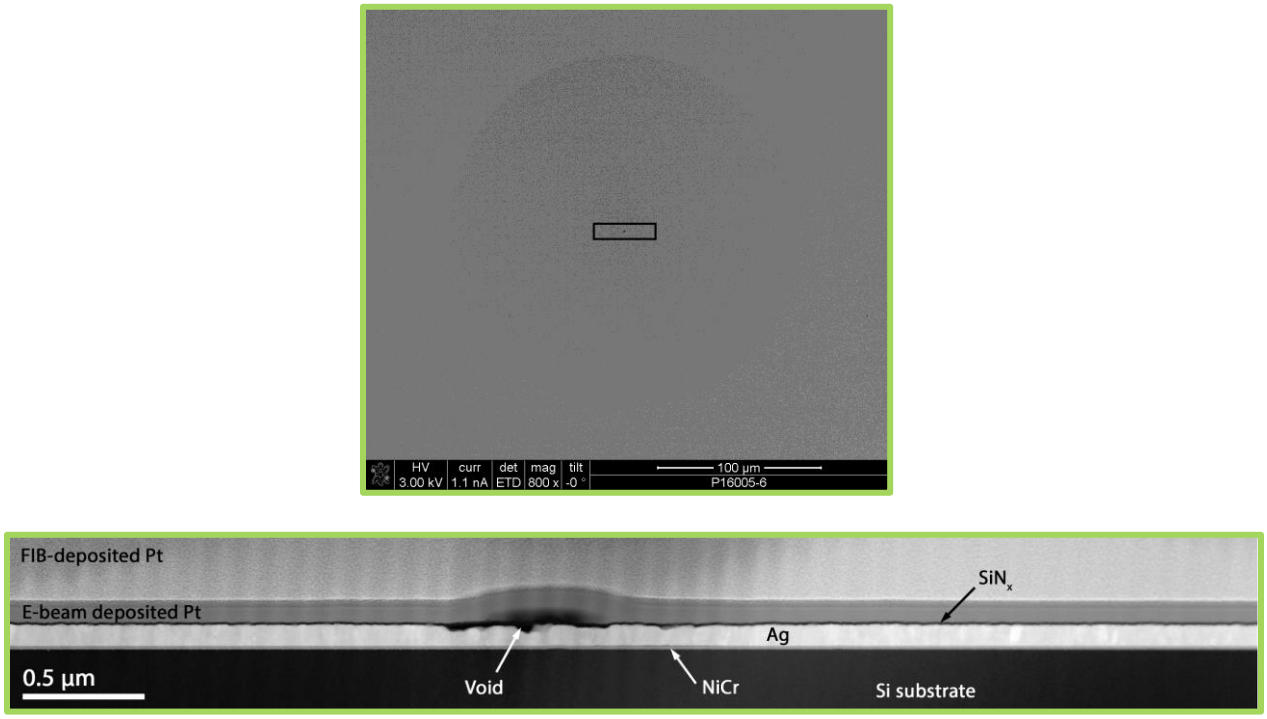

Figure 19. Plan-view SEM (top) and cross-section TEM (lower) micrographs of a corrosion feature on the CrN_x adhesion layer mirror.

The Ag-CrN_x-SiN_x interface is readily susceptible to corrosive attack, as evidenced by the large radial extent of the circular corrosion regions. Attack of the silver layer itself is far less extensive. The absence of blisters and delamination at the Ag-SiN_x interface suggests that the CrN_x adhesion layer improves adhesion and stability at this interface when compared to the no adhesion layer mirror. Though it's also possible that the adhesion layer material is affecting the electrochemical potential at the top of the silver layer; this will be discussed further in subsequent sections. The corrosive attack of the interface and the attack of the silver layer itself are considered to be two competing processes; their relative influence and interaction are not fully understood.

3.3.5 $NiCrN_x$ Adhesion Layer Mirror

The corrosion features on the $NiCrN_x$ adhesion layer mirror are substantially different than the features observed on the previous two mirrors, indicating that the corrosion process is also different. Figure 20 shows plan-view SEM of a corrosion feature on the $NiCrN_x$ adhesion layer mirror. A circular corrosion region is present, though much smaller in radial extent, and a large central agglomerate is surrounded by voids that are nearly entirely depleted of silver. Previous researchers have reported similar agglomerated silver corrosion features on other protected silver mirrors [10, 15, 23, 52]. Figure 21 shows cross-sectional TEM micrographs of the corrosion feature shown in Figure 20. The corrosion process is significantly more disruptive to the layered structure of the mirror coating near to the silver agglomerate. However, farther from the central agglomerate, the layered structure of the coating is largely preserved. Notably, voiding and silver depletion occurs from the lower silver-base layer interface, the NiCr-Ag interface, while the upper Ag-$NiCrN_x$-SiN_x interface appears intact across the corrosion region. No breaks were found in the SiN_x layer, suggesting they are either elsewhere on the corrosion feature or are too small to observe.

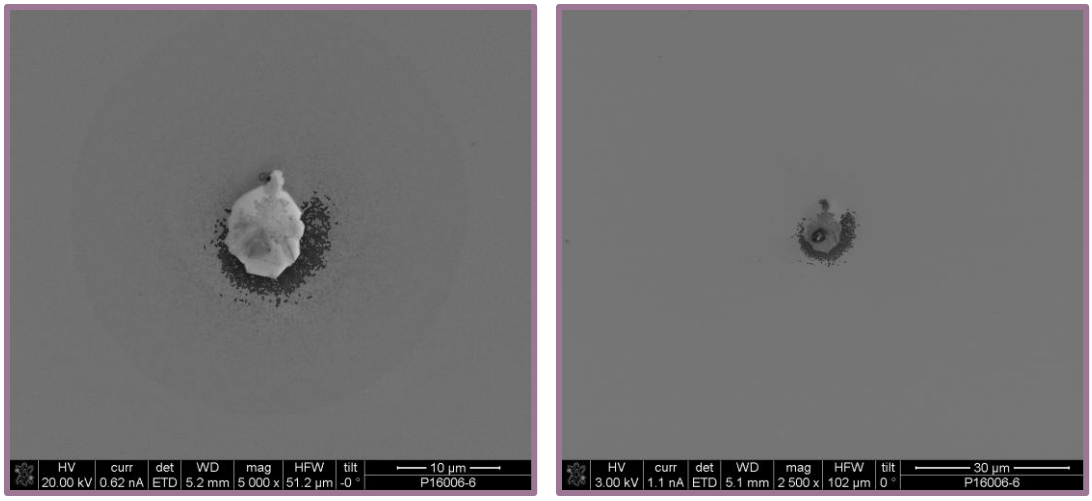

Figure 20. Plan-view SEM micrographs of a corrosion feature on the $NiCrN_x$ adhesion layer mirror. 20 kV accelerating voltage (left) and 3 kV accelerating voltage (right).

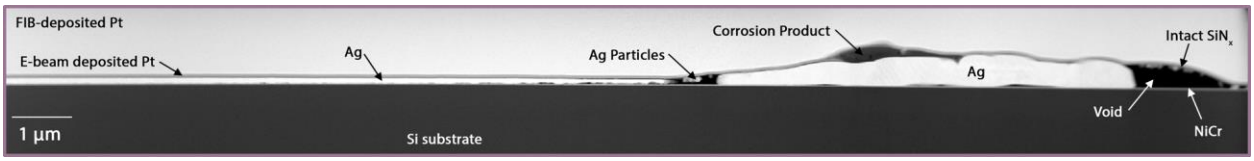

Figure 21. Cross-section TEM micrographs of a corrosion feature on the $NiCrN_x$ adhesion layer mirror, taken through the central defect shown in Figure 20.

The central agglomerate is largely silver, though limited chlorine, sulfur, and oxygen were also detected. Chlorine and oxygen were similarly detected in the silver-depleted regions surrounding the central agglomerate. The corrosion product on top of the SiN_x layer consists of nickel, sulfur, chlorine, oxygen, carbon, and phosphorous. The varied distribution of the corrosion products suggests that the corrosion of nickel and the corrosion of silver are two competing reactions, possibly driven by different electrochemical mechanisms.

As corrosive species penetrate the SiN_x layer, the $NiCrN_x$ adhesion layer prevents interfacial attack at the Ag-SiN_x interface. Rather, the corrosive species attack the silver and the lower silver-base layer interface. This creates the smaller circular corrosion region at the NiCr-Ag interface and the lateral transport of silver results in the large central agglomerate. The

improved stability at the Ag-$NiCrN_x$-SiN_x interface is likely due to the nickel in the $NiCrN_x$ adhesion layer as the mechanism that enabled interfacial corrosion in the CrN_x adhesion layer mirror is no longer available in the $NiCrN_x$ adhesion layer mirror. The XPS data (Figure 12) show nickel extending furthest in to the silver, possibly improving adhesion at the interface, though the exact nature of the nickel-silver interaction is not available from these data. The nickel in the $NiCrN_x$ adhesion layer may also be affecting the electrochemical potential at the top of the silver layer to change the mechanism of corrosion.

3.4 Conclusions

Corrosion feature development was shown to depend largely on the composition of the very thin (5Å) adhesion layer between the silver and the protective overcoat of SiN_x. The corrosion features originate at small defects in the dielectric protection layers and grow laterally along various layer interfaces, only sometimes resulting in significant layer disruption and silver corrosion or agglomeration. The morphology of the corrosion features and the extent of layer disruption varies significantly based on the adhesion layer material.

On the no adhesion layer mirror, large circular corrosion regions form along the Ag-SiN_x interface, leading to delamination of the protective SiN_x from the silver. The layer structure of the silver is largely preserved, as there is limited attack of the silver itself. The interfacial mechanism of corrosion results in substantial attack at the edges of the no adhesion layer mirror. On the CrN_x adhesion layer mirror, similar large circular corrosion regions form along the Ag-CrN_x-SiN_x interface, also with limited disruption to the layered structure of the coating. Delamination of the SiN_x does not occur; rather, limited attack of the silver results in a small amount of silver voiding. The interfacial attack and the attack of the silver layer itself are considered to be two competing

processes. While the corrosion features and processes are analogous to those in the no adhesion layer mirror, the CrN_x adhesion layer has changed the mechanism of corrosion at the Ag-SiN_x interface, resulting in far less corrosion at the edges of the mirror.

On the $NiCrN_x$ adhesion layer mirror, much smaller corrosion features form that are significantly more disruptive to the layered structure of the coating. Substantial silver agglomeration and large voids occur. As corrosive species enter the coating through defects in the dielectric protection layer, attack of the Ag-$NiCrN_x$-SiN_x interface does not occur due to improved stability provided by the nickel in the adhesion layer. Rather, corrosive species attack the silver and, eventually, the lower NiCr-Ag interface. The adhesion layers may be affecting the electrochemical potential at the top of the silver layer to change the mechanism of corrosion feature development and growth. Ultimately, both the lower and upper silver interfaces play important roles in the corrosion process.

Chapter 4. Development and Growth of Corrosion Features

4.1 Introduction

Chapter 3 showed that the corrosion process in these Gemini-style protected silver mirrors depends largely on the composition of the adhesion layer between the silver and its protective dielectric overcoat. Corrosion features appear to originate at small defects in the SiN_x protection layer and grow laterally along various layer interfaces, only sometimes resulting in significant layer disruption and silver corrosion. The morphology of the corrosion features and the extent of layer disruption depends on the composition of the adhesion layer. Silver mirrors with no adhesion layers or CrN_x adhesion layers experienced corrosion primarily along the silver-dielectric interface, resulting in large circular corrosion regions with limited disruption to the layered structure of the coating. In contrast, silver mirrors with $NiCrN_x$ adhesion layers experienced substantial layer disruption as the nickel in the adhesion layer improved the stability at the silver-dielectric interface and enabled the corrosion reaction to attack the lower silver interface.

This chapter extends this work to further investigate the compositional effects at the silver interfaces on the mechanisms of corrosion feature development and growth. Accelerated environmental exposure testing of protected silver mirrors with various NiCr- and Cr-based layers on either side of the silver layer was used to investigate the corrosion processes that occur at the Ag-Cr interfaces and their effects on mirror durability. We will show that the Ag-Cr interfaces are particularly susceptible to corrosive attack by chlorine and oxygen, and that this interfacial corrosion drives the development of corrosion features, impacting the optical properties of the mirrors.

4.2 Experimental Methods

4.2.1 Deposition Processes

The deposition of the protected silver mirrors by plasma beam sputtering was described in Chapter 3.

4.2.2 Silver Mirror Designs

For this study, two model mirror coatings were investigated in which the composition of the base layer below the silver and the adhesion layer above the silver were varied to differentiate between the Ag-Cr and the Ag-NiCr interfaces, and their location within the layered structure (Figure 22). The CrN_x adhesion layer mirror has a NiCr base layer with a CrN_x adhesion layer. The Cr base layer mirror has a Cr base layer and a $NiCrN_x$ adhesion layer. The other layers, Ag and SiN_x, are the same between the two mirrors. By changing only the location of the Ag-Cr interface within the mirror stack, this study will investigate how the absence of nickel contributes to the interfacial attack previously observed. Chromium is often utilized as an underlayer in various protected silver mirror designs [24, 78].

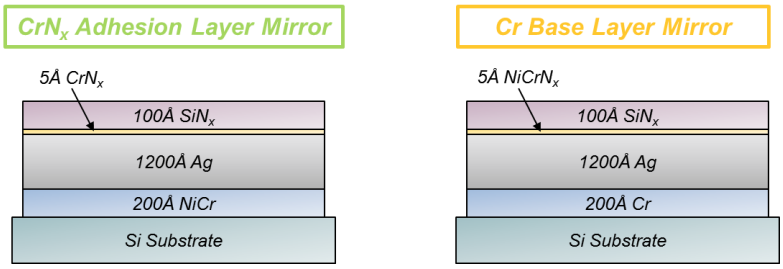

Figure 22. CrN_x adhesion layer mirror and Cr base layer mirror designs deposited for this study.

4.2.3 Accelerated Environmental Exposure

As described in Chapter 3, durability and corrosion resistance of the mirrors were evaluated by MFG exposure. Throughout exposure, the mirrors were characterized to observe changes in optical properties and coating morphology. As previously described, reflectance and scatter were measured at the mirror center, degradation of the mirror surface was imaged under dark field conditions, and corrosion features were imaged with an optical microscope under DIC mode.

After MFG exposure, high sensitivity chemical analyses of the layered structure of the corrosion features were performed by Time of Flight-Secondary Ion Mass Spectrometry (ToF-SIMS) depth profiles using a Physical Electronics TRIFT-V nanoTOF. The TRIFT-V is a triple focusing time-of-flight mass spectrometer equipped with a pulsed bismuth cluster liquid metal ion gun (LMIG). Secondary ions are generated by impact ionization using bismuth as the primary species. A 1 kV Cesium LMIG source was used to remove material during the depth profiles. Mass spectral data was obtained at 5 second intervals during the cesium sputtering over a 400x400 μm area to show the corroded area of interest.

4.3 Results & Discussion

4.3.1 Corrosion Feature Growth

Both mirrors showed good durability after 10 days of MFG exposure (Figure 23 and Figure 24). The CrN_x adhesion layer mirror exhibited no loss in reflectance and only a slight increase in scatter, indicating that the corrosion features on this mirror have not significantly disrupted the layered structure of the coating and that the thick silver reflective layer is largely intact. In comparison, the Cr base layer mirror exhibited a small (1% at 600 nm) decrease in reflectance and a significant increase in scatter after MFG exposure, suggesting that the morphology of the

corrosion features on the two mirrors are different. The corrosion features on the Cr base layer mirror are likely more disruptive to the layered structure of the mirror coating, thereby reducing its optical performance.

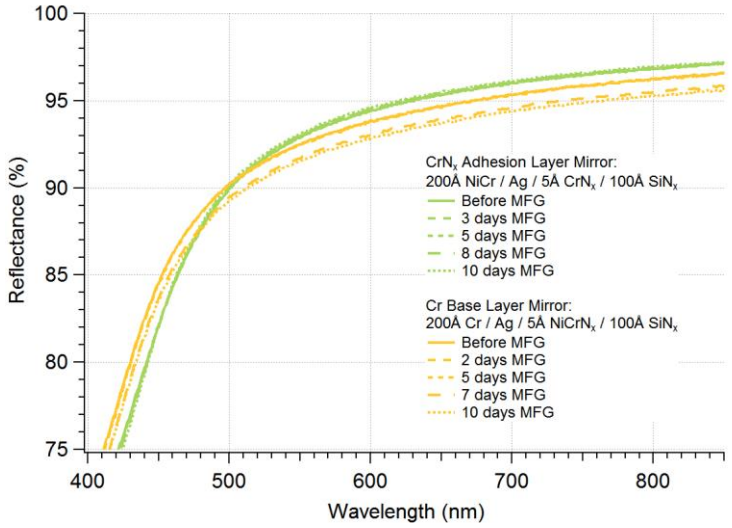

Figure 23. Reflectance spectra of the silver mirrors during MFG exposure.

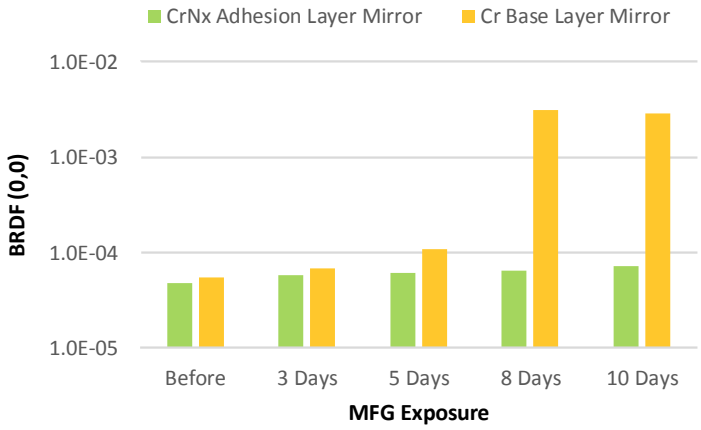

Figure 24. Scatter of the silver mirrors during MFG exposure.

While the optical performance of both mirrors was still good after MFG exposure, degradation is apparent in dark field images of the mirror surfaces (Figure 25). Prior to MFG exposure, the smooth, reflective surfaces of both mirrors appear black under dark field imaging

conditions; following MFG exposure, degradation on the mirrors appears white. Both mirrors show degradation around the edges of the coating, as well as many small scattered corrosion features across the entire surface of each mirror. Due to the way the oblique lighting was oriented, the corrosion features in the upper half of the Cr base layer mirror appear particularly bright, though the features do exist across the entire mirror surface.

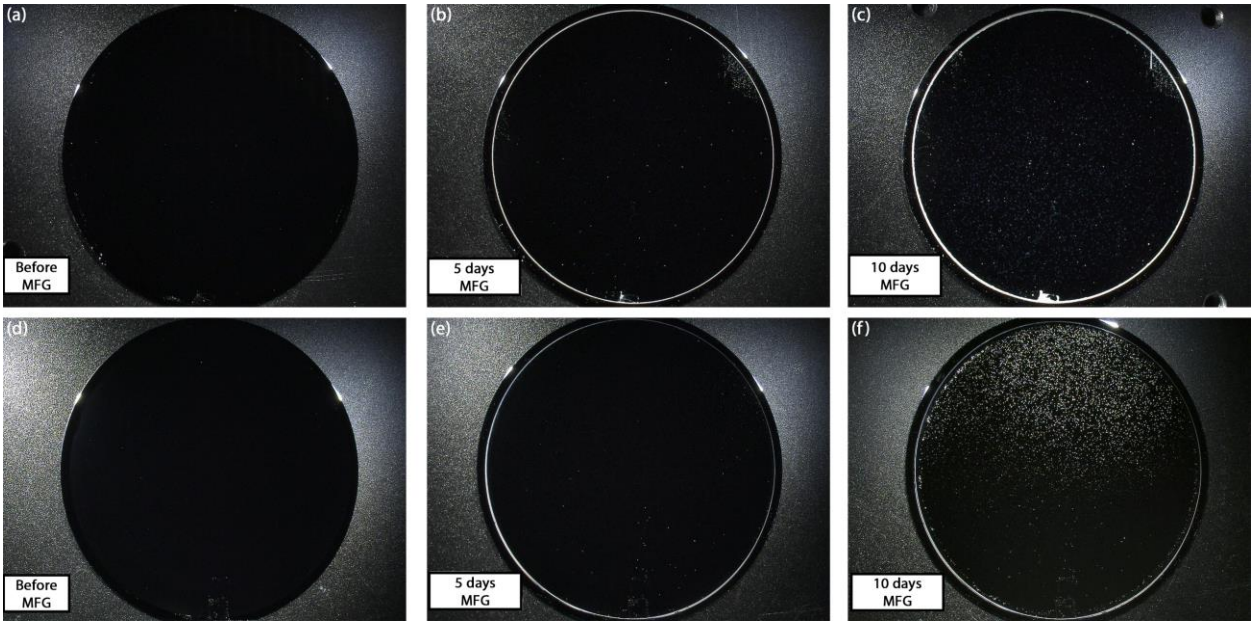

Figure 25. Dark field images of the CrN_x adhesion layer mirror (a,b,c) and Cr base layer mirror (d,e,f) during MFG exposure. Before MFG exposure (a,d), after 5 days MFG exposure (b,e), after 10 days MFG exposure (c,f).

Optical micrographs of the development and growth of the corrosion features at the center of the CrN_x adhesion layer mirror and the Cr base layer mirror during MFG exposure are shown in Figure 26 and Figure 27, respectively. As described previously, the features on the CrN_x adhesion layer mirror are large circular corrosion regions that grow radially out from a central defect as the corrosion reaction proceeds laterally within the coating structure. The areas of the coating surrounding the circular corrosion regions appear intact and unaffected by the corrosion process. Close inspection of the pre-MFG image in Figure 26 shows that some of the circular

corrosion regions on the CrN_x adhesion layer mirror originate at pre-existing defect sites, whereas many others do not. Likewise, there are other pre-existing defects sites that do not develop into circular corrosion regions. From these images, it is unclear why this occurs. While the circular corrosion regions grow radially in size with MFG exposure, they do not change substantially in appearance. Their low contrast, compared to the uncorroded portions, again suggests that there is limited disruption to the layers of the coating, thus preserving the optical properties of this mirror after MFG exposure.

The Cr base layer mirror shows similar large circular corrosion regions that also grow radially out from a central defect during MFG exposure. Initially, the features on both mirrors are similar in appearance and growth rate, suggesting that similar corrosion reactions are occurring in both mirrors. However, after 7 days of MFG exposure, many additional features appear within the circular corrosion regions on the Cr base layer mirror that correspond to the notable increase in measured scatter (Figure 24). The patterning on these additional features suggests topographical and morphological differences that are likely due to delamination at layer interfaces, with the layers themselves remaining largely intact.

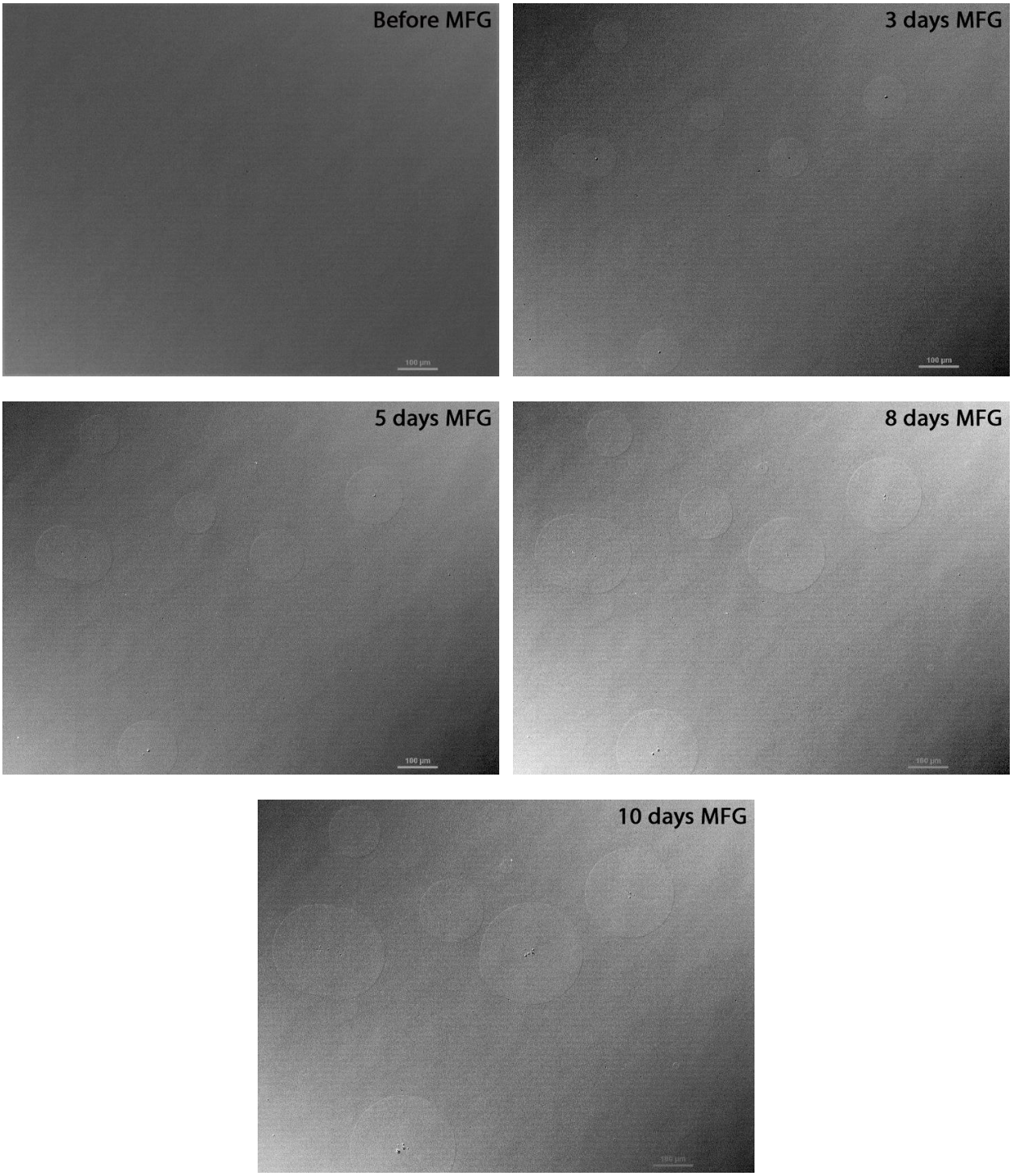

Figure 26. Optical micrographs of corrosion feature growth on the CrN_x adhesion layer mirror during MFG exposure.

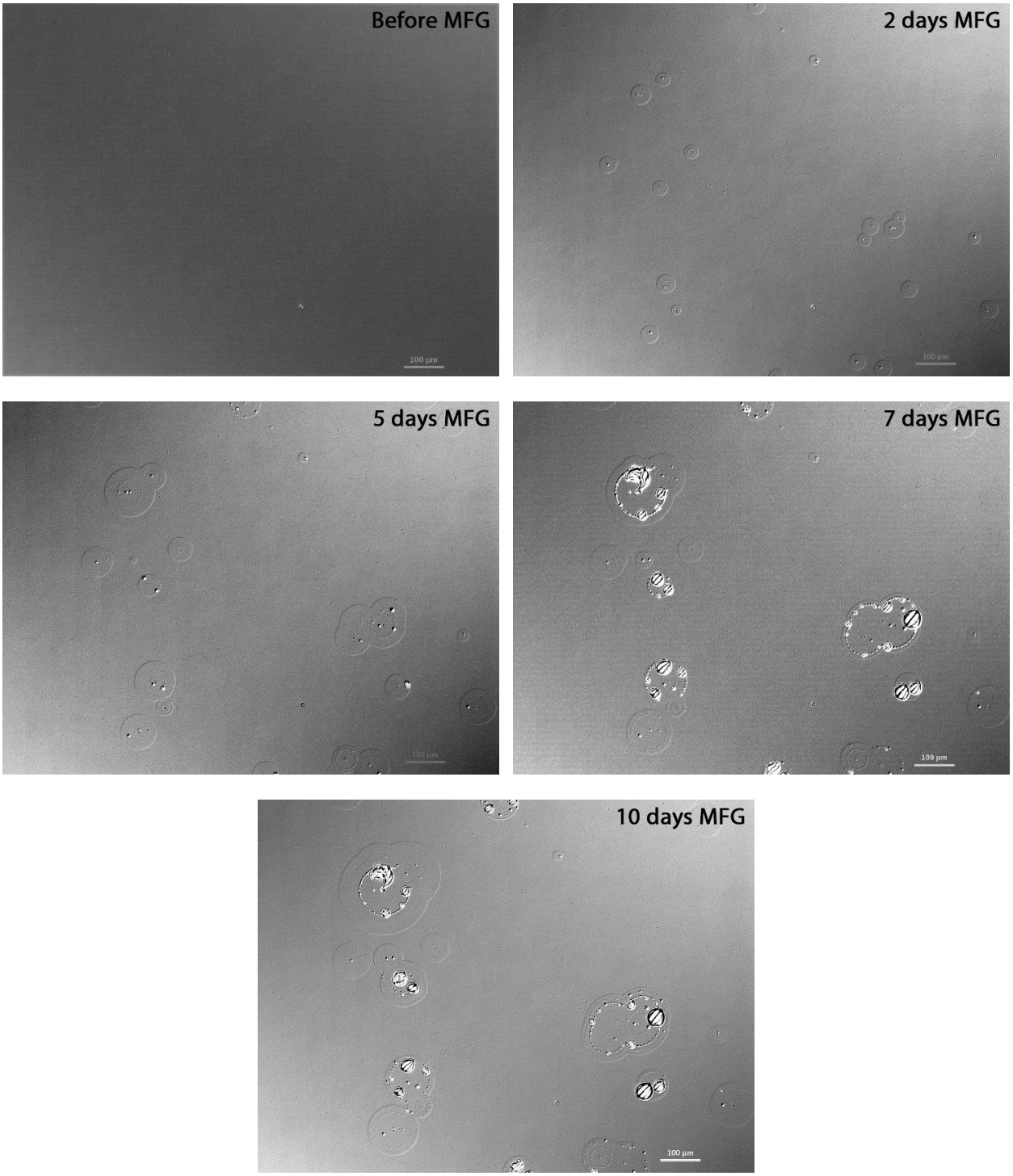

Figure 27. Optical micrographs of corrosion feature growth on the Cr base layer mirror during MFG exposure.

4.3.2 Corrosion Feature Layered Structure

Following MFG exposure, corrosion features on both mirrors were cross-sectioned for TEM analysis to investigate the layered structure of the coating within the circular corrosion regions. A micrograph obtained during the FIB process of the CrN_x adhesion layer mirror is shown in Figure 28 and marks the location of the TEM cross-section shown in Figure 29. The SEM micrograph was obtained in secondary electron mode with low accelerating voltage to provide a near-surface image of the corrosion feature. The low contrast between the circular corrosion region and the uncorroded portion of the mirror suggests that there is limited topographical variation or disruption to the layered structure of the coating within the circular corrosion regions. This is confirmed by the TEM cross-section, which shows the layers largely intact. There is a small amount of voiding at the top of the silver layer, but no significant silver agglomeration is present. Because the layered structure of the mirror coating is largely preserved, the optical performance of the mirror is maintained after MFG exposure.

As discussed previously, the corrosion process is believed to begin with corrosive species entering the coating through small defects in the protective dielectric layer and proceeding laterally along the silver-dielectric interface, i.e. the Ag–CrN_x-SiN_x interface, creating the large circular corrosion regions. This interfacial corrosion process is evidenced by the small amount of voiding at the top of the silver layer, which suggests that the corrosion reaction is occurring at the top of the silver layer. Limited attack of the silver has begun, suggesting that lateral transport of this silver is occurring, though it is not entirely clear what drives this process. The low spatial resolution and poor signal to noise of both SEM- and TEM-based EDS were inconclusive on the quantity, composition, and distribution of trace corrosion products within the circular corrosion regions.

The large radial extent of the circular corrosion regions indicates that the Ag–CrN_x-SiN_x interface is readily susceptible to corrosive attack. Attack of the silver layer itself is far less extensive. The absence of blisters and delamination at the Ag-SiN_x interface suggests that the CrN_x adhesion layer improves adhesion and stability at this interface when compared to mirrors with no adhesion layer. It is also possible that the CrN_x adhesion layer is affecting the electrochemical potential of the silver layer to influence how the corrosion process evolves [2, 18, 39, 61]. The corrosive attack at the interface and the attack of the silver layer itself are considered to be two competing processes; their relative influence and interaction are not fully understood.

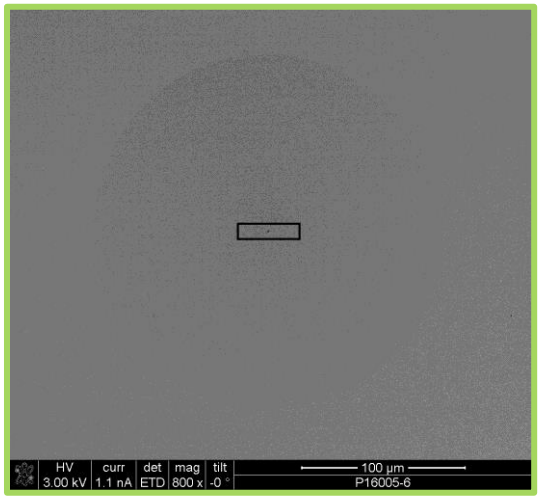

Figure 28. Plan-view SEM micrograph of a circular corrosion region on the CrN_x adhesion layer mirror showing the location of the TEM cross-section. Reprint of Figure 19.

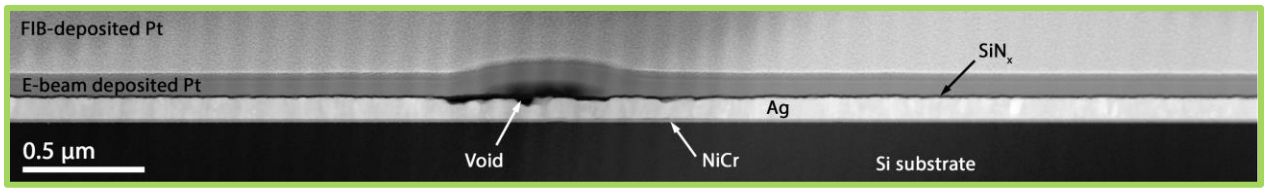

Figure 29. TEM cross-section near the center of a circular corrosion region on the CrN_x adhesion layer mirror. Reprint of Figure 19.

As the corrosion process originates at small defects in the protective dielectric layer, corrosive species enter the coating layers and proceed laterally along the silver-dielectric interface, creating the large circular corrosion regions at the Ag–CrN_x-SiN_x interface. The absence of nickel in the CrN_x adhesion layer appears to increase the susceptibility of this interface to attack compared to silver mirrors with $NiCrN_x$ adhesion layers. Therefore, it was hypothesized that the circular corrosion regions on the Cr base layer mirror would also occur at the silver interface that does not contain nickel, i.e. the lower silver interface in the Cr base layer mirror.

Micrographs obtained during the FIB process of the Cr base layer mirror are shown in Figure 30, and mark the location of the TEM cross-section shown in Figure 31. As noted with the CrN_x adhesion layer mirror, the low contrast between the circular corrosion regions and the uncorroded coating suggests that the layered structure of the coating is largely intact. However, there is topographical variation associated with the additional features within the circular corrosion regions on the Cr base layer mirror; they appear in the micrographs as blisters or delaminations. The cross-section location was chosen to pass through a blister to clearly show the changes in the layered structure of the coating. The TEM image confirms that the layered structure of the coating is preserved across the circular corrosion region except where the intact silver layer has delaminated from the Cr layer below.

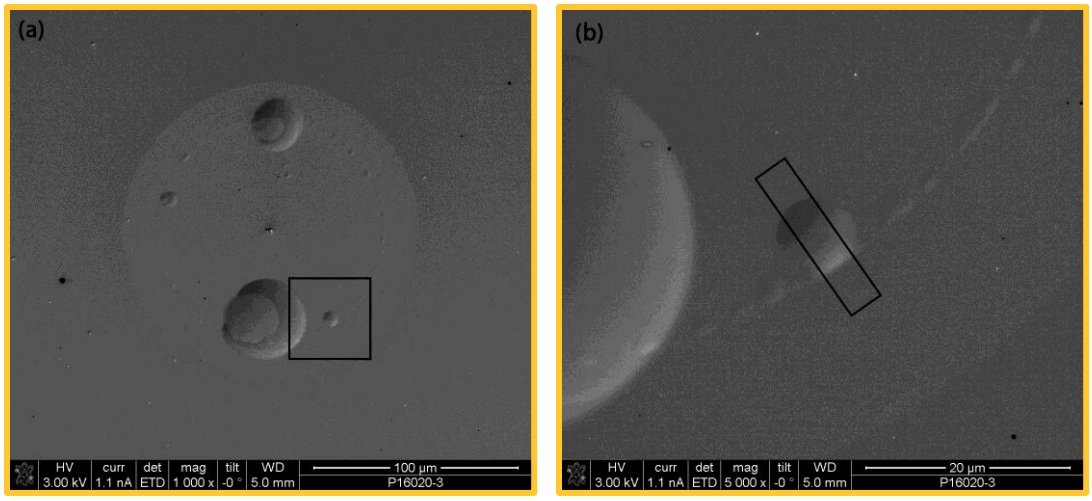

Figure 30. SEM micrographs of a circular corrosion region on the Cr base layer mirror showing the location of the TEM cross-section through the small blister delamination.

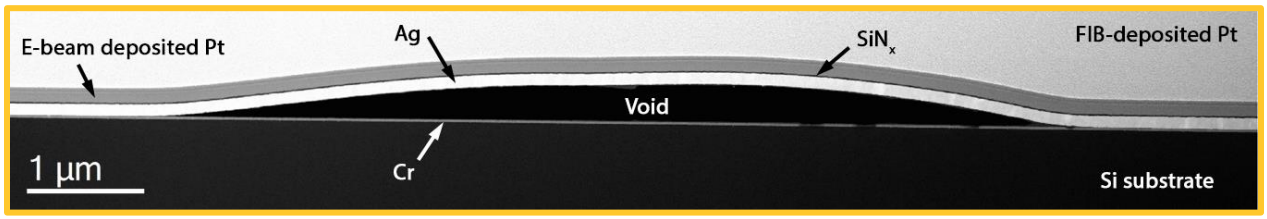

Figure 31. TEM cross-section of a delamination within a circular corrosion region on the Cr base layer mirror.

As with the CrN_x adhesion layer mirror, the corrosion reaction in the Cr base layer mirror is proceeding along the silver-chromium interface, i.e., the silver interface that lacks nickel. In the Cr base layer mirror, the corrosion process similarly enters the coating through a small defect in the dielectric protection layer but cannot proceed along the silver-dielectric interface because of the improved interface stability associated with the $NiCrN_x$ adhesion layer. Rather, the reactants attack the silver and proceed along the lower silver-chromium interface to create the circular corrosion regions.

As the corrosion reaction proceeds along the silver-chromium interface, it is likely reducing the adhesion and integrity of that interface, leading to delamination of the intact silver layer from

the chromium base layer below. The blisters are a result of stress in the coating layers [23, 75 – 77]. The delaminations leave behind voids between the two layers and cause the patterning observed in the optical micrographs due to light scatter from the now-topographical silver layer.

There is a small amount of voiding in the chromium base layer and some buildup of corrosion products at the edge of the delaminations. These corrosion products contain silver, chromium, and silicon, as well as chlorine and oxygen, as determined by EDS. However, no significant silver voiding is observed. On both mirrors, it is not immediately clear why the corrosive species do not simply attack the silver layer rather than the silver-chromium interfaces. While it is possible that the interface is simply more susceptible to corrosive attack than an intact layer, there are likely also chemical, electrochemical, and kinetic effects to the corrosion process. The layers on either side of the silver layer may affect the electrochemical behavior of the silver [23, 75 – 77]; this will be discussed in subsequent chapters.

4.3.3 Corrosion Feature Development

The circular corrosion regions that develop on these protected silver mirrors often originate at pre-existing defect sites, as illustrated in the optical micrographs of corrosion feature development and growth in Figure 26 and Figure 27. To investigate these defect structures, a TEM cross-section was prepared through the central feature on a circular corrosion region on the Cr base layer mirror (Figure 32 and Figure 33). The TEM cross-section again shows that the coating layers are largely intact within the circular corrosion region, except where the intact silver layer has delaminated from the Cr base layer below, creating the large void. The central defect appears as a low-Z nodule protruding above the mostly intact layers.

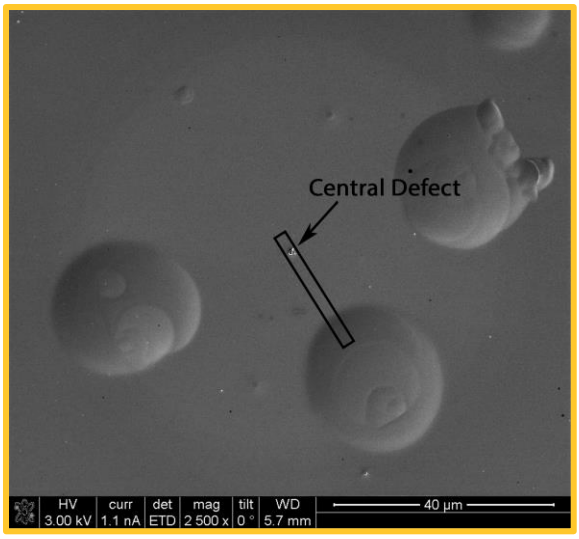

Figure 32. SEM micrograph of a circular corrosion region on the Cr base layer mirror showing the location of the TEM cross-section through the central defect.

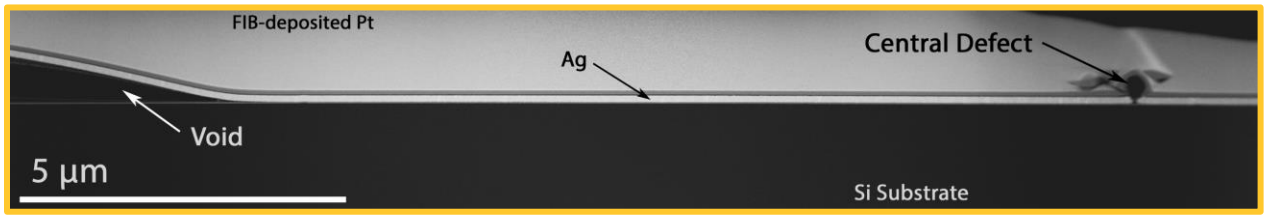

Figure 33. TEM cross-section through the central defect on a circular corrosion region on the Cr base layer mirror.

A high-resolution image of the central defect is shown in Figure 34 along with EDS maps of the region. The large nodule of the central defect is predominately silicon, with a nonuniform signal of nitrogen. This defect is a coating "spit" deposited during reactive sputtering of the silicon nitride protective layer. The SiN_x layer is sputtered from a silicon target in a mixture of argon and nitrogen, such that poisoning of the silicon target occurs readily because the target bias is provided by a DC power supply. Buildup of a SiN_x dielectric layer on the silicon target results in arcing, or breakdown, which can eject lumps of silicon from the target. These deposit on the substrate as nodules of silicon, rather than individual molecules of SiN_x, disrupting the layered structure of the thin film and shadowing further deposition of the protective SiN_x layer. For silicon spits that

deposit early in the deposition of the SiN_x layer, it's possible that only a few angstroms of protective SiN_x are present below. This provides entry points for corrosive species to attack the coating layers, leading to the large circular corrosion regions.

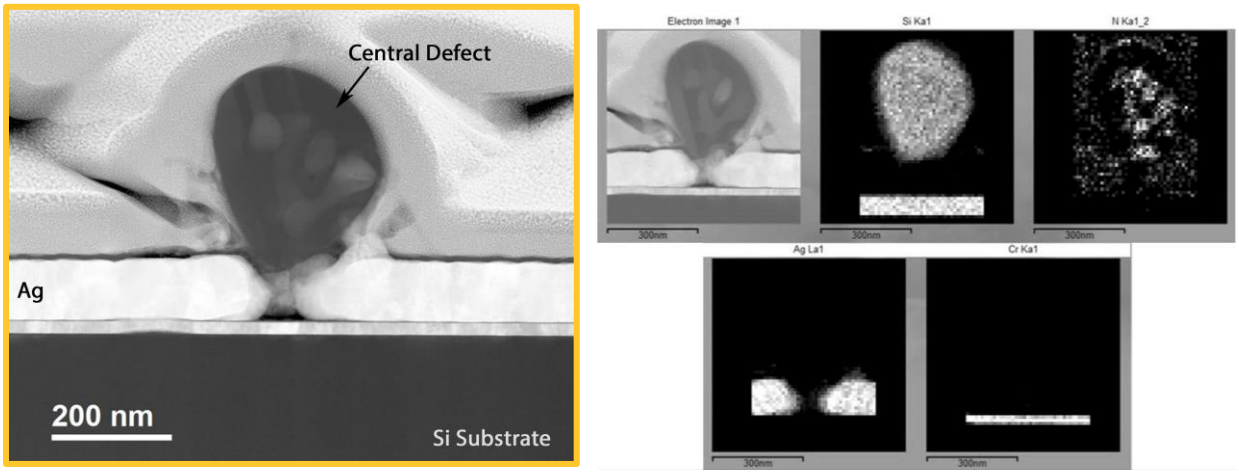

Figure 34. (Left) TEM cross-section through the central defect on a circular corrosion region on the Cr base layer mirror. (Right) EDS maps of the central defect.

The corrosion and degradation of these silver mirrors is therefore considered to be, at least in part, a defect-mediated process, with the coating spits providing entry points for corrosive attack within the layers, below the mostly-intact SiN_x layer. It was pointed out previously that only some pre-existing defects evolved into circular corrosion regions (Figure 26 and Figure 27). These are likely silicon spits that were deposited early in the SiN_x deposition and resulted in only a few, poorly-protective angstroms of SiN_x below. The defects that did not evolve into corrosion features were likely deposited later in the SiN_x deposition, with much thicker protective layers below. Similarly, the circular corrosion regions that showed no obvious pre-existing defect to start are believed to be the result of spits that are too small to observe in the optical micrographs.

4.3.4 Corrosion Feature Interface Chemistry

Once the corrosion process is initiated, the TEM cross-sections and previous low-voltage EDS measurements [79] suggest that similar corrosion processes are occurring in both mirrors, but that the attack is occurring at different stratigraphic locations within the coating layers. In the CrN_x adhesion layer mirror, corrosive species enter the coating through small defects in the dielectric protective layer and proceed laterally along the Ag–CrN_x-SiN_x interface. In the Cr base layer mirror, the addition of nickel at the Ag–$NiCrN_x$-SiN_x interface results in the corrosion occurring along the lower Cr-Ag interface. In both mirrors, the circular corrosion regions form only at the silver-chromium interfaces. To investigate the corrosion chemistry at these interfaces, ToF-SIMS depth profile maps at the silver interfaces are presented. These maps provide chemical information of the area inside the circular corrosion regions compared to the un-corroded coating at different stratigraphic locations within the layered structure. Blue boxes on the coating depth gauges indicate the vertical location of the ToF-SIMS maps. The regular grid of small bright squares, as well as the brightness gradients, are measurement artifacts from non-uniformity in the detector.

ToF-SIMS maps of the CrN_x adhesion layer mirror at the upper silver-dielectric interface are shown in Figure 35, while those for the lower base layer-silver interface are shown in Figure 36. At the silver-dielectric interface, the chemical signature of the corrosion features is evident, as chlorine and oxygen enrichment are apparent within the circular corrosion regions. This suggests that corrosion feature development and growth is driven by the oxidation and chloridation of both silver and chromium at the Ag–CrN_x-SiN_x interface. Sulfur enrichment is apparent only at the very center of the circular corrosion region and is believed to be associated with attack and voiding of the silver directly below the central defect (Figure 29). At the lower silver-base layer

interface, no indication of the circular corrosion regions is evident. The corrosion process in the CrN_x adhesion layer mirror occurs only at the silver-dielectric interface, i.e. the interface that lacks nickel.

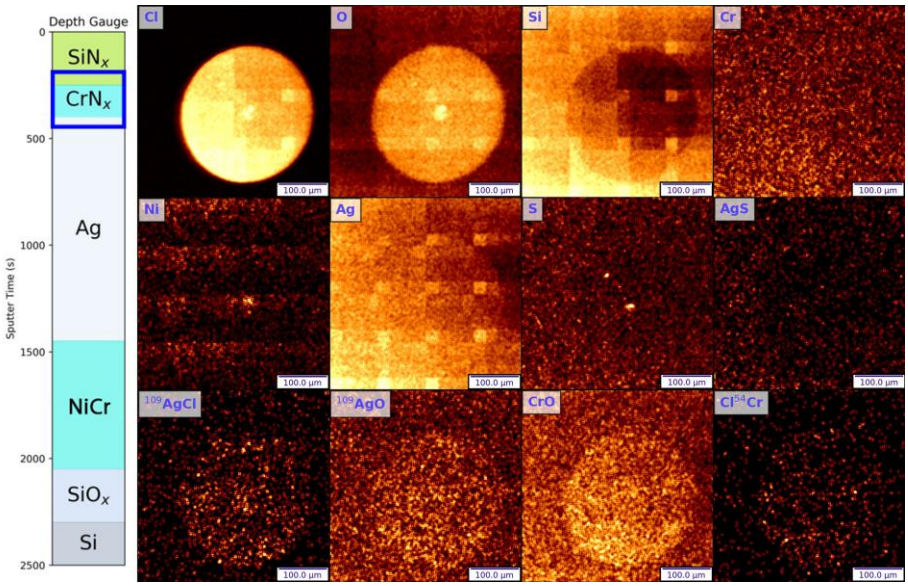

Figure 35. ToF-SIMS depth profile maps at the Ag–CrN_x-SiN_x interface of a circular corrosion region on the CrN_x adhesion layer mirror.

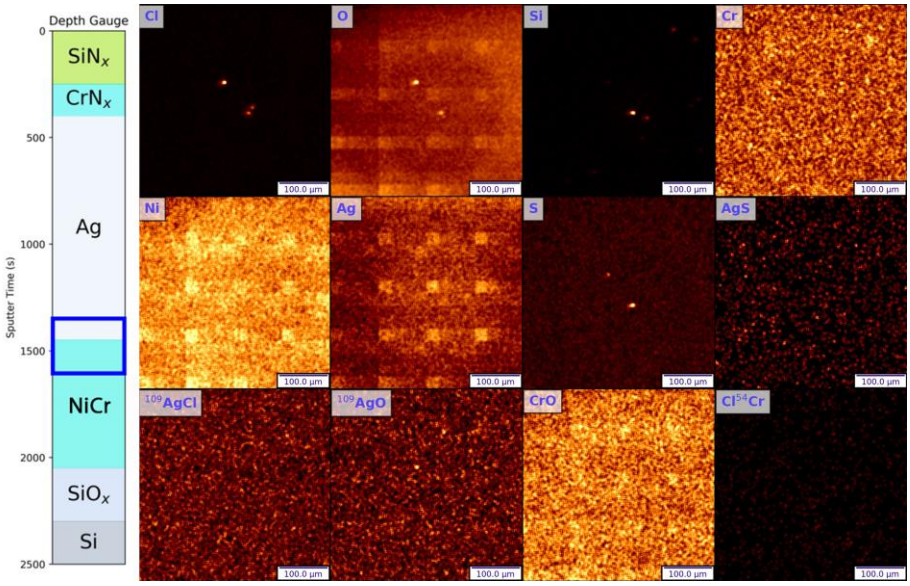

Figure 36. ToF-SIMS depth profile maps at the NiCr-Ag interface of a circular corrosion region on the CrN_x adhesion layer mirror.

ToF-SIMS maps of the Cr base layer mirror at the upper and lower silver interfaces are shown in Figure 37 and Figure 38, respectively. Analogous to the CrN_x adhesion layer mirror, the corrosion features are evident at the Cr-Ag interface. Oxygen and chlorine enrichment within the circular corrosion regions occurs only at the lower base layer-silver interface, i.e. the interface that lacks nickel. There is no evidence of the circular corrosion regions at the upper silver-dielectric interface. The three features present at the upper interface are small blisters or delaminations that are apparent throughout the ToF-SIMS sputtering process due to topographical differences. As with the CrN_x adhesion layer mirror, sulfur enrichment is only apparent at the very center of the circular corrosion region in the Cr base layer mirror, suggesting attack of the silver directly below the central defect (Figure 34). Ultimately, the $NiCrN_x$ adhesion layer is believed to enhance the stability of the Ag-SiN_x interface in the Cr base layer mirror, such that the corrosion reaction is limited there. Rather, corrosive species attack the silver, reaching the lower Cr-Ag interface, where the circular corrosion regions preferentially develop.

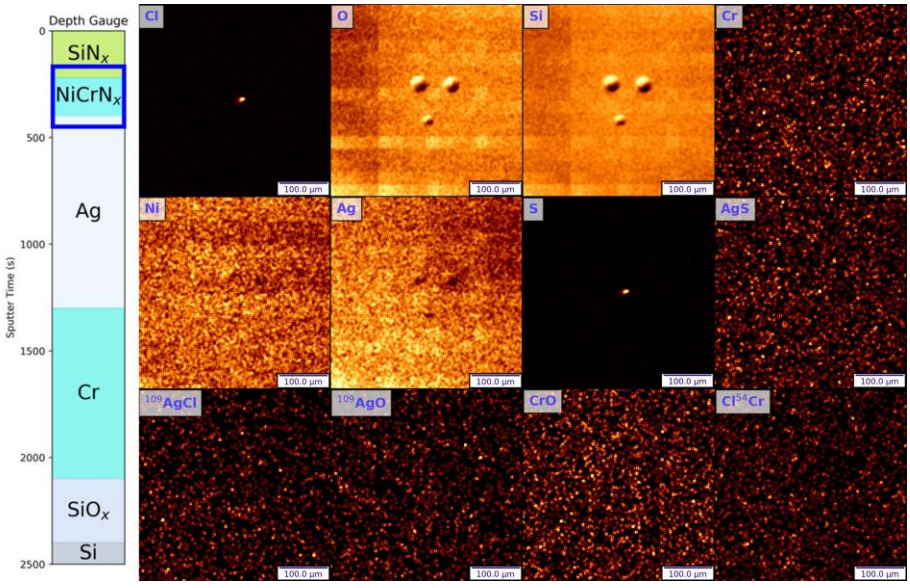

Figure 37. ToF-SIMS depth profile maps at the Ag–$NiCrN_x$-SiN_x interface of a circular corrosion region on the Cr base layer mirror.

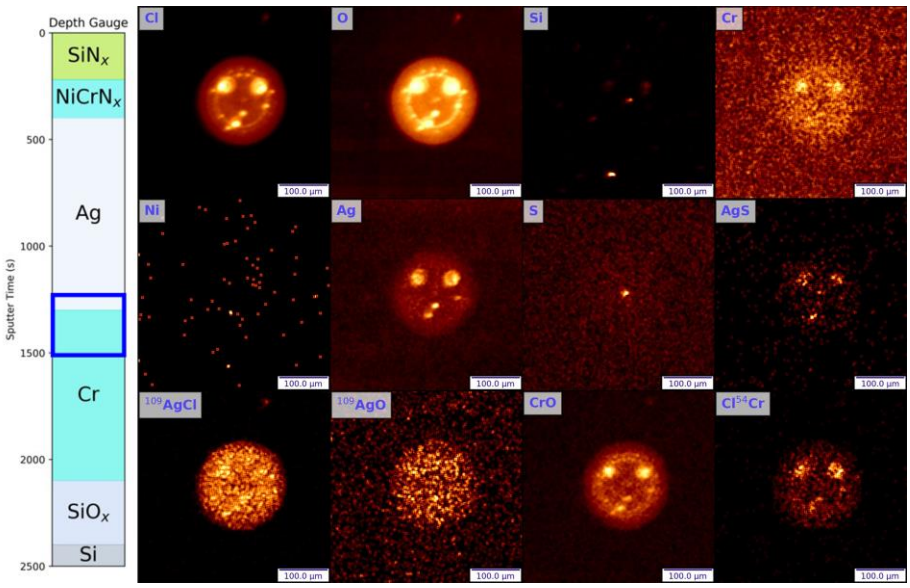

Figure 38. ToF-SIMS depth profile maps at the Cr-Ag interface of a circular corrosion region on the Cr base layer mirror.

The ToF-SIMS data provide insight into the electrochemical mechanism of corrosion associated with the silver-chromium interfaces. While silver chloride and silver oxide are possible corrosion products during any silver corrosion process, the susceptibility of chromium to corrosive attack by chlorine and oxygen is likely a driving force for the growth of the circular corrosion regions at the Ag-Cr interfaces. The standard Gibbs free energy of formation of chromium oxide and chromium chlorides have the highest negative values of the oxides and chlorides formed with chromium, nickel, and silver (Table 2) [80]. Based on these data, a more reactive behavior is expected for chromium, followed by nickel, and then silver. As the corrosive species enter the coatings through small defects in the dielectric protective layer, oxidation and chloridation of the silver-chromium interfaces occur. This results in the circular corrosion regions forming along the silver-dielectric interface in the CrN_x adhesion layer mirror but along the silver-base layer interface in the Cr base layer mirror. Thus, the mechanisms by which these corrosion features form are due, in part, to compositional effects at the silver interfaces.

Table 2. Standard Gibbs Free Energy of Formation at 25°C of Possible Corrosion Products

Compound	ΔG_f^0 (kJ/mol)
AgCl	-110
$NiCl_2$	-259
$CrCl_2$	-356
$CrCl_3$	-486
Ag_2O	-11.2
NiO	-212
Ni_2O_3	--
Cr_2O_3	-1058
Ag_2S	-41.7
NiS	-79.5
Ni_3S_2	-197
Cr_2S_3	--

4.4 Conclusions

Corrosion features throughout MFG exposure of two model silver mirrors were studied to investigate how compositional effects within the layers on either side of the silver layer influence the mechanisms of corrosion feature development and growth. It was shown that corrosion features originate at small defects in the protective dielectric layer and grow laterally along various layer interfaces, only sometimes resulting in significant layer disruption. Initial corrosion feature development occurs at pre-existing coating "spit" defects in the SiN_x layer, as the thickness of the protective layer is likely inadequate beneath these defects.

Subsequently, the growth of the corrosion features is highly dependent on the composition of the layers on either side of the silver layer. In the CrN_x adhesion layer mirror, the CrN_x adhesion layer allows the corrosion reaction to proceed along the silver-dielectric interface. This leads to the growth of large circular corrosion regions that do not significantly disrupt the layered structure of the coating, thus maintaining its optical performance. In the Cr base layer mirror, the addition

of nickel in the $NiCrN_x$ adhesion layer prevents the corrosion reaction from proceeding along the silver-dielectric interface, likely due to improved stability associated with the nickel-silver interaction there. Rather, the silver underneath the central defect is attacked, opening a channel for corrosive species to reach the base layer below the silver. As a result, the material at the lower silver interface encounters a larger driving force to react, and the circular corrosion regions form as the corrosion reaction proceeds along the lower silver-chromium interface. This leads to reduced adhesion at this interface and delamination of the silver from the chromium below, which reduces the optical performance of this mirror. The differences in morphology and properties associated with the blisters on the Cr base layer mirror are a result of the different vertical location of the Ag-Cr interface in the layered structure. In both mirrors, similar circular corrosion regions form only at the silver-chromium interfaces, indicating that the corrosion mechanism is similar and largely dependent on these Ag-Cr interfaces.

In contrast, from Chapter 3, mirrors with only NiCr-based layers adjacent to the silver experience limited growth of circular corrosion regions at the silver interfaces, but extensive corrosive attack of the silver layer itself. This disrupts the layered structure of the mirror and increases its scatter, suggesting that a CrN_x adhesion layer may be better than a $NiCrN_x$ one in terms of preserving the mirror's optical properties over time as corrosion features grow. However, as the corrosion features develop along the Ag–CrN_x-SiN_x interface, they are likely reducing the adhesion and stability of the interface, which could lead to removal of the protective layer if the mirror were disturbed during operations, such as washing or inspection. This will be explored in the following chapter.

In summary, silver mirrors with one Cr-based layer on either side of the silver experience substantial interfacial corrosion along the silver-chromium interface, regardless of where this

interface is located within the layered structure of the mirror. The Ag-Cr interfaces are preferentially attacked by the oxidation and chloridation of both silver and chromium. The thermodynamic stability of the chromium corrosion products is a possible driving force for the corrosion reaction to proceed preferentially along these interfaces. Though it's also possible that the different NiCr- and Cr-based layers are affecting the electrochemical potential at the top of the silver layer to change how the corrosion process evolves. Ultimately, the growth of the corrosion features and the mechanisms of corrosion depend on the layers on both sides of the silver, not just the layer above.

Chapter 5. Influence of Environmental Variables on Corrosion Behavior

5.1 Introduction

Atmospheric corrosion is complex due to the large number of natural variables in the environment. Determining the influence of each of these contributing factors is crucial to understanding the underlying causes of corrosion and degradation in these silver mirrors. Mixed flowing gas exposure utilizes the synergistic effects of multiple atmospheric pollutants in combination with humidity to accelerate corrosion [16]. The MFG test was designed to simulate the kinetics and degradation mechanisms of real-world corrosion in order to evaluate the behavior of materials in an accelerated time frame. The standard MFG exposure consists of specific concentrations of Cl_2, H_2S, and NO_2, in purified air at increased relative humidity and temperature. Only the most durable silver mirrors can survive extended exposure to these environments.

By utilizing multiple atmospheric pollutants to accelerate corrosion, MFG exposure complicates interpretation of the controlling factors in the mirror corrosion process. This chapter assesses the underlying causes of corrosion and degradation during environmental exposure of Gemini-style protected silver mirrors, specifically to investigate the relative importance of the environmental variables. To isolate the effects of the atmospheric pollutants, single flowing gas (FG) testing was used in which a single atmospheric pollutant was combined with the humidity and temperature levels from the MFG environment to investigate the corrosion process: Cl_2 FG exposure, H_2S FG exposure, and NO_2 FG exposure. These single FG exposures were compared to standard MFG exposure, salt fog exposure, and long-term exposure to investigate the corrosion mechanisms and behavior of three model mirror coatings.

5.2 Experimental Methods

5.2.1 Deposition Processes

The deposition of protected silver mirrors by plasma beam sputtering was described in Chapter 3.

5.2.2 Silver Mirror Designs

Several model mirror coatings were deposited in which the composition of the base layer below the silver and the adhesion layer above the silver were varied (Figure 39). The mirror layers were designed to investigate the different corrosion mechanisms that occur at the Ag-Cr and Ag-NiCr interfaces with respect to their location within the layered structure of the mirrors. As described previously, the CrN_x adhesion layer mirror has a NiCr base layer and a CrN_x adhesion layer. The Cr base layer mirror has a Cr base layer and a $NiCrN_x$ adhesion layer. The $NiCrN_x$ adhesion layer mirror has a NiCr base layer and a $NiCrN_x$ adhesion layer. The other layers, Ag and SiN_x, are the same in each of the three mirrors. By changing the location of the nickel-based layers within the mirror stack, this study will further investigate how nickel contributes to the interfacial stability previously observed.

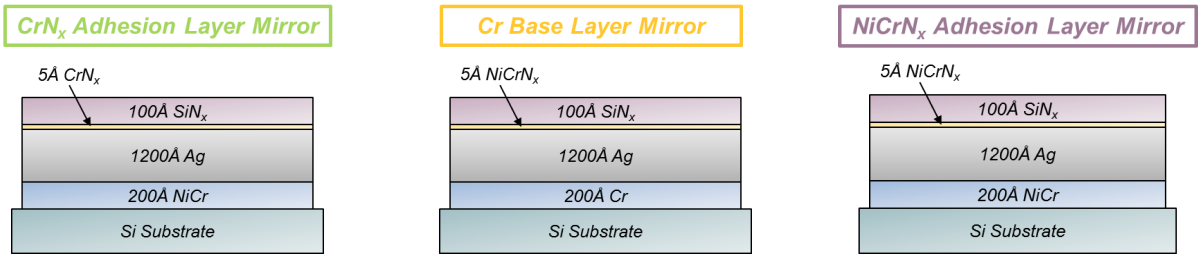

Figure 39. CrN_x adhesion layer mirror (left), Cr base layer mirror (center), and $NiCrN_x$ adhesion layer mirror (right) designs deposited for this study.

All the samples for each type of mirror design were deposited in the same coating run. This allowed direct comparison between the different environmental exposures. In addition, the three mirror designs were deposited in three sequential coating runs to ensure that the silver and SiN_x layers were consistent. All samples of each mirror type were stored in individual polypropylene sample holders after deposition and before testing. The interlocking sample holders significantly reduced air flow at the sample surface but were not completely air-tight. The samples were stored in a cleanroom environment for up to one year.

5.2.3 Accelerated Environmental Exposure

5.2.3.1 Mixed Flowing Gas (MFG) Exposure

The durability and corrosion behavior of the mirrors were first evaluated by MFG exposure, as described previously. This accelerated environmental exposure test was designed to evaluate the behavior of materials in an accelerated time frame by utilizing the synergistic effects of multiple atmospheric pollutants in combination with humidity to accelerate corrosion [16]. The Class II MFG exposure utilizes specific concentrations of three air pollutants, 10 ppb Cl_2, 10 ppb H_2S, and 200 ppb NO_2, in purified air at 70% RH and 30°C. Recently, Chu et al. [67] has shown that these standard Class II MFG conditions may be too harsh for protected silver mirror designs in that they cause extensive degradation that does not correlate with long-term behavior. As a result, the air pollutant concentrations were lowered while the RH and temperature settings were maintained. This reduced MFG environment consisted of 60% of the Cl_2, H_2S, and NO_2 gas concentrations from the Class II environment in purified air at 70% RH and 30°C (Table 3). It should be noted that the Cl_2 concentration fluctuated throughout testing; Cl_2 adsorption onto internal surfaces of the MFG chamber has been reported by Abbott [16]. As such, the nominal

concentrations are provided in Table 3. The mirrors were tested for a total of 10 days in 2, 3, or 5-day increments.

5.2.3.2 Single Flowing Gas (FG) Exposure

By design, the MFG exposure test utilizes multiple atmospheric pollutants to accelerate corrosion. This complicates interpretation of the controlling factors in the mirror corrosion process. To better understand the relative importance of the environmental variables, the MFG exposure test was modified. The goal was to isolate the effects of the three air pollutants in the MFG environment. These single flowing gas (FG) exposures were designed to be performed with only one air pollutant, either Cl_2, H_2S, or NO_2, in purified air at 70% RH and 30°C (Table 3). However, after testing, it was found that residual chlorine was present in the MFG system and interfered with the results of the H_2S FG and NO_2 FG exposures; this will be discussed in detail in the subsequent sections.

Table 3. Nominal MFG and Single FG Test Conditions Based on Class II Environments

Method	Cl_2 (ppb)	H_2S (ppb)	NO_2 (ppb)	Temperature (°C)	Relative Humidity (%)
MFG (60%)	6	6	120	30	70
Cl_2 FG	10	--	--	30	70
H_2S FG	--*	10	--	30	70
NO_2 FG	--*	--	200	30	70

*Residual Cl_2 during testing

During all MFG and single FG exposures, 0.5-inch square copper coupons were used to verify the reactivity of the corrosive gas environments by measuring the weight gain before and after MFG exposure per ASTM B810-01a [81]. The average copper coupon weight gain measurement enables quantitative comparison of corrosivity between the MFG and single FG exposure conditions.

5.2.3.3 Salt Fog Exposure

Mirror durability and corrosion behavior were also evaluated by salt fog exposure. The standard ASTM B117 salt fog exposure test is often used to assess the long-term durability of protected silver mirrors [24, 31, 82]. The salt fog exposure was conducted in a BEMCO P700XL salt-spray chamber maintained at 95°F with a 5% NaCl solution per ASTM B117. The mirrors were tested for a total of 8 hours, in 2-hour increments. Many silver mirrors degrade significantly under these conditions [24, 31].

5.2.4 Characterization Techniques

As described previously, the mirrors were characterized throughout accelerated testing. Reflectance and scatter were measured at the mirror center; degradation of the surface was imaged under dark field conditions; corrosion features were imaged under DIC mode. Following exposures, chemical analyses were performed by ToF-SIMS depth profiles.

5.3 Results & Discussion

5.3.1 MFG and Single FG Exposures

During the MFG and single FG exposures, copper coupons were exposed concurrently with the silver mirrors to provide information on the corrosivity of the environments. The average copper coupon weight gains during the four exposure conditions are shown in Table 4. Even at the reduced gas concentrations utilized during the MFG conditions (60% Class II), the copper coupon weight gain is significantly higher than the weight gain observed during any of the single

FG exposures. This is believed to be due to the synergistic effects of multiple atmospheric pollutants that accelerates copper corrosion in the MFG environment [16].

Table 4. Average Copper Coupon Weight Gain during MFG and Single FG Exposures

Method	**Weight Gain (mg/cm^2-day)**
MFG (60%)	5.6
Cl_2 FG	2.6
H_2S FG	3.5
NO_2 FG	3.8

5.3.2 Protected Silver Mirrors

All three model mirror coatings show very good durability after exposure to accelerated testing environments. After 10 days of MFG exposure, only small losses in reflectance and moderate increases in scatter are apparent (Figure 40). The larger increase in scatter of the Cr base layer mirror is due to the topographical nature of delaminations associated with corrosion features on this mirror. The change in reflectance of the CrN_x adhesion layer mirror is also associated with the development of corrosion features, in this case, at the Ag–CrN_x-SiN_x interface. As described in previous chapters, corrosion feature development and growth depend on the layers on either side of the silver layer. Mirrors with one Cr-based layer adjacent to the silver exhibit characteristic circular corrosion regions, with attack occurring at the Ag-Cr interface. Mirrors with only NiCr-based layers adjacent to the silver exhibit characteristic corrosion nodules due to more extensive attack of the silver layer itself. These differences influence the optical performance of the mirrors.

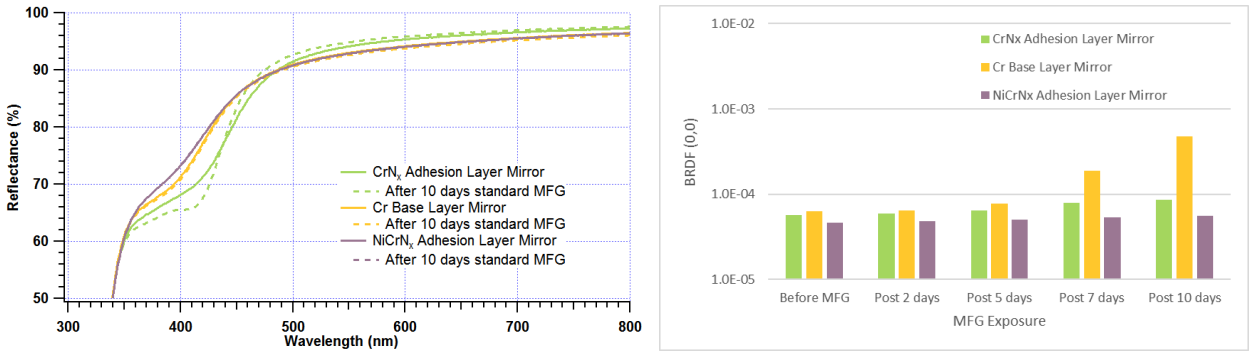

Figure 40. Reflectance spectra (left) and scatter (right) of three mirror coatings during 10 days MFG exposure.

5.3.3 Corrosion Features on the CrN_x Adhesion Layer Mirror

While the optical performance of the CrN_x adhesion layer mirror was still good after MFG exposure, the dark field image (Figure 41) shows degradation around the edge of the coating, as well as many small scattered corrosion features across the entire surface of the mirror. These corrosion features are characteristic of the CrN_x adhesion layer mirror. The large circular corrosion regions grow radially out from central defects, increasing in size with exposure, but not significantly disrupting the layered structure of the coating.

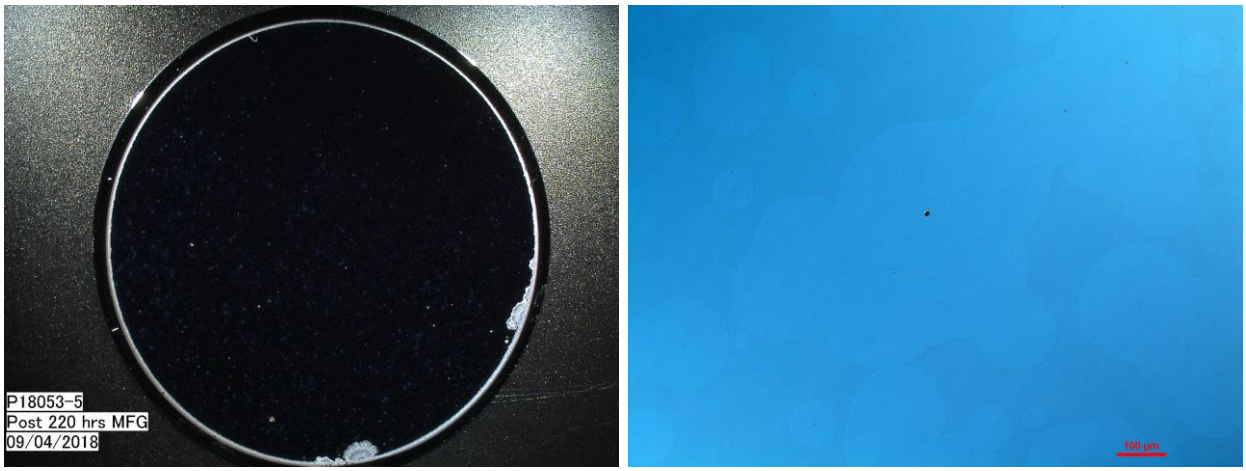

Figure 41. Dark field image (left) of a CrN_x adhesion layer mirror with corresponding optical micrograph (right) of corrosion features after 10 days MFG exposure.

For comparison, dark field images and optical micrographs of the CrN_x adhesion layer mirror after the single FG exposures are shown in Figure 42. Similar corrosion is evident around the coating edges as well as with the corrosion features across the surfaces of each mirror. The optical micrographs show very similar corrosion features for each of the single FG conditions, as well as for the MFG exposure. In all four exposures, the corrosion features are large circular corrosion regions with low contrast between the corroded and uncorroded portions of the mirror. The similar morphologies suggest that similar corrosion reactions are occurring during the four exposure conditions. The extent of corrosion, however, is different. As expected, the MFG exposure results in slightly larger circular corrosion regions, on average, corresponding to the slightly larger loss in reflectance (Figure 43). This correlates with the copper coupon measurements that showed notably larger weight gain during the MFG exposure compared to any of the single FG exposures (Table 3). This is believed to be due to the synergistic effects of multiple atmospheric pollutants designed to accelerate corrosion, characteristic of the MFG environment. However, the differences in the optical properties of the mirrors were small; no substantial difference in scatter was measured. While the corrosion features cover a significant portion of the mirror surfaces, the layered structure is largely preserved, thus maintaining the optical performance.

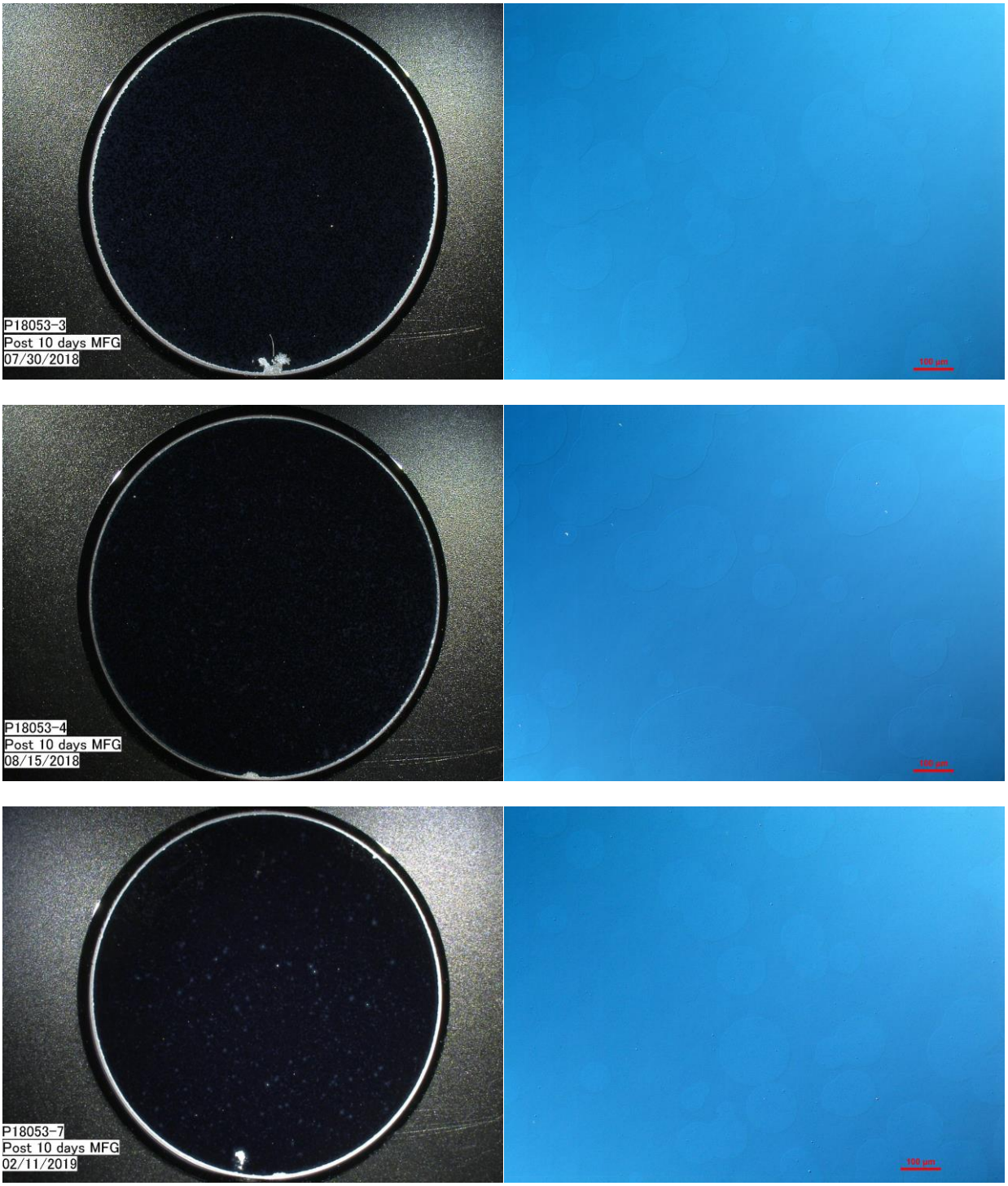

Figure 42. Dark field images of CrN_x adhesion layer mirrors with corresponding optical micrographs of corrosion features after 10 days single FG exposures. (Top) Cl_2 FG, (center) H_2S FG, (bottom) NO_2 FG exposures.

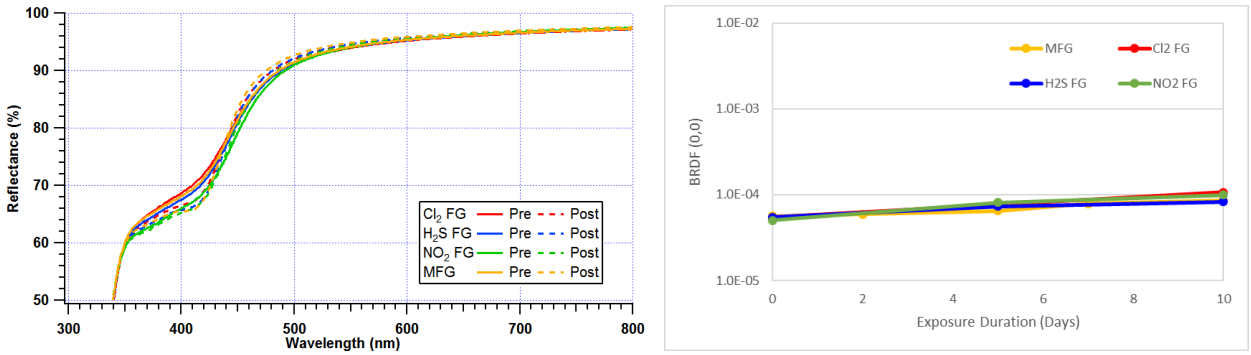

Figure 43. Reflectance spectra (left) and scatter (right) of CrN_x adhesion layer mirrors during MFG and single FG exposures.

The four mirrors show similar number of corrosion features, suggesting that all four of the exposure conditions are harsh enough to cause degradation through the pre-existing coating defects in the SiN_x layer, which allow pathways for corrosive species to enter the coating layers. The similar number and morphology of the corrosion features during the four exposures provide insight into the mechanism of corrosion in the CrN_x adhesion layer mirror. Previously, we showed that oxidation and chloridation of both the silver and chromium at the Ag–CrN_x-SiN_x adhesion interface influenced the development of the circular corrosion regions; ToF-SIMS depth profile maps at the silver-dielectric interface showed chemical signatures of chlorine and oxygen enrichment within the circular corrosion regions on CrN_x adhesion layer mirrors exposed to the standard MFG environment (Figure 35). Similar ToF-SIMS maps for the single FG exposures are shown in Figure 44. Oxygen and chlorine enrichment are again apparent, further suggesting that these species play an important role in the corrosion process.

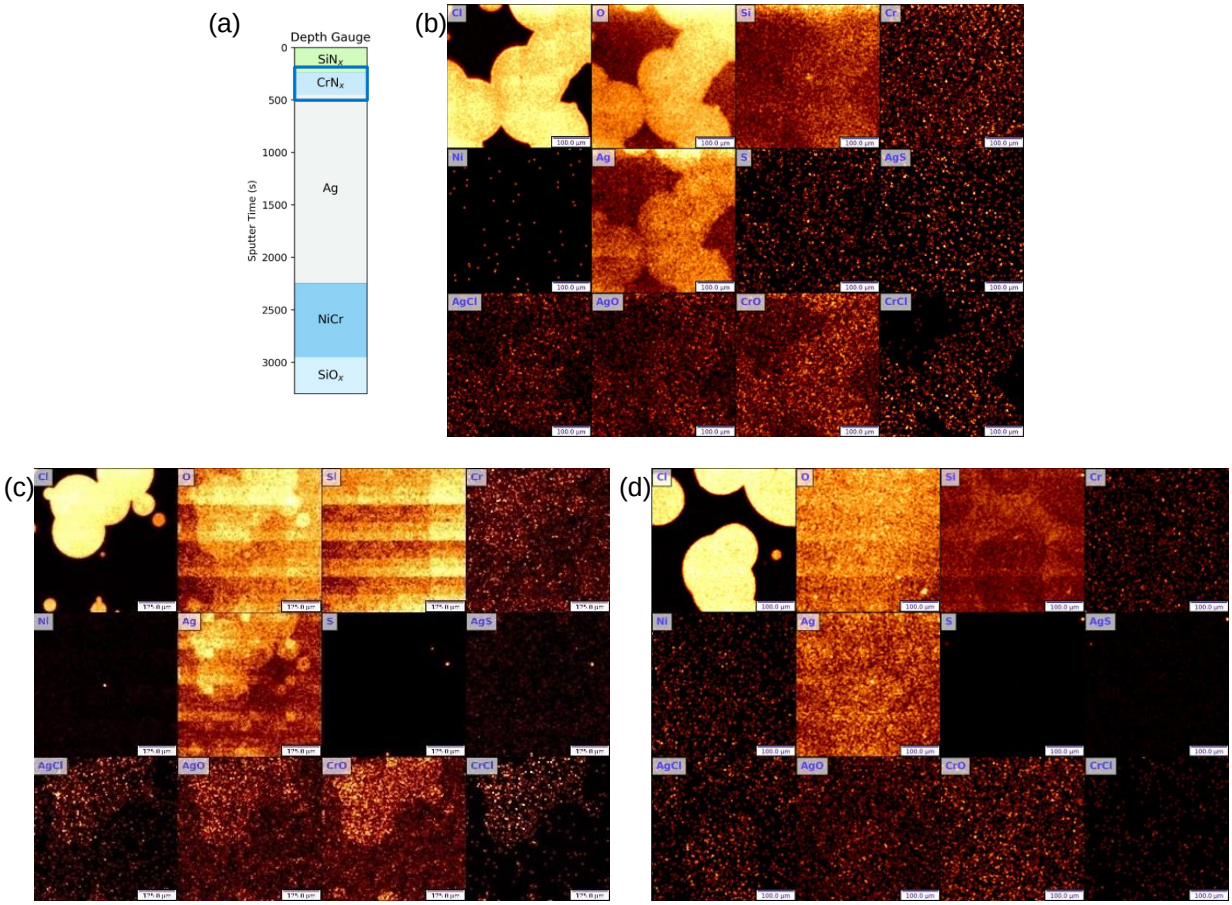

Figure 44. ToF-SIMS depth profile maps at the Ag–CrN_x-SiN_x interface of circular corrosion regions on the CrN_x adhesion layer mirrors after 10 days of single FG exposure: (b) Cl_2 FG, (c) H_2S FG, (d) NO_2 FG. (a) Depth gauge showing vertical location within layered structure of coating.

While the single FG experiments were designed to limit exposure to only one atmospheric pollutant at a time, the ToF-SIMS data suggest that a small amount of residual chlorine in the MFG system was present in all the environments at concentrations high enough to promote corrosion. The similar morphologies of the corrosion features and the extent of corrosion on all four mirrors further supports this conclusion. It was not possible to monitor the chlorine concentration during exposures due to interference in the chlorine analyzer with humidity and the other flowing gases. After residual chlorine was suspected, measurements were performed under a variety of conditions to investigate the residual concentration. Purging the system with dry air reduced, but did not

eliminate, the residual chlorine. Approximately 3 ppb residual chlorine was measured under conditions similar to those before and during the H_2S FG and NO_2 FG exposures.

The similar sizes, number density, and chemical signatures of the circular corrosion regions in the Cl_2 FG exposure compared to the H_2S FG and NO_2 FG exposures suggests that above a critical low level of chlorine, additional chlorine in the environment may not further accelerate the corrosion process, i.e. the corrosion process saturates. The growth of the corrosion features, therefore, may be limited by the transport of corrosive reactants and products between the central defects and the growing radii of the circular corrosion regions.

While the residual chlorine complicates interpretation of the single FG results, the relative humidity and temperature were kept constant in all MFG and single FG exposures: 70% RH and 30°C. The role of humidity therefore must be considered as a possible controlling factor in the development of the circular corrosion regions. On bare surfaces, the atmospheric corrosion process begins with a water layer adsorbing on the surface; the thickness of the water layer is a function of temperature, humidity, and surface energy [83 – 86]. Pollutant gases dissolve into the water layer, along with any salts present on the surface. As the local ion concentration increases, corrosion processes occur. At increased relative humidity, such as the 70% RH used during testing, water adsorption is expected to be a minimum of five monolayers and to increase dramatically with increasing water vapor pressure [83 – 86]. Previous researchers have reported an increase in size and number density of defect sites on various protected silver mirrors with increasing humidity and temperature [10]. Therefore, adsorbed moisture on the mirror surface is believed to provide transport of the corrosive species from the central defects to the growing circular corrosion regions. The dissolution of Ag and Cr at the Ag–CrN_x-SiN_x interface then occurs due to oxidation and

chloridation. The Ag and Cr dissolution likely reduces adhesion at the interface, allowing the circular corrosion regions to develop. This will be discussed in more detail in the next section.

While the CrN_x adhesion layer mirror performed well in the MFG and single FG environments, optical measurements and dark field images during salt fog exposure show much more extensive degradation (Figure 45 and Figure 46, respectively). A significant increase in scatter is evident, along with a notable loss in reflectance above 500 nm. It is worth noting that the scatter measurements and the oblique lighting technique used in the dark field images are very sensitive to coating disruptions caused by the corrosion features. The broadband reflectance measurement, on the other hand, requires extensive degradation to measure significant losses. The degradation after 8 hours of salt fog exposure corresponds to only a 3% loss in reflectance at 600 nm. While the extensive degradation on the CrN_x adhesion layer mirror suggests that the salt fog environment is more severe than the MFG environment, insight into the mechanisms of corrosion and degradation will show that is not necessarily the case.

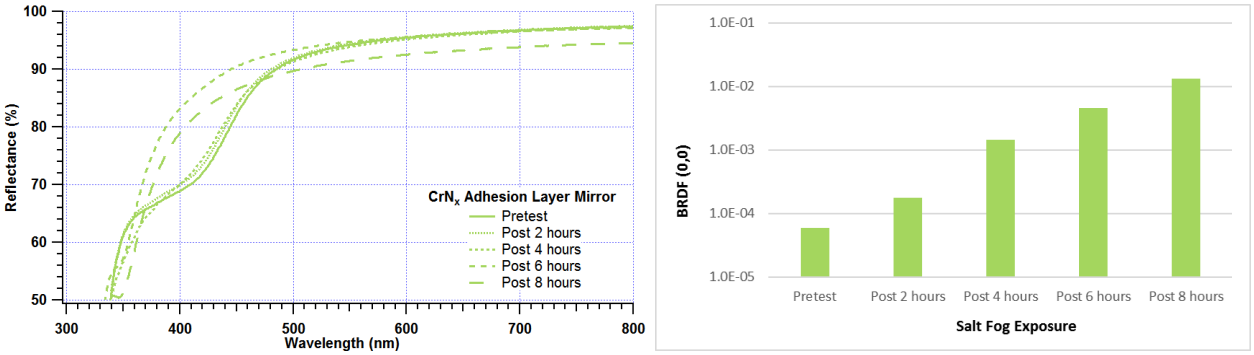

Figure 45. Reflectance spectra (left) and scatter (right) of a CrN_x adhesion layer mirror during salt fog exposure.

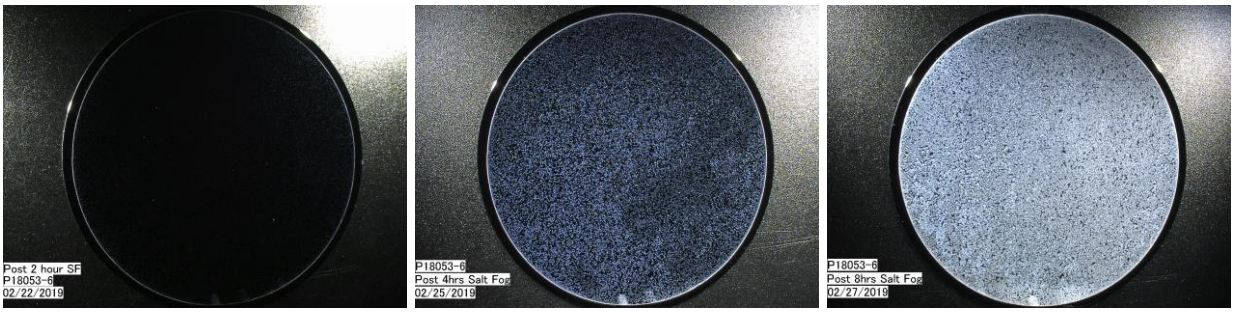

Figure 46. Dark field images of a CrN_x adhesion layer mirror during salt fog exposure. (Left) 2 hr exposure, (center) 4 hr exposure, (right) 8 hr exposure.

Optical micrographs of the corrosion features on the CrN_x adhesion layer mirror during salt fog exposure are shown in Figure 47. After two hours of exposure, small circular corrosion regions are evident on the mirror, similar to those observed in the MFG and single FG environments. However, the SiN_x protective layer appears to be partially removed at many of these features. This is believed to be due to gentle washing of the mirror after the salt fog exposure to remove salt from the surface in order to perform the optical measurements [82]. Removing the SiN_x protective layer exposes the silver directly to the harsh salt fog environment upon subsequent exposure, thereby allowing extensive attack of the silver itself. The small crystallites on the surface after 8 hours of salt fog exposure are largely silver, likely photo-reduced from AgCl [17, 87].

The removal of the SiN_x protective layer is also evident in the reflectance measurements; after 6 hours of salt fog exposure, the reflectance below 500 nm has recovered to levels above the pretest reflectance. In the pretest spectrum, the absorption shoulder centered at 370 nm is due to surface plasmon resonance (SPR) at the interface between the rough silver surface and the dielectric layer above it [20, 34 – 38]. Once the SiN_x is removed from washing, the SPR absorption feature is significantly reduced as the reflectance of the bare silver is measured directly. After additional salt fog exposure, the silver is more extensively attacked, and the broadband reflectance begins to drop. While the washing process is designed to be gentle, the relatively easy removal of

the SiN_x layer suggests that adhesion at the silver-dielectric interface has been reduced considerably during the corrosion process. The SiN_x layer on a freshly-deposited silver mirror withstands the washing process with no removal.

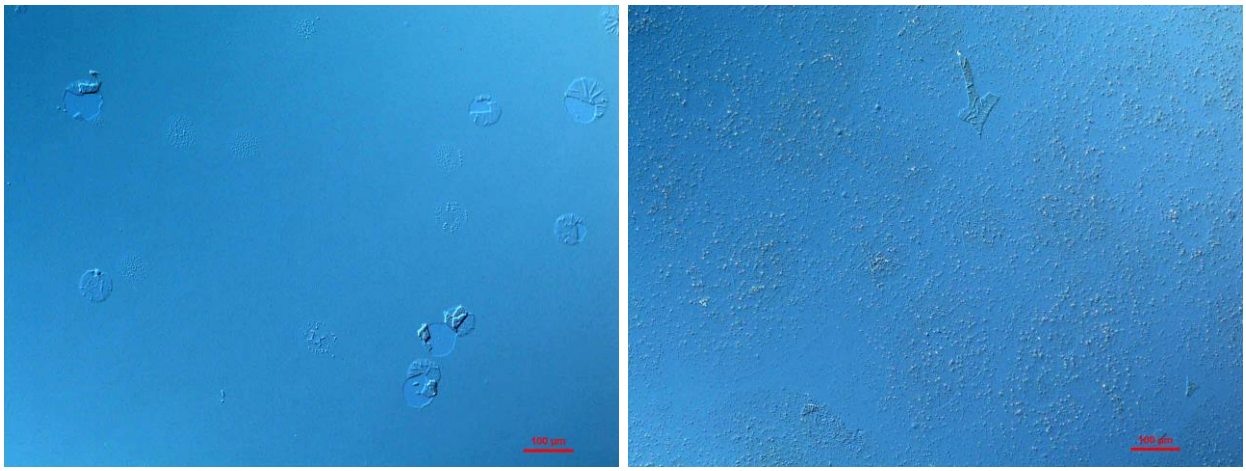

Figure 47. Optical micrographs of corrosion features on a CrN_x adhesion layer mirror after (left) 2 hr and (right) 8 hr salt fog exposure.

The mechanism of corrosion in the CrN_x adhesion layer mirror during salt fog exposure, is therefore believed to be similar to that observed during MFG and single FG exposures. Corrosive species enter the coating through pre-existing coating defects in the SiN_x layer and proceed along the Ag–CrN_x-SiN_x interface, creating similar circular corrosion regions. The interfacial attack reduces adhesion of the dielectric to the silver, such that washing the mirror removes the SiN_x protective layer and exposes the silver directly to the salt fog environment. The salt fog environment is not necessarily harsher than the MFG environment; the additional washing causes the more extensive degradation. Understanding the testing environments and procedures is, therefore, critical to appropriately applying accelerated testing.

It has been reported that bulk silver does not experience extensive corrosion or degradation during salt fog exposure [13, 88], whereas the exposed silver on the CrN_x adhesion layer mirror experiences notable corrosion and degradation. While the presence of the CrN_x adhesion layer

may affect the electrochemical behavior of the exposed silver, bare silver coatings have previously been shown to be susceptible to corrosive attack during salt fog exposure in our laboratory [31]. The presence of ozone in the room air supply to the salt fog chamber is believed to act as an oxidizer to enable corrosion during our salt fog exposures [12, 13].

5.3.4 Corrosion Features on the Cr Base Layer Mirror

The Cr base layer mirror after MFG exposure also shows degradation around the edge of the coating, as well as many small scattered corrosion features across the surface of the mirror (Figure 48). The corrosion features are characteristic of the Cr base layer mirror. The large circular corrosion regions grow radially out from central defects, increasing in size with exposure, and developing additional features whose topography indicate delamination at the Cr-Ag interface. The number of circular corrosion regions is significantly fewer than the number observed on the CrN_x adhesion layer mirror. On the Cr base layer mirror, the corrosive species must penetrate through the silver layer to reach the Cr-Ag interface; the development of the circular corrosion regions, therefore, may be slower or otherwise limited. This is likely associated with the stability of the $NiCrN_x$ adhesion layer, whose role will be discussed in the following section.

Figure 48. Dark field image of a Cr base layer mirror with corresponding optical micrograph of corrosion features after 10 days MFG exposure.

For comparison, dark field images and optical micrographs of the Cr base layer mirror after the single FG exposures (Figure 49) show similar edge corrosion and scattered corrosion features. The circular corrosion regions are similar in morphology, size, and number in each of the single FG exposures, as well as in the MFG exposure, suggesting that similar corrosion reactions are occurring in all four environments. Differences in extent of corrosion are not obvious; the circular corrosion regions are not significantly larger or further developed in any of the environments. However, the MFG exposure results in a larger increase in scatter than the single FG exposures (Figure 50), which is believed to be due to the synergistic effects of multiple atmospheric pollutants in the MFG environment.

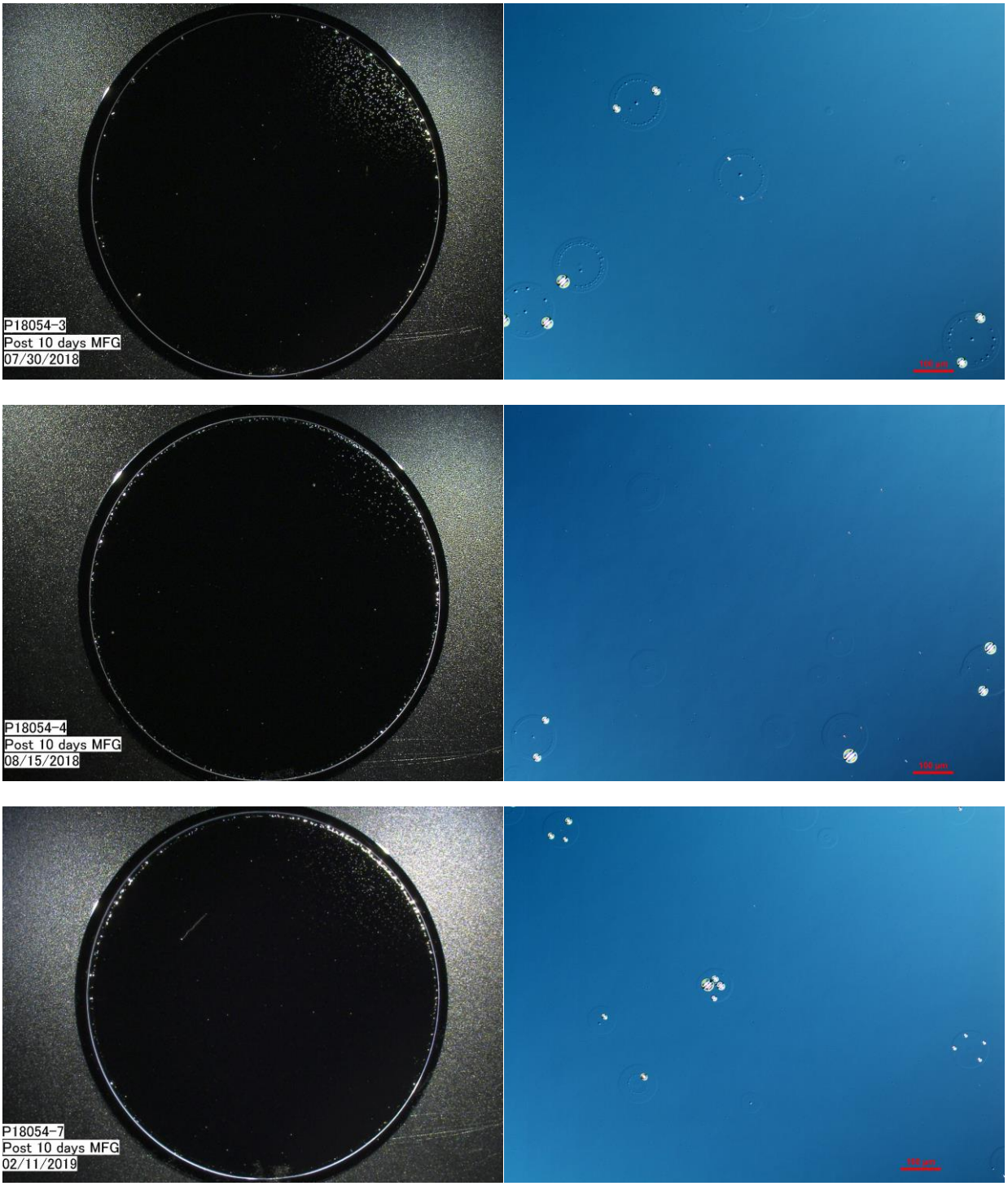

Figure 49. Dark field images of Cr base layer mirrors with corresponding optical micrographs of corrosion features after 10 days single FG exposure. (Top) Cl_2 FG, (center) H_2S FG, (bottom) NO_2 FG exposures.

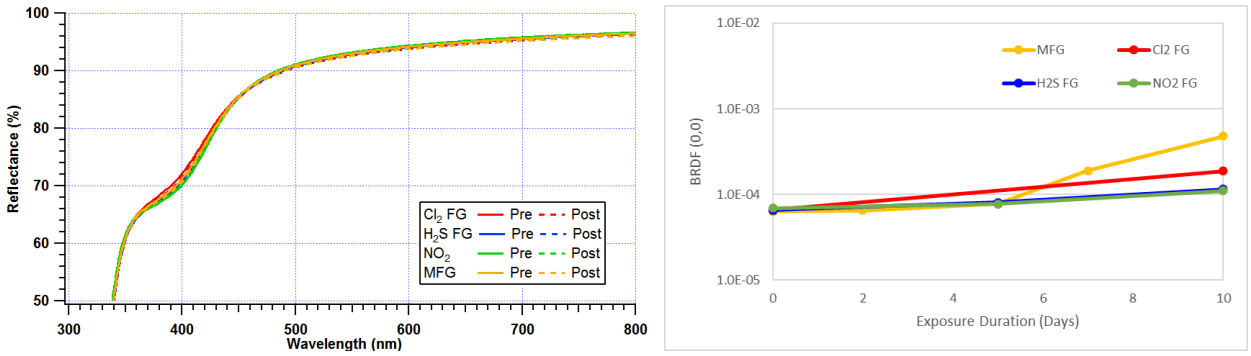

Figure 50. Reflectance spectra (left) and scatter (right) of Cr base layer mirrors during MFG and single FG exposures.

As with the CrN_x adhesion layer mirror, the similar morphology of the corrosion features during the four exposures provide insight into the mechanism of corrosion in the Cr base layer mirror. Corrosive species enter the coating through pre-existing coating defects in the SiN_x protective layer and attack the silver rather than the silver-dielectric interface due to the $NiCrN_x$ adhesion layer; upon reaching the base layer, the attack proceeds along the Cr-Ag interface. ToF-SIMS depth profile maps at the Ag-Cr interface in the Cr base layer mirrors during the single FG exposures are shown in Figure 51. As with the maps previously presented for MFG exposure (Figure 38), oxygen and chlorine enrichment are apparent within the circular corrosion regions, further suggesting these species play an important role in the corrosion process.

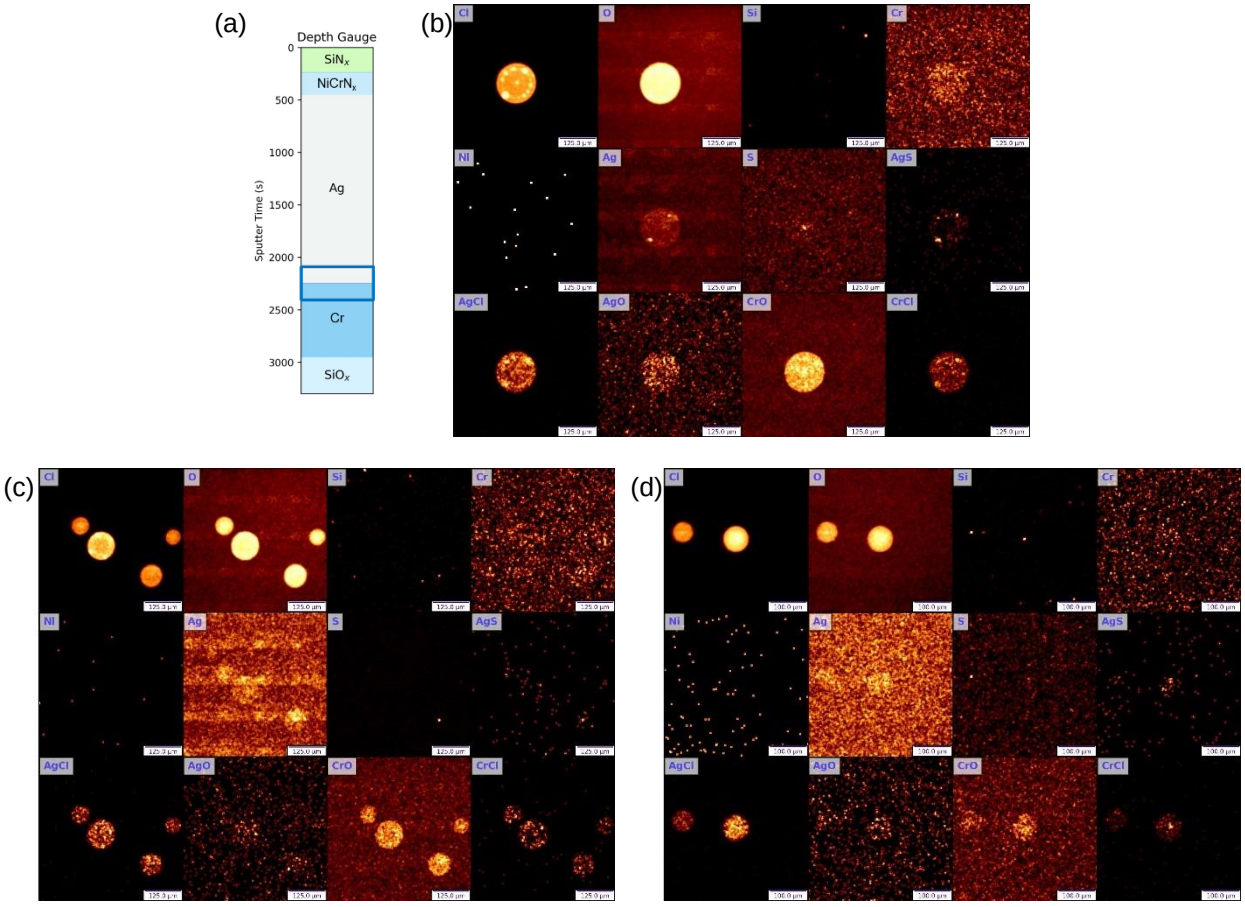

Figure 51. ToF-SIMS depth profile maps at the Cr-Ag interface of circular corrosion regions on the Cr base layer mirrors after 10 days of single FG exposure: (b) Cl_2 FG, (c) H_2S FG, (d) NO_2 FG. (a) Depth gauge showing vertical location within layered structure of coating.

As was discussed in the previous section, residual chlorine in the MFG system during the H_2S FG and NO_2 FG exposures was at sufficient concentration to promote corrosion. The similar chemical signatures from the ToF-SIMS measurements therefore suggest a low level of chlorine influences the corrosion processes at the Ag-Cr interfaces. Though, the role of water in providing a means of transport for corrosive species and dissolution mechanisms must also be considered. It's also possible that the different layers on either side of the silver layer in the CrN_x adhesion layer mirror and the Cr base layer mirror affect the electrochemical behavior of the silver to change the dissolution and corrosion behavior; this will be discussed in subsequent chapters.

The role of stress in the layered mirror structure must also be considered in relation to the corrosion mechanisms in these mirrors. In the Cr base layer mirror, delamination of the Ag from the Cr below occurs during growth of the circular corrosion regions creating voids and high-scatter features. This has been ascribed to stress in the layers relieved as delamination following reduced adhesion at the Cr-Ag interface caused by the interfacial corrosive attack [23, 75, 76]. The SiN_x is known to be highly compressive, while the Cr is strongly tensile [28, 49, 89, 90]. The stresses in the coating layers, therefore, may also play a role in the development of the circular corrosion regions themselves. Attack and dissolution of the silver and chromium reduces adhesion at the Ag-Cr interfaces, possibly allowing the stress to propagate the corrosion reaction [23, 46]; this will be discussed further in subsequent chapters. Similar behavior could also play a role in the growth of the circular corrosion regions on the CrN_x adhesion layer mirror.

While the CrN_x adhesion layer mirror performed poorly in salt fog exposure, the Cr base layer performed quite well. The dark field image after 8 hours of exposure (Figure 52) shows some corrosion around the edge and across the surface of the coating. No increase in scatter was observed, and only a very small drop in reflectance below 450 nm was measured, as the corrosion features are smaller in size and less extensively developed, with few apparent delamination blisters. The corrosion features are characteristic of the Cr base layer mirror: circular corrosion regions that grow radially in size from a central defect. The mechanism of corrosion during salt fog exposure is therefore considered to be similar to that during MFG and single FG exposures, with chlorine and moisture driving the corrosion process at the Cr-Ag interface. These corrosive species enter the coating and attack the Cr-Ag interface. As this interface is below the silver, washing the mirror after salt fog exposure does not cause the same degradation as observed with the CrN_x adhesion layer mirror. While the Cr-Ag interface also experiences reduced adhesion, the

thick, intact silver layer above it may be more resistant to the gentle washing action, thereby preserving the layered structure.

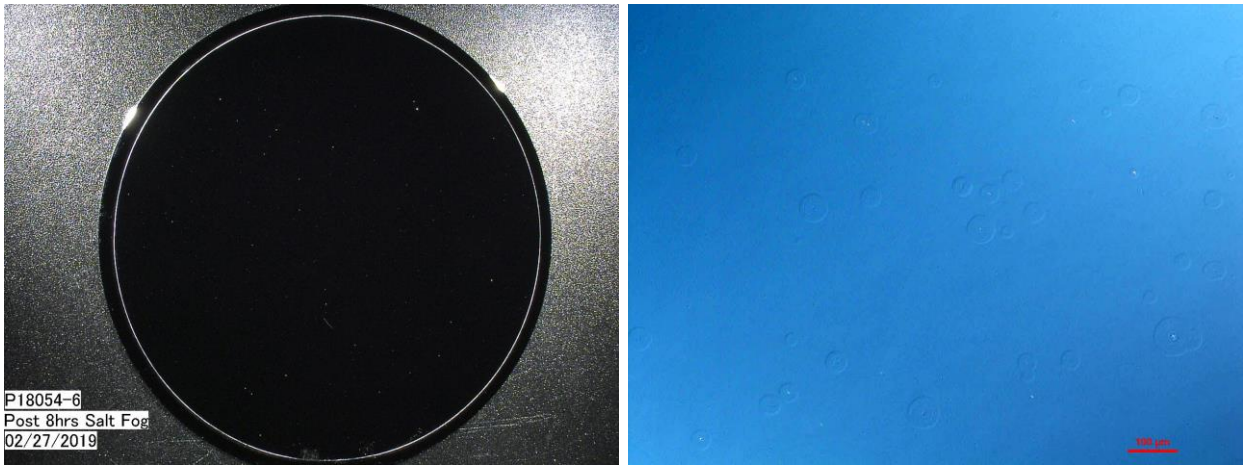

Figure 52. Dark field images of a Cr base layer mirror with corresponding optical micrograph of corrosion features after 8 hrs salt fog exposure.

During the salt fog exposure, the salt solution condenses on the surface of the mirrors, resulting in droplets of water on the mirror surfaces. There is substantially more water on the surface during salt fog exposure compared to the adsorbed water on the surfaces during MFG or single FG exposures; in addition, the concentration of dissolved chloride ions is higher in salt fog exposure. While these factors affect the extent of corrosion, they do not appear to change the mechanism of corrosion, suggesting that the corrosion process is substantially controlled by the defects in the SiN_x layer allowing corrosive species to enter the coating.

5.3.5 Corrosion Processes at NiCr-Ag Interfaces

The corrosion processes that occur in mirrors with NiCr-based layers on either side of the silver have been shown to be significantly different than those that occur in mirrors with at least one Cr-based layer adjacent to the silver. $NiCrN_x$ adhesion layer mirrors experience substantial

attack of the silver layer, resulting in characteristic corrosion nodules; the interfacial attack is significantly reduced.

While the optical performance of the $NiCrN_x$ adhesion layer mirror was very good after MFG exposure (Figure 40), the dark field image shows degradation around the edge and small scattered corrosion features across the surface (Figure 53); the corrosion features are characteristic corrosion nodules. The corrosion nodules are substantially smaller in size than the circular corrosion regions on the mirrors with a Cr-based layer adjacent to the silver; the nodules are on the order of tens of microns in diameter rather than the hundreds of microns in diameter for the circular corrosion regions. The corrosion nodules are also significantly fewer in number, suggesting that nickel may slow the corrosion process. However, the corrosion nodules do not increase substantially in radial size with exposure; rather, they appear to erupt more, which is due to the progression of the silver attack. Localized disruption to the layered structure occurs as the silver is attacked, which indicates a change in the corrosion mechanism rather than only a change in kinetics.

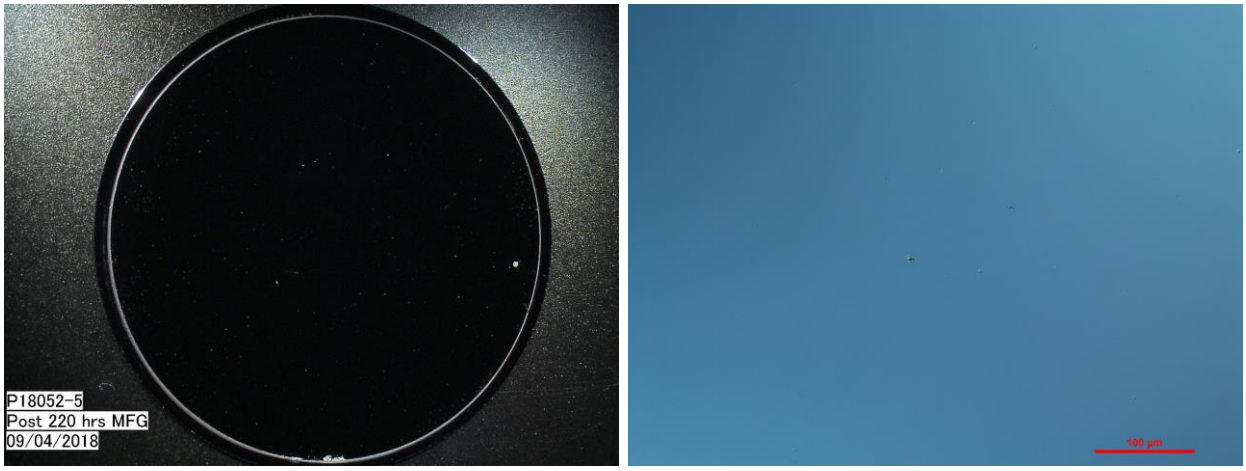

Figure 53. Dark field image of a $NiCrN_x$ adhesion layer mirror with corresponding optical micrograph of corrosion features after 10 days MFG exposure. Note scale difference from other micrographs.

For comparison, dark field images and optical micrographs of the $NiCrN_x$ adhesion layer mirror after the single FG exposures are shown in Figure 54. Similar corrosion is evident around the edge of the coating as well as the scattered features across the surface. Strikingly, the Cl_2 FG exposure shows significantly more corrosion than both the MFG and other single FG exposures; there are significantly more features and they are larger and more extensively corroded. These features correspond to the significant increase in scatter observed after Cl_2 FG exposure (Figure 55). Nonetheless, the corrosion nodules that develop during the four exposures exhibit similar morphologies, indicating that the mechanism of corrosion is similar.

The star-like corrosion nodules observed during Cl_2 FG exposure are more extensively corroded than the rounded nodules observed during the other exposures. As the attack of the silver proceeds, silver is being depleted from the silver layer and transported to the agglomerate. The star-like features likely develop as arms or dendrites growing out from the initially circular nodule as the region around the agglomerate becomes entirely depleted of silver. This may be associated with favorable crystallographic directions and the distance the silver must migrate from the intact coating to the central agglomerate.

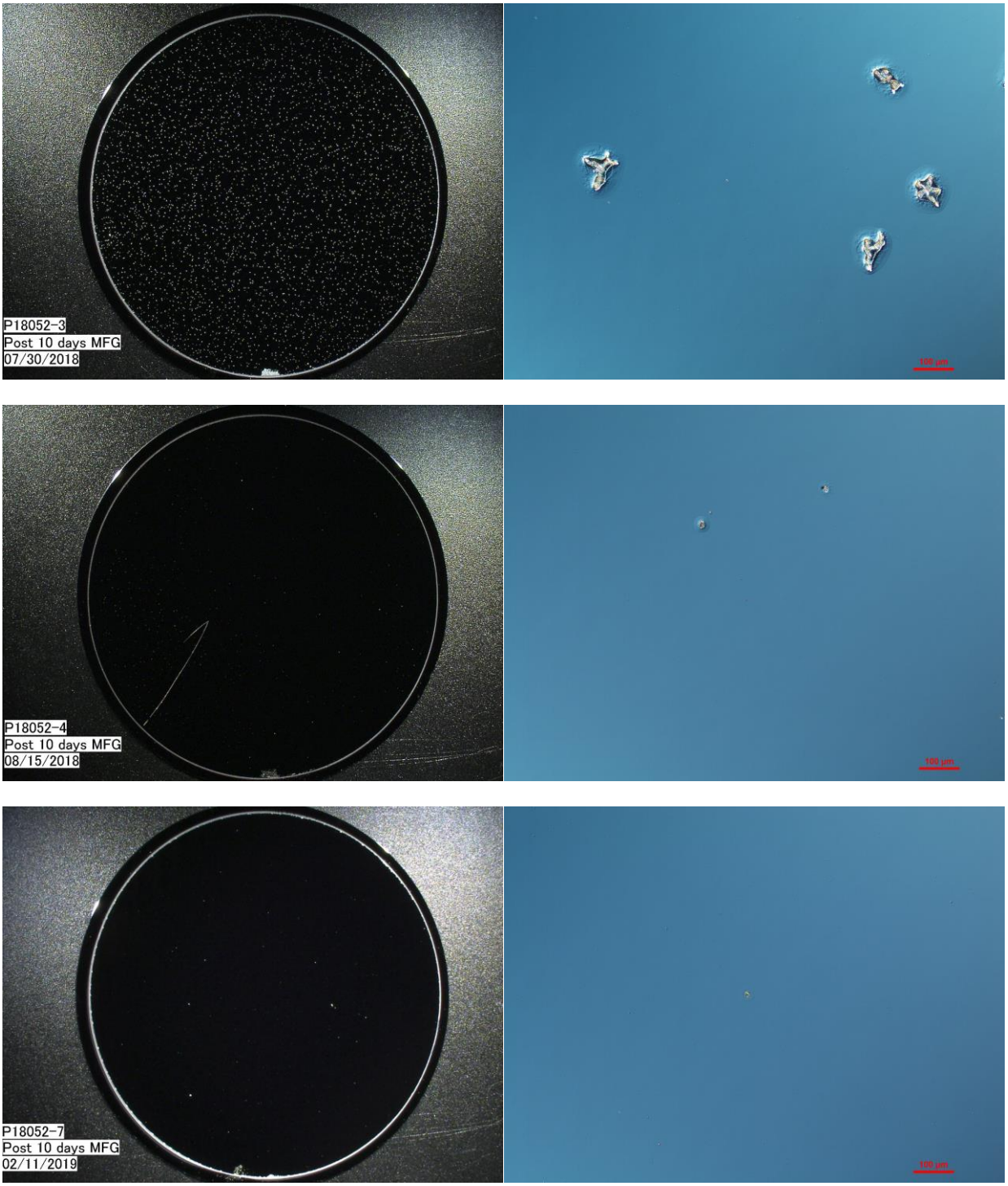

Figure 54. Dark field images of $NiCrN_x$ adhesion layer mirrors with corresponding optical micrographs of corrosion features after 10 days single FG exposure. (Top) Cl_2 FG, (center) H_2S FG, (bottom) NO_2 FG exposures.

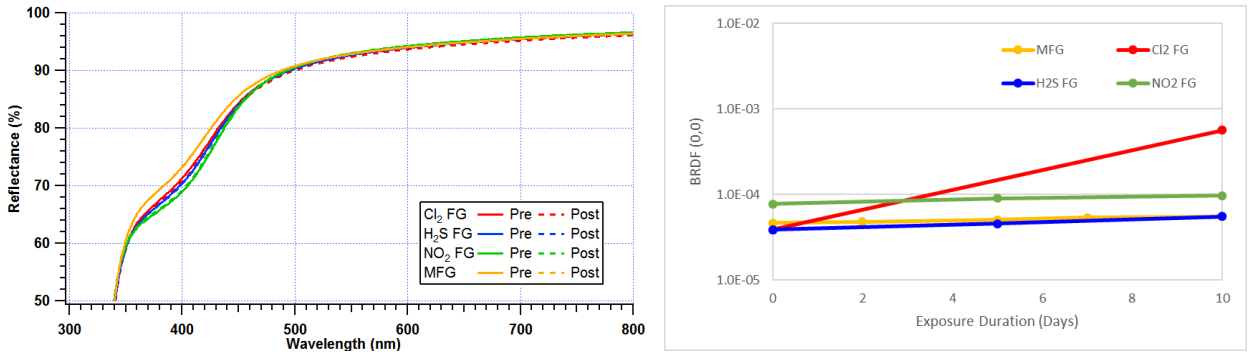

Figure 55. Reflectance spectra (left) and scatter (right) of $NiCrN_x$ adhesion layer mirrors during MFG and single FG exposures.

The more extensive corrosion during the Cl_2 FG exposure suggests that chlorine plays a critical role in the corrosion behavior of the $NiCrN_x$ adhesion layer mirrors. The addition of nickel to the layers adjacent to the silver results in substantial attack of the silver layer itself. The chloridation of Ag, whereby adsorbed water dissolves chlorine gas, which then reacts with the silver to dissolve and precipitate AgCl, is well-reported [8, 13, 91]. In addition, the partial pressure of Cl_2 has been shown to significantly increase the corrosion rate of nickel, whereas H_2S was shown to have little influence on nickel corrosion [92, 93]. The susceptibility of silver and nickel to chloridation may explain the extensive attack observed during the Cl_2 FG exposure; possible galvanic interactions between these materials will be investigated in subsequent chapters.

The $NiCrN_x$ adhesion layer mirror also performs extremely well in salt fog exposure. The dark field image shows some corrosion around the edge and scattered corrosion features across the surface; the higher resolution optical micrograph shows few, small characteristic corrosion nodules (Figure 56). The similar morphologies of the corrosion nodules indicate that similar corrosion reactions are occurring during the salt fog exposure and the MFG and single FG exposures. As corrosive species enter the coating through pre-existing defects in the SiN_x layer, attack of the silver occurs as the nickel in the $NiCrN_x$ adhesion layer limits the interfacial attack at the silver-dielectric interface.

Figure 56. Dark field images of a $NiCrN_x$ adhesion layer mirror with corresponding optical micrograph of corrosion features after 8 hrs salt fog exposure.

As mentioned in the previous section, more water condenses on the mirror surface with a higher concentration of dissolved chloride ions during salt fog exposure than during MFG or single FG exposures. The more extensive corrosion observed during Cl_2 FG exposure suggests that the chlorine gas may also act as an oxidizer to increase corrosion; however, the effect of exposure duration on extent of corrosion should be investigated in more detail to fully understand this effect.

5.3.6 Correlation to Long-Term Storage

The Gemini-style protected silver mirrors are very durable; after several years stored in closed containers in the laboratory, minimal corrosion is evident on most of the mirrors. However, small corrosion features are apparent on some of the mirrors. The CrN_x adhesion layer mirror exhibits observable characteristic circular corrosion regions after just 6 months in laboratory storage (Figure 57). These features are significantly smaller in size and fewer in number than the features observed after accelerated testing. However, the similar morphologies suggest that the mechanism of corrosion is similar.

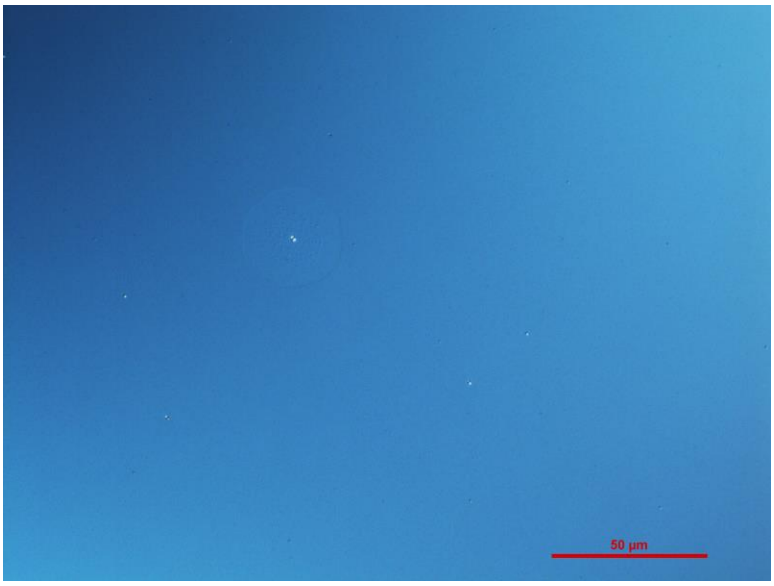

Figure 57. Optical micrograph of a corrosion feature on the CrN_x adhesion layer mirror after 6 months of laboratory storage. Note the difference in scale from previous micrographs of this mirror type.

ToF-SIMS depth profile maps at the silver-dielectric interface of a circular corrosion region on a CrN_x adhesion layer mirror stored in the laboratory for one year are shown in Figure 58. As with mirrors exposed to accelerated testing environments, the circular corrosion region shows oxygen and chlorine enrichment, suggesting that similar corrosion mechanisms are operating during both accelerated testing and real-world corrosion. The chlorine level in the laboratory was measured to be less than 0.5 ppb, while the humidity averages approximately 50%. This small amount of chlorine present in the laboratory environment along with limited adsorbed moisture on the surface is enough to affect corrosion. These data further emphasize the important role of dissolved chlorine and water during the growth of the circular corrosion regions on the CrN_x adhesion layer mirror.

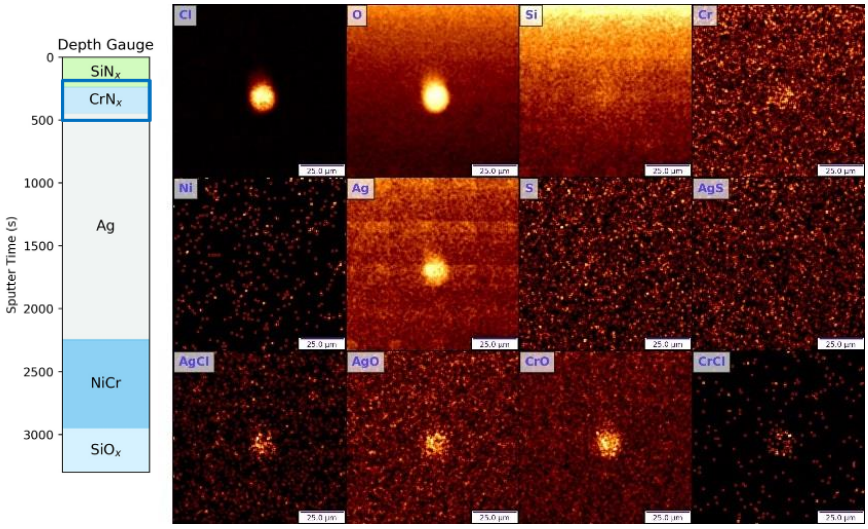

Figure 58. ToF-SIMS depth profile maps at the Ag–CrN_x-SiN_x interface of a circular corrosion region on a CrN_x adhesion layer mirrors after 1 year of laboratory storage.

The correlation of corrosion features and mechanisms during accelerated testing and real-world corrosion enables the determination of acceleration factors for the accelerated testing. The circular corrosion regions on the CrN_x adhesion layer mirror after 1 year in laboratory storage average 25 µm in diameter. The circular corrosion regions after 10 days in MFG exposure average 200 µm in diameter. This suggests that 10 days of MFG exposure correlates with approximately 8 years of laboratory storage conditions. However, this correlation should be utilized with caution, as the data herein indicate that accelerated corrosion behavior depends critically on the design of the mirror coating, the layers on either side of the silver, in combination with the environmental variables.

5.4 Conclusions

Degradation and corrosion behavior of three model silver mirrors were studied in a variety of environmental conditions to investigate the controlling factors in the mirror corrosion processes, including the relative importance of the environmental variables. We have shown that corrosion

feature morphology, and corresponding mechanism of corrosion, is dependent on the mirror design, specifically the layers on either side of the silver layer. In all the environmental conditions, mirrors with one Cr-based layer adjacent to the silver develop characteristic circular corrosion regions at the Ag-Cr interfaces, driven by the dissolution of silver and chromium, the resulting reduced adhesion at the Ag-Cr interface, and stress in the layers. These characteristic corrosion features develop in MFG, single FG, as well as long-duration environments, indicating that the accelerated testing reproduces real-world corrosion mechanisms. Comparatively, mirrors with NiCr-based layers on either side of the silver develop characteristic corrosion nodules during all exposure environments; substantial attack of the silver occurs while the interfacial attack is significantly reduced. The characteristic corrosion features on all three mirror designs during all exposure environments indicate that the mechanism of corrosion is largely dependent on the materials within the layered structure of the coatings.

Differences in extent of corrosion were observed on all three mirror designs between the various accelerated testing environments, providing insight into the role of the environmental variables. The corrosion behavior of mirrors with one Cr-based layer adjacent to the silver is influenced by low levels of chlorine in the environment. In addition, adsorbed moisture on the surface provides transport of corrosive species that enables dissolution of silver and chromium at the Ag-Cr interfaces; this reduces adhesion and allows stress-induced corrosion processes to create the circular corrosion regions. The corrosion process is, therefore, limited by the transport of chlorine species to the growing circular corrosion regions. In contrast, the corrosion behavior of mirrors with NiCr-based layers on either side of the silver is significantly affected by the concentration of chlorine in the environment. Far more extensive corrosion is observed in the Cl_2 FG exposure, suggesting that attack of the silver and nickel is significantly influenced by the

amount of chlorine available to participate in the corrosion reactions. The various NiCr- and Cr-based layers adjacent to the silver layer may also be affecting the electrochemical behavior of the silver to change the dissolution and corrosion behavior.

The variations in corrosion behavior in the various environmental conditions show that understanding the testing environment is critical to appropriately applying accelerated testing. Moreover, understanding the interactions of each mirror design with these accelerated testing environments is necessary, as the various layers adjacent to the silver cause each mirror design to be susceptible to the environmental variables in different ways. Ultimately, the layers on either side of the silver layer dominate the corrosion behavior and control the mechanism of corrosion.

Chapter 6. Effects of Stress on Corrosion Behavior

6.1 Introduction

The role of stress in the development and growth of corrosion features on the Gemini-style protected silver mirrors was discussed in Chapter 5. Coating stress is one of several factors that is known to influence the stability of thin films in general [58, 94] and may be important for the long-term durability of silver mirrors in particular [21, 23, 24, 49]. Stress can develop in thin films during high-energy, nonequilibrium deposition processes and is significantly dependent on the deposition conditions used. Ion flux, ion energy, chamber pressure, gas ratios, and substrate conditions can influence the stress state of a thin film [58, 94, 95]. High levels of stress can damage the film or substrate, degrade the properties of the film, or cause the film to lose adhesion [58]. Compressive stress can cause the film to buckle, while tensile stress can cause the film to crack and peel [58, 76, 77, 96]. Preventing these types of failures is important for long-term coating reliability.

In protected silver mirrors, the state of stress in the multilayer coating is compounded by the different materials used for each layer and the very thin layer thicknesses, which can create large stress gradients. The metal layers are generally tensile, while the dielectric layers are usually compressive [58, 89, 90, 97, 98]. The resultant stress state of a mirror is a combination of the stress in each layer weighted by the thickness of each layer; however, the situation is more complex than simply the sum of the stresses of the individual layers. When deposited in a mirror stack, the tensile metal layers and compressive dielectric layers can create large stresses at the layer interfaces, even if the overall stress state of the mirror coating is balanced. Stress in a mirror coating may affect the corrosion processes that occur, impacting durability. For example, stress-induced failure of the dielectric protection layers can expose the silver directly to corrosive species.

Stress-induced corrosion cracking can occur whereby stress accelerates crack growth [46, 99]. Stress gradients can also accelerate solid state diffusional processes [100], which may affect mirror durability as well.

This chapter investigates the role of stress in the durability and corrosion behavior of Gemini-style protected silver mirrors by reducing stress in the highest stress layers of the mirror coatings. Sputtered SiN_x is known to have high compressive stress [28, 46, 90, 97], while sputtered chromium has high tensile stress [24, 89]. A variety of deposition conditions were explored to reduce the stress in these two layers. $NiCrN_x$ adhesion layer mirrors and Cr base layer mirrors were then deposited utilizing the deposition conditions for either lower stress SiN_x or Cr layers. The durability and corrosion behavior of these lower stress mirrors were evaluated by MFG exposure to investigate the effects of stress on the extent and mechanisms of corrosion.

6.2 Experimental Methods

6.2.1 Coatings and Deposition Processes

The deposition of protected silver mirrors by plasma beam sputtering was described in Chapter 3.

Single layers of the mirror materials were also deposited on polished silicon substrates to investigate the effects of deposition conditions on reducing stress in the layers. The conditions used during deposition of the various SiN_x and Cr single layers are shown in Table 5. The thickness of the single layer coatings was either 500Å or 1000Å depending on the deposition conditions and rates used. These thicknesses were required to reduce errors in the stress measurements. As with layers of the mirror coatings, thickness of the single layers was controlled

by quartz crystal monitors calibrated by profilometry or ellipsometry. Optical constants of the SiN_x films were measured by ellipsometry from 200 to 1700 nm.

Table 5. Deposition Conditions of SiN_x and Cr Layers for Protected Silver Mirrors

Layer Type	Layer Material	RF Power (W)	Target Bias Power (W)	Chamber Pressure (mTorr)	Substrate Condition
Standard SiN_x	SiN_x	1300	1000	2.0	Grounded
Low-bias SiN_x	SiN_x	2500	500	2.0	Grounded
High-pressure SiN_x	SiN_x	1300	1000	4.0	Grounded
Standard Grounded Cr	Cr	1000	1000	2.0	Grounded
Floating Cr	Cr	1000	1000	2.0	Floating

6.2.2 Stress Measurements

Stress in a thin film can induce a curvature to the substrate as the thin film lengthens or contracts and the substrate bends in response to the applied stress [24, 101]. For elastic isotropic substrates, Stoney's equation relates the radius of curvature, *R*, of an initially flat substrate to the biaxial stress, σ_f, of the deposited thin film:

$$\sigma_f t_f = \frac{E_s h^2}{6(1-\nu_s)R} \quad (1)$$

where t_f is the thickness of the film, h is the thickness of the substrate, E_s is Young's modulus of the substrate, and ν_s is Poisson's ratio of the substrate [58, 102]. By measuring the various properties of the film and substrate, the coating stress can be determined.

Stress in single layers of the mirror coatings was characterized by measuring the change in radius of curvature of the silicon substrates due to deposition of the coatings. The profile of the silicon substrates was pre-characterized before depositions using a 4D AccuFiz phase-shifting Fizeau interferometer. After the coatings were deposited, the profile of the coated substrates was measured. The radius of curvature of the uncoated and coated substrates was determined using Zygo MetroPro interferometry software. As the silicon substrates were not flat to begin with,

substrates with the most radially symmetric profiles were chosen for depositions. Even so, the errors in the radius of curvature measurements were large enough that small differences in stress could not be detected. After the radius of curvature values were determined, a modified version of Stoney's equation [101] was used to calculate coating stress, accounting for the anisotropy of the silicon substrates:

$$\sigma_f t_f = \frac{h^2}{6(S_{11}^{Si} - S_{12}^{Si})R} \quad (2)$$

where $1/(S_{11}^{Si} - S_{12}^{Si})$ is the biaxial modulus of Si (001), which has a value of 1.803×10^{11} Pa. Positive stress corresponds to tensile stress in the film; negative stress corresponds to compressive film stress.

6.2.3 Silver Mirror Designs

Two model silver mirror designs were used to investigate the effects of reducing stress in the layers of the mirror coatings (Figure 59). The $NiCrN_x$ adhesion layer mirror was utilized to explore the role of reduced stress in the SiN_x protective layer. Three $NiCrN_x$ adhesion layer mirrors were deposited with identical NiCr, Ag and $NiCrN_x$ layers, but with different SiN_x layers – either standard, low-bias, or high-pressure SiN_x. The Cr base layer mirror was utilized to explore the role of reduced stress in the Cr base layer or in the SiN_x protective layer. Three Cr base layer mirrors were deposited with identical Ag and $NiCrN_x$ layers. One Cr base layer mirror was deposited with the standard grounded Cr and the standard SiN_x, while a second Cr base layer mirror was deposited with floating Cr and standard SiN_x. A third Cr base layer mirror was deposited with standard grounded Cr and high-pressure SiN_x.

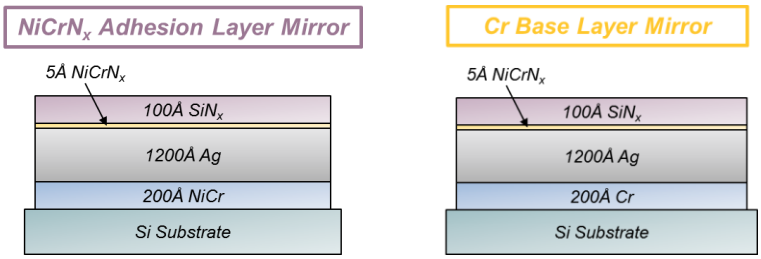

Figure 59. $NiCrN_x$ adhesion layer mirror (left) and Cr base layer mirror (right) designs deposited for this study.

6.2.4 Accelerated Environmental Exposure

Durability and corrosion behavior of the mirrors were evaluated by standard MFG exposure, as described previously. Before, during, and after MFG exposure, the mirrors were characterized to observe changes in optical properties and coating morphology. Reflectance and scatter were measured at the mirror center, degradation of the mirror surface was imaged under dark field conditions, and corrosion features were imaged with an optical microscope under DIC mode.

6.3 Results & Discussion

6.3.1 Effects of Deposition Conditions on Coating Stress

The standard layers used in the mirror coatings have been optimized through years of depositions and experience for both optical performance and durability [24, 31, 47, 74]. The standard SiN_x is reactively deposited at moderate power, 1300 W of RF power to the plasma source and 1000 W of power to the DC target bias, and a chamber pressure of 2.0 mTorr. This standard SiN_x exhibits excellent optical properties, as shown in Table 6, and has been shown to provide very good durability when utilized in various protected silver mirror coatings. However, it is highly compressive. Compressive stresses in reactively-sputtered dielectric coatings are thought to arise primarily from bombardment of the growing film by energetic particles, a process referred

to as atomic peening [65, 94, 95, 103]. Volumetric strain associated with incorporation of film impurities as well as reaction of the sputtered metal atoms with the process gas can also increase compressive stresses [94]. To lower stress in the SiN_x layer, a variety of deposition conditions were investigated utilizing modified power settings as well as higher chamber pressures (Table 5).

Table 6. Stress and Optical Properties of SiN_x Layers

Layer	Stress, σ (MPa)	Index of Refraction, n [+]	Extinction Coefficient, k [+]
Standard SiN_x	-1100 ± 200	2.014	3.26×10^{-4}
Low-bias SiN_x	-1200 ± 200	1.954	2.87×10^{-2}
High-pressure SiN_x	-550 ± 200	1.821	2.85×10^{-3}

[+] n & k at 550 nm

The low-bias SiN_x layer was deposited at 2500 W of RF power and 225 V of DC target bias, which generates approximately 500 W of power to the target. Lowering the target bias is intended to reduce the energy with which the sputtered atoms and reflected neutrals arrive at the substrate, thereby reducing stress in the deposited coating [24, 94]. However, lowering the target bias also reduces the deposition rate. To maintain a reasonable deposition rate, the power to the RF plasma source was increased, which increased the plasma ion density without increasing the ion energy [63]. A variety of RF and target bias power combinations were investigated, but none exhibited significantly lower stress than the conditions used for the standard SiN_x coatings. Within the range of power settings attainable in the deposition chamber, it was not possible to reduce the SiN_x stress in this manner. Moreover, the low-bias SiN_x coatings have significantly reduced optical properties. The high k-value is associated with significantly increased arcing that occurred during the low-bias SiN_x depositions, resulting in substantially more spit defects in the coatings. As described in previous chapters, breakdown of SiN_x dielectric buildup on the silicon target during reactive sputtering can eject lumps of silicon from the target that deposit in the growing film. These spit defects act as absorbers in the SiN_x layer, thereby reducing its optical properties.

A high-pressure SiN_x layer was deposited at 4.0 mTorr to significantly reduce the stress in this layer. Increasing the chamber pressure reduces the mean free path in the vacuum environment, thereby increasing the number of collisions of the gas and ion species [55, 65, 94, 103]. This reduces the energy with which the sputtered atoms and reflected neutrals arrive at the substrate, thereby reducing stress in the deposited coating. As shown in Table 6, the high-pressure SiN_x deposition reduced the coating stress by a factor of two. However, it also reduced the index of refraction of the SiN_x. This is believed to be due to the higher chamber pressure and corresponding lower sputtered atom energy, which results in a less dense SiN_x layer [24].

The standard Cr coating has rather high tensile stress, as shown in Table 7. The tensile stresses observed in metallic coatings, such as Cr, are generally believed to be due to grain boundary relaxation phenomena that occur during film growth [94, 95, 98, 103]. The standard sputtering configuration for all layers of the mirror coatings occurs with the substrate plate grounded, which prevents charge buildup at the substrates. Removing the grounding strap from the substrate plate, such that the substrates were now floating electrically, resulted in significant stress reduction in the Cr layer by a factor of two. The floating charge on the substrate plate is negative, as expected from plasma exposure. This likely yields increased argon ion bombardment of the substrates, which increases the compressive stress in the film, thereby making the Cr layer less tensile.

Table 7. Stress in Cr Layers

Layer	**Stress, σ (MPa)**
Standard Grounded Cr	780 ± 100
Floating Cr	350 ± 100

The deposition conditions used to reduce stress in the SiN_x and Cr single layers were employed in the deposition of full mirror coating stacks. This is believed to result in reduced stress

within the modified mirror coatings, particularly at the layer interfaces of the reduced stress layer. However, differences in measured stress in the modified mirror coatings compared to the standard mirror coatings were within the margin of error, such that the stress in the mirrors is not reported here. This is likely due to the much thinner layers used in the mirror coatings, 100Å of SiN_x and 200Å of Cr, and the large errors in the stress measurements due to non-radially-symmetric silicon substrates.

6.3.2 Nodular Corrosion Feature Development on $NiCrN_x$ Adhesion Layer Mirrors

The $NiCrN_x$ adhesion layer mirror with standard SiN_x exhibits excellent optical performance and durability, as shown in Figure 60 and Figure 61. With the highest initial reflectance and low scatter, the optical properties of this mirror are maintained throughout MFG exposure. In contrast, the $NiCrN_x$ adhesion layer mirror with high-pressure SiN_x exhibits slightly reduced initial reflectance, though it is also maintained throughout MFG exposure, and a larger increase in scatter. This is due to an increase in the size or number of corrosion features, the primary contributors to scatter increase in $NiCrN_x$ adhesion layer mirrors during MFG exposure. Similarly, the $NiCrN_x$ adhesion layer mirror with low-bias SiN_x exhibits significantly reduced initial reflectance that is further reduced by 1% at 600 nm during MFG exposure. The reduced reflectance and very high initial scatter of this mirror are due to the increased number of spit defects in the low-bias SiN_x layer.

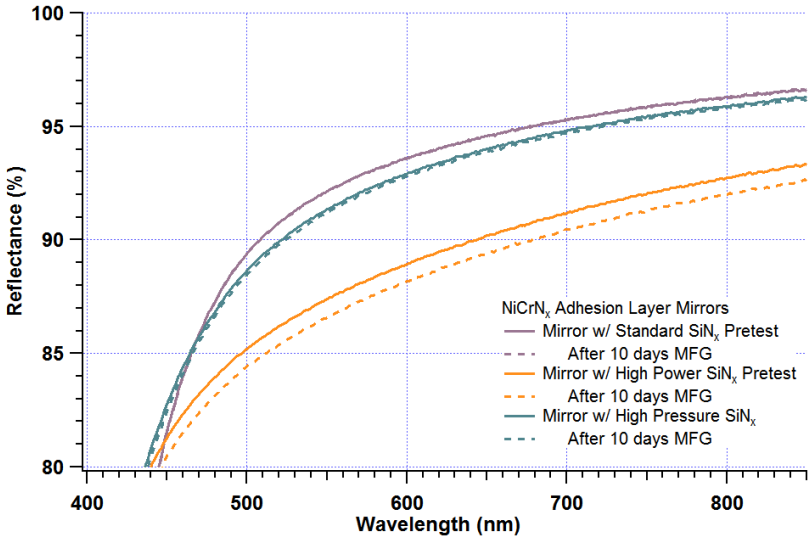

Figure 60. Reflectance of $NiCrN_x$ adhesion layer mirrors before and after MFG exposure.

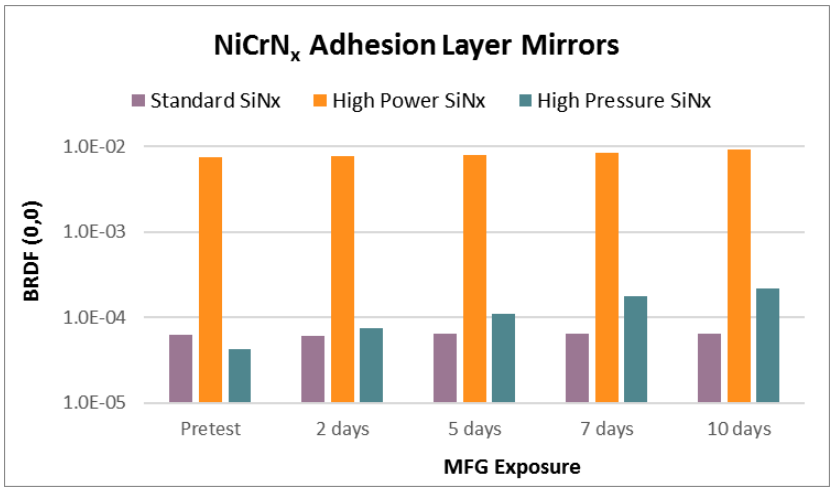

Figure 61. Scatter of $NiCrN_x$ adhesion layer mirrors during MFG exposure.

Dark field images of the three $NiCrN_x$ adhesion layer mirrors before and after MFG exposure are shown in Figure 62. The markings that occur at 6 o'clock on several of the mirrors prior to MFG exposure are due to handling of the substrates prior to coating. After MFG exposure, degradation is apparent around the edge and with scattered corrosion features across the surface of the mirror with standard SiN_x (Figure 62a,b). However, the mirrors with low-bias and high-pressure SiN_x are clearly far more degraded. The mirror with high-pressure SiN_x exhibits more

corrosion features across the surface (Figure 62e,f), corresponding to the larger increase in scatter of this mirror. The mirror with low-bias SiN_x also exhibits increased scattered corrosion features across the surface (Figure 62c,d), including some very bright spots. More notable, however, is the gray color of this mirror prior to MFG exposure. As mentioned previously, a smooth reflective mirror appears black under these oblique lighting conditions. The gray color of the $NiCrN_x$ adhesion layer mirror with low-bias SiN_x is a result of the increased scatter associated with increased number of spit defects in the SiN_x layer. The poor surface quality of this mirror corresponds to the significantly reduced optical properties of the SiN_x layer (Table 6).

Optical micrographs of representative corrosion features on the three $NiCrN_x$ adhesion layer mirrors are shown in Figure 63. All three mirrors exhibit characteristic corrosion nodules typical of $NiCrN_x$ adhesion layer mirrors, indicating that the composition of the layers adjacent to the silver controls the mechanism of corrosion. As discussed in previous chapters, the corrosion nodules are a result of disruption to the layered structure of the coating resulting from attack of the silver layer itself. While the nodules are characteristic of $NiCrN_x$ adhesion layer mirrors, the extent of corrosion, both in number and size of corrosion features, differs considerably between the three mirrors with variations in SiN_x.

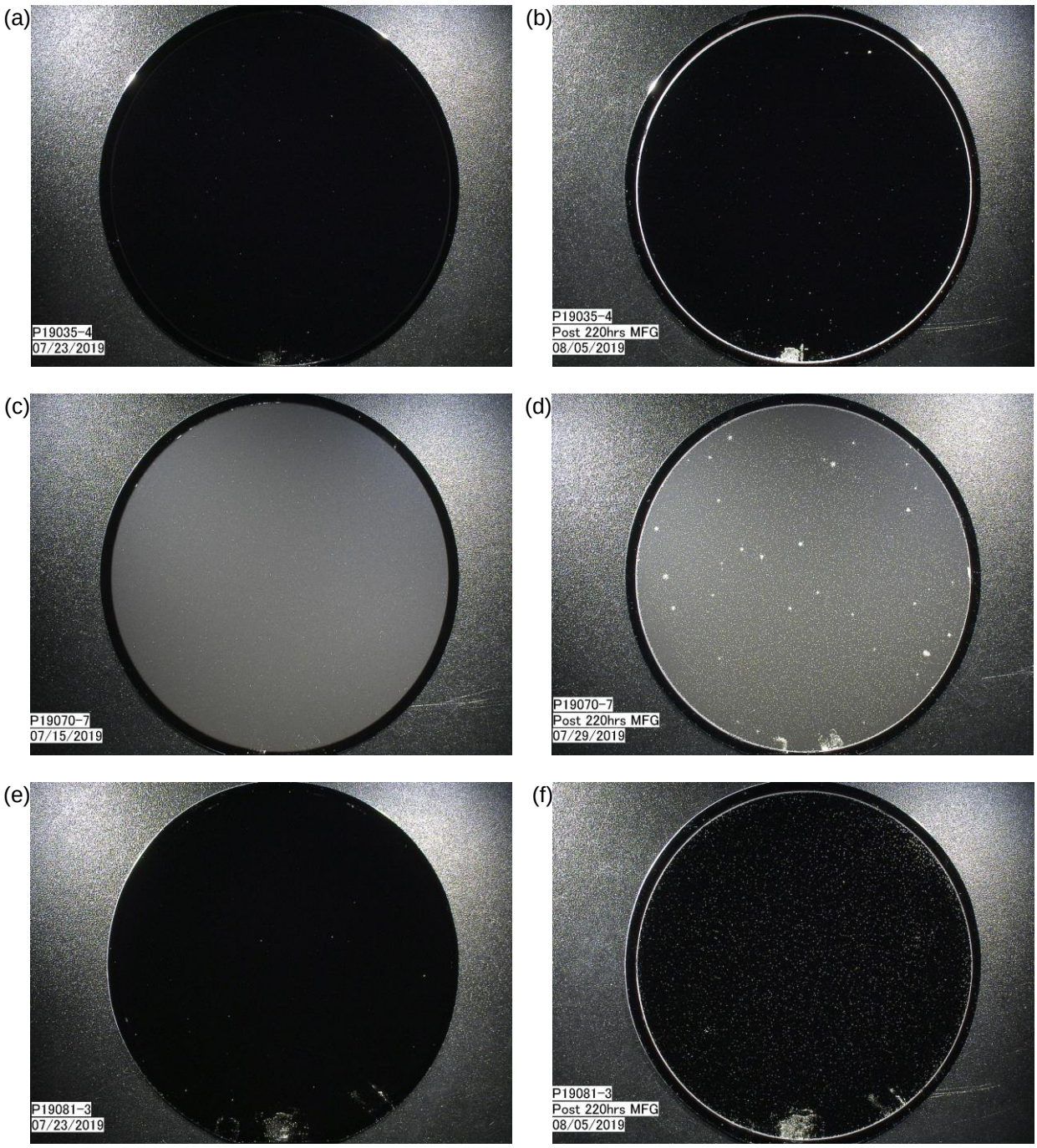

Figure 62. Dark field images of the $NiCrN_x$ adhesion layer mirrors before (a,c,e) and after (b,d,f) 10 days MFG exposure. Mirrors with (a,b) standard SiN_x, (c,d) low-bias SiN_x, and (e,f) high-pressure SiN_x protective layers.

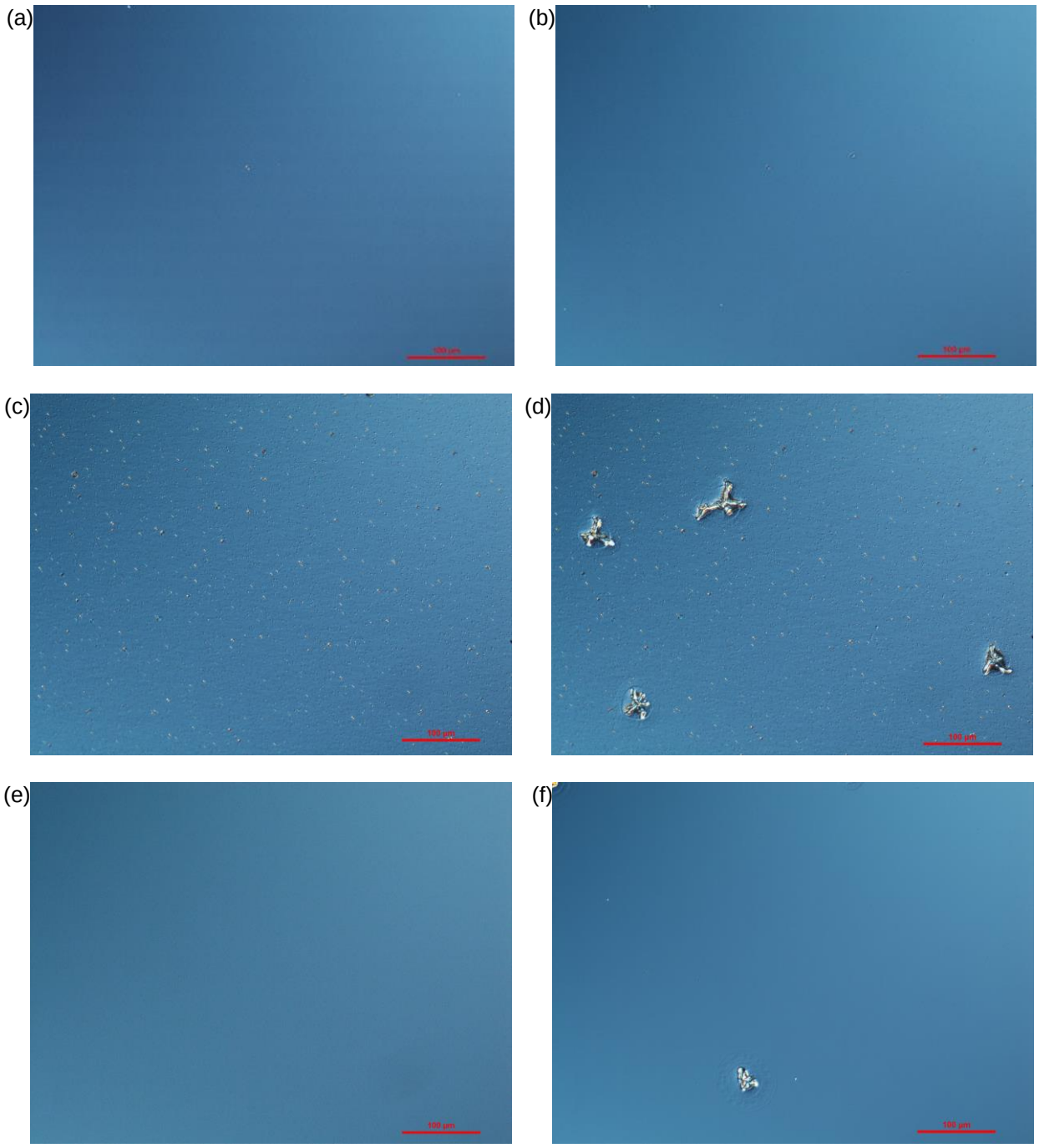

Figure 63. Optical micrographs of corrosion features on the $NiCrN_x$ adhesion layer mirrors before (a,c,e) and after (b,d,f) 10 days MFG exposure. Mirrors with (a,b) standard SiN_x, (c,d) low-bias SiN_x, and (e,f) high-pressure SiN_x protective layers.

The $NiCrN_x$ adhesion layer mirror with standard SiN_x exhibits few, small characteristic corrosion nodules (Figure 63b); this is typical of these standard mirrors. The $NiCrN_x$ adhesion

layer mirror with high-pressure SiN_x exhibits both larger and higher number of characteristic corrosion nodules (Figure 63f). This is likely due to the decreased density of the high-pressure SiN_x layer, which may allow corrosive species to more easily reach the Ag layer, thereby increasing the extent of corrosion. The increased number and size of corrosion nodules is directly related to the increased scatter of this mirror during MFG exposure. While the high-pressure SiN_x layer exhibits substantially reduced compressive stress, the extent of corrosion of the $NiCrN_x$ adhesion layer mirror with this high-pressure SiN_x is increased, resulting in reduced durability.

The $NiCrN_x$ adhesion layer mirror with low-bias SiN_x exhibits significantly larger and greater number of characteristic corrosion nodules (Figure 63d). The star-like corrosion nodules are more extensively corroded than the more rounded nodules observed on the other mirrors. The more extensive corrosion on this mirror is due to the significantly increased number of pre-existing spit defects in the SiN_x layer, as shown in Figure 63c, which are due to increased arcing during deposition. As discussed in Chapter 4, the development of corrosion features on these mirrors is due, at least in part, to a defect mediated process associated with the pre-existing coating spit defects. The durability and optical performance of the $NiCrN_x$ adhesion layer mirror with low-bias SiN_x is significantly reduced, with no benefit in reduced stress in the SiN_x layer.

The process changes implemented to reduce stress in the SiN_x layer of the $NiCrN_x$ adhesion layer mirrors resulted in reduced mirror durability, both in terms of reduced optical properties and more extensive corrosion. The low-bias SiN_x did not exhibit reduced stress and mirrors with this layer also developed more and larger corrosion features due to increased spit defect density. While the high-pressure SiN_x did exhibit substantially reduced compressive stress, the corresponding $NiCrN_x$ adhesion layer mirror had more and larger corrosion features due to decreased density of the SiN_x layer. SiN_x layer quality, in terms of spit defects and density, is therefore believed to

significantly influence the extent of corrosion. Reduced stress does not appear to reduce the extent of corrosion, at least within the parameter space explored with this study. Although differing in corrosion extent, all three $NiCrN_x$ adhesion layer mirrors developed characteristic corrosion nodules, suggesting that the NiCr-based layers on either side of the silver layer largely control the mechanisms of corrosion feature development and growth. The composition of the layers adjacent to the silver are more important for long-term durability.

6.3.3 Circular Corrosion Feature Development on Cr Base Layer Mirrors

The three Cr base layer mirrors deposited for this study exhibit very good optical properties and durability, as shown in Figure 64 and Figure 65. No difference in initial reflectance or loss in reflectance during MFG exposure are apparent. Differences in initial scatter and scatter increases are small. Notably, the Cr base layer mirror with standard grounded Cr exhibits slightly larger increase in measured scatter, suggesting that the corrosion features on this mirror are more developed. As this mirror includes both the higher stress standard Cr and SiN_x layers, it is notable that the scatter of this mirror is the largest after MFG exposure.

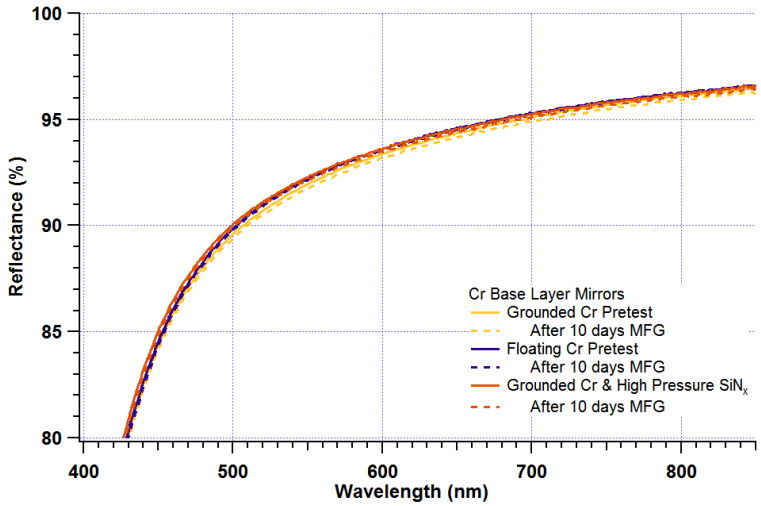

Figure 64. Reflectance spectra of Cr base layer mirrors before and after MFG exposure.

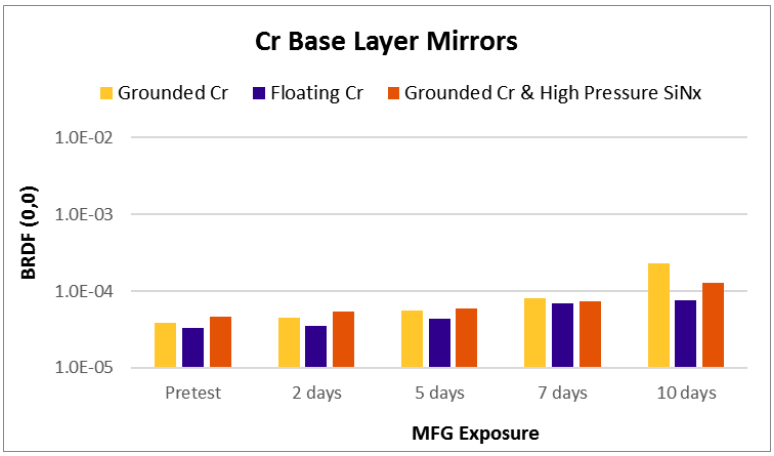

Figure 65. Scatter of Cr base layer mirrors during MFG exposure.

Dark field images of the three Cr base layer mirrors before and after MFG exposure are shown in Figure 66. Prior to MFG exposure, the markings on the mirrors that appear at 6 o'clock, as well as at 9 and 1 o'clock on one mirror, are due to handling and substrate thickness measurements prior to coating. After MFG exposure, some corrosion is evident on all the mirrors with no clear differences in the extent of corrosion around the edges or in the scattered corrosion features across the surfaces of each mirror.

Optical micrographs of representative corrosion features on the three Cr base layer mirrors are shown in Figure 67. All three mirrors exhibit characteristic circular corrosion regions typical of Cr base layer mirrors, indicating that the composition of the layers adjacent to the silver controls the mechanism of corrosion. As discussed in previous chapters, the circular corrosion regions develop at the Ag-Cr interface, as both the Ag and Cr are susceptible to oxidation and chloridation. As the corrosion and dissolution proceeds along the interface, reduced adhesion results in delamination of the Ag layer from the Cr below, creating blisters that increase the measured scatter of the mirrors. In the optical micrographs, differences in the extent of corrosion between the characteristic corrosion features on each mirror are not obvious.

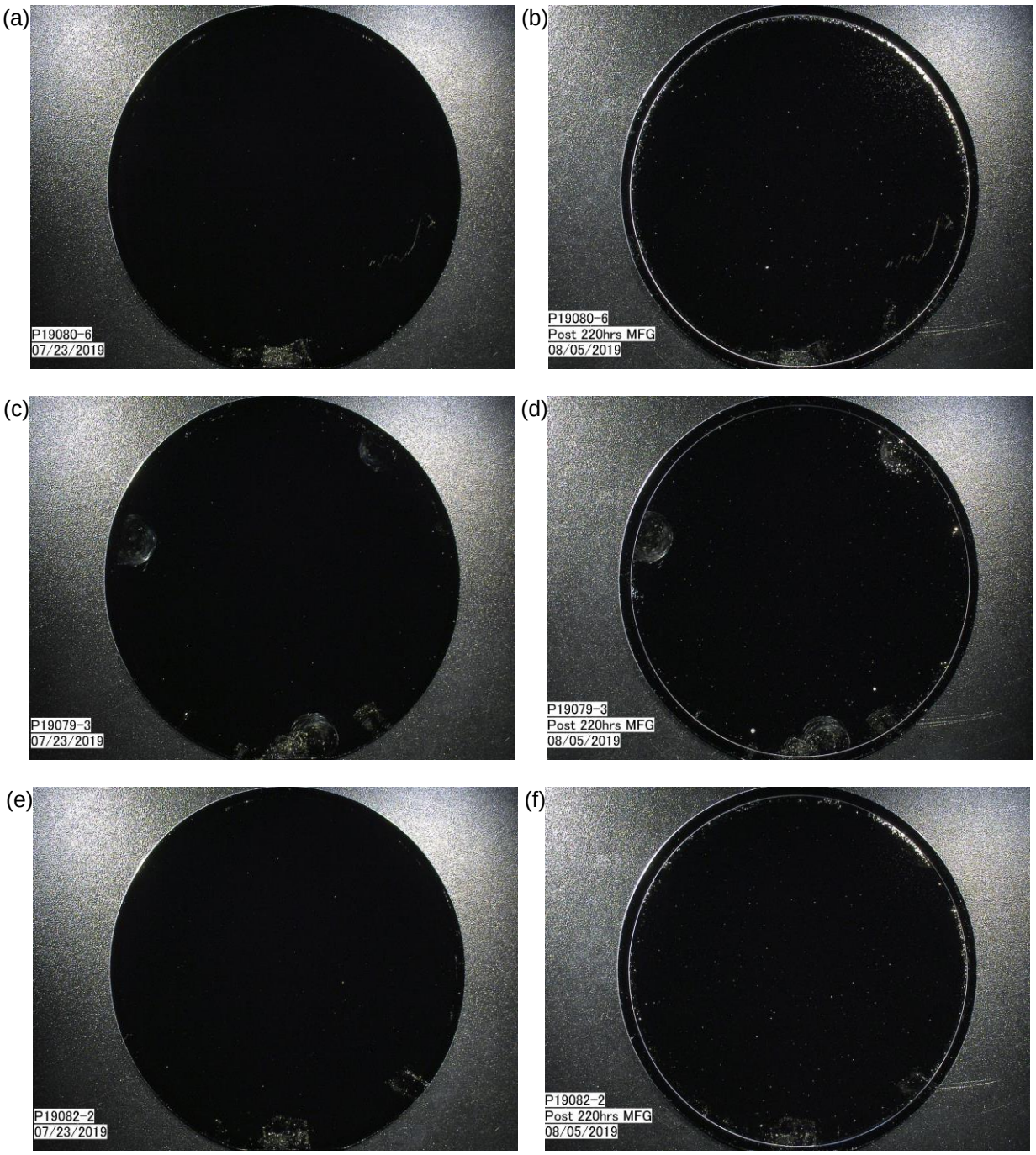

Figure 66. Dark field images of the Cr base layer mirrors before (a,c,e) and after (b,d,f) 10 days MFG exposure. Mirrors with (a,b) grounded Cr base layer, (c,d) floating Cr base layer, and (e,f) grounded Cr base layer and high-pressure SiN_x protective layer.

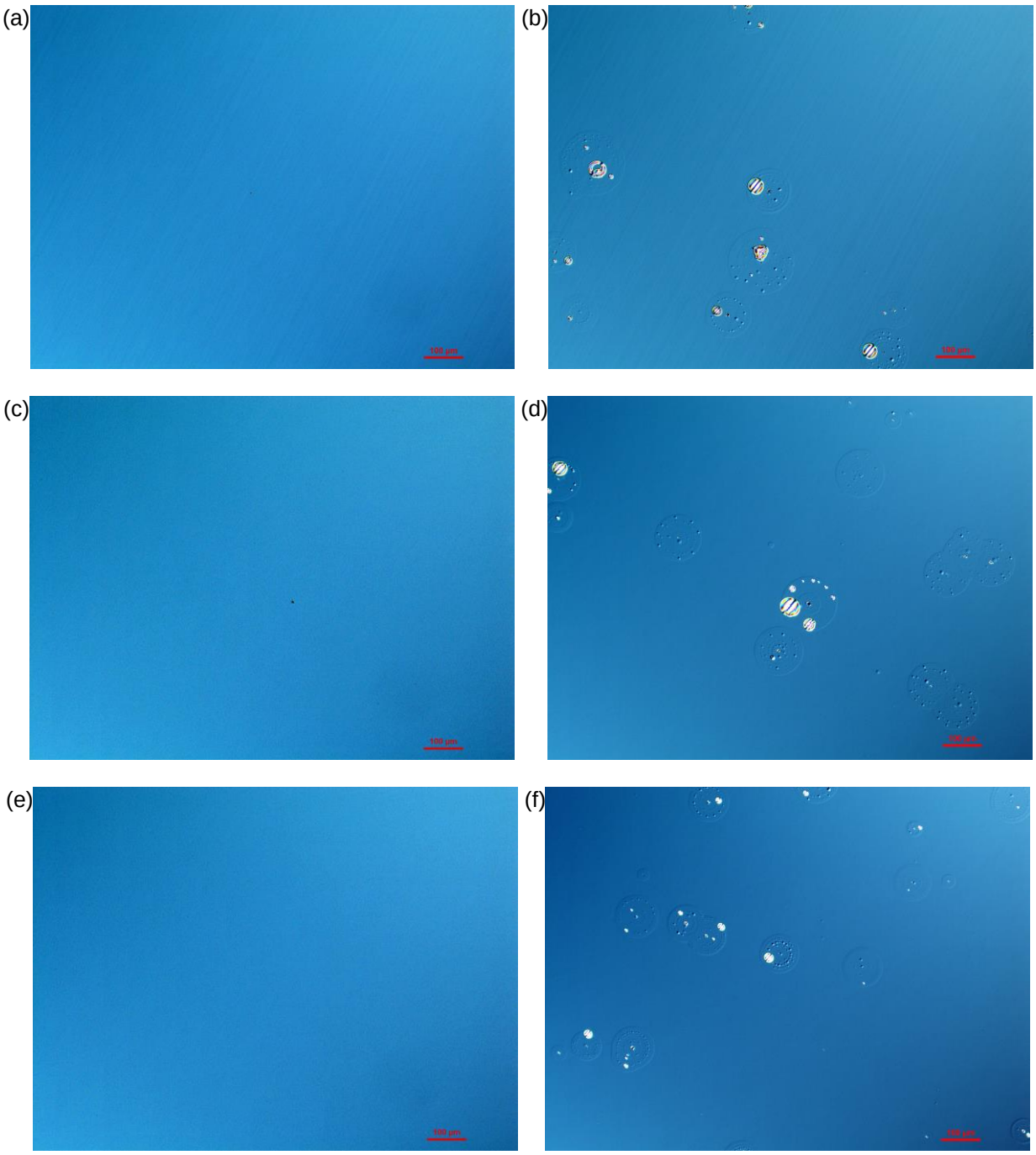

Figure 67. Optical micrographs of corrosion features on the Cr base layer mirrors before (a,c,e) and after (b,d,f) 10 days MFG exposure. Mirrors with (a,b) grounded Cr base layer, (c,d) floating Cr base layer, and (e,f) grounded Cr base layer and high-pressure SiN_x protective layer.

The Cr base layer mirror with standard grounded Cr exhibits characteristic circular corrosion regions (Figure 67b), as is typical for these standard mirrors. The Cr base layer mirror

with floating Cr exhibits similar size and number density of characteristic circular corrosion regions (Figure 67d). This suggests that the lower stress associated with the floating Cr layer does not obviously affect the extent of corrosion in this mirror. However, it should be noted that fewer of the circular corrosion regions on this mirror have developed delamination blisters, corresponding to the smaller increase in measured scatter of this mirror. This suggests that lower stress in the Cr base layer may play a role in the stress required for blister formation as the corrosion reaction reduces adhesion at the Ag-Cr interface [46, 76]. However, the effect is small and further study is needed to fully elucidate any changes.

The Cr base layer mirror with standard grounded Cr and high-pressure SiN_x also exhibits similar size and number density of characteristic circular corrosion regions (Figure 67e). This mirror was designed to investigate the role of reduced stress in the SiN_x layer. No significant differences in extent of corrosion are apparent from the optical images of the corrosion features, indicating that reduced stress in the SiN_x layer does not obviously reduce the extent of corrosion in this mirror. However, the slightly lower increase in measured scatter associated with this mirror compared to the standard Cr base layer mirror may be related to fewer circular corrosion regions that have developed delamination blisters. This may be related to reduced stress in the SiN_x, though, again, the effect is small and further study is needed.

The process changes implemented to reduce stress in the Cr base layer mirrors did not produce significant differences in durability, in terms of reduction in optical properties, or in corrosion extent, either in size or number of corrosion features. Small differences in scatter were apparent, which appear to be related to the development of delamination blisters. As the dissolution of silver and chromium reduces adhesion at the Ag-Cr interface, the formation of delamination blisters is reduced due to lower stress in the coating. Even so, within the range of

stresses explored in this study, lower stress in the Cr or SiN_x layers does not substantially affect the extent of corrosion in these mirrors. Moreover, all three mirrors develop characteristic circular corrosion regions, suggesting that the Ag-Cr interface controls the mechanism of corrosion feature development in mirrors with one Cr-based layer adjacent to the silver. The composition of the layers adjacent to the silver are most important for long-term durability.

6.4 Conclusions

The effect of stress on the durability and corrosion behavior of protected silver mirrors was studied by reducing stress in the highest stress layers of the mirror coatings. A significant reduction in stress in the SiN_x layer was possible with an increase in sputtering pressure, whereas changes to the RF and target bias power did not reduce stress in the SiN_x layer. However, neither process change resulted in an improvement in durability. In fact, both high-pressure SiN_x and low-bias SiN_x layers resulted in more extensive corrosion in $NiCrN_x$ adhesion layer mirrors, including an increase in both number and size of corrosion features. Within the range of SiN_x stresses studied, the SiN_x layer quality, in terms of the number of spit defects and the density of the layer, is more important in determining the extent of corrosion.

It was not possible to isolate changes in stress in the SiN_x layer from changes in defect density and layer nanostructure. Therefore, reducing stress in the Cr layer was explored by removing the grounding strap from the substrate plate. This resulted in a floating substrate condition that significantly reduced the stress in the Cr layer, though it did not have a significant effect on the durability of the Cr base layer mirrors. A small improvement in scatter was observed, related to reduced number of delamination blisters in the mirrors with lower stress Cr or SiN_x layers. This suggests that stress may also contribute to the growth of the circular corrosion regions

in Cr base layer mirrors and also in CrN_x adhesion layer mirrors; however, within the range of stresses attainable with this deposition chamber, the effect was small. Overall, within the range of Cr and SiN_x stresses studied, reducing coating stress did not significantly reduce the extent of corrosion.

Furthermore, within the range of stresses studied, reducing stress in the SiN_x and Cr layers does not appear to change the mechanisms of corrosion in these mirrors. In all $NiCrN_x$ adhesion layer mirrors, regardless of the stress state or layer quality of the SiN_x layer, characteristic corrosion nodules formed. Similarly, in all Cr base layer mirrors, regardless of the stress state or layer quality of the Cr or SiN_x layers, characteristic circular corrosion features formed. While stress may play a role in the extent of corrosion and the corrosion kinetics, the composition of the layers on either side of the silver have a larger influence on the mechanisms of corrosion feature development and growth.

Chapter 7. Electrochemical Assessment of Corrosion Behavior

7.1 Introduction

Electrochemical methods enable rapid assessment of corrosion behavior [104]. These techniques can elucidate the thermodynamic and kinetic aspects of corrosion phenomena, including the active corrosion mechanisms and the corresponding corrosion rates. While a certain reaction may be thermodynamically favored, it may not be the driver of the corrosion process if it happens too slowly. To this end, this chapter explores the application of several electrochemical techniques to the corrosion of Gemini-style protected silver mirrors to investigate the controlling factors in the mirror corrosion process.

During atmospheric corrosion of protected silver mirrors, when two dissimilar metals are in electrical and ionic contact at the interfaces of the coating, galvanic corrosion can occur. Corrosion of the less noble material can be accelerated while the more noble material can be protected. Characterization of galvanic interactions between dissimilar metals is obtained through polarization curve measurements [104]. These data can be used to generate a galvanic series in the environment of interest, which enables prediction and understanding of corrosion behavior based on mixed potential theory.

After corrosion has occurred, the coulometric reduction technique can be used to quantify the amount and identify the type of corrosion products found on silver surfaces [12, 13, 17, 88, 105]. This galvanostatic technique utilizes a cathodic current to reduce metal ions in Ag corrosion products on the surface back to their elemental form. The total charge passed during reduction is proportional to the mass transformed, while the reduction voltage plateaus allow the corrosion products to be identified. Identifying and quantifying the Ag corrosion products enables understanding of the electrochemical reactions that occur during the corrosion process.

The purpose of this chapter is to characterize the electrochemical effects of the layers adjacent to the silver to further understand the underlying causes of corrosion and degradation in these mirrors. Initial work focused on the development of the electrochemical techniques for application to protected silver mirror coatings. Then, coulometric reduction was used to identify and quantify the corrosion products formed on several mirror designs after accelerated environmental exposure. Finally, polarization curve measurements, verified by galvanic couple measurements, were performed to assess possible galvanic interactions in the layers. Together these electrochemical data provide the basis for understanding the controlling factors in the silver mirror corrosion processes.

7.2 Experimental Methods

7.2.1 Coatings and Deposition Process

Protected silver mirror coatings, bare silver mirror coatings, and single layers of the mirror materials were deposited by plasma beam sputtering, which was described in Chapter 3. Four protected silver mirror designs were used in this study: the no adhesion layer mirror, the CrN_x adhesion layer mirror, the $NiCrN_x$ adhesion layer mirror, and the Cr base layer mirror (Figure 68). The mirrors were deposited on polished silicon substrates that had small platinum tabs deposited at the edges, as shown in Figure 69. The platinum tabs were required for the coulometric reductions.

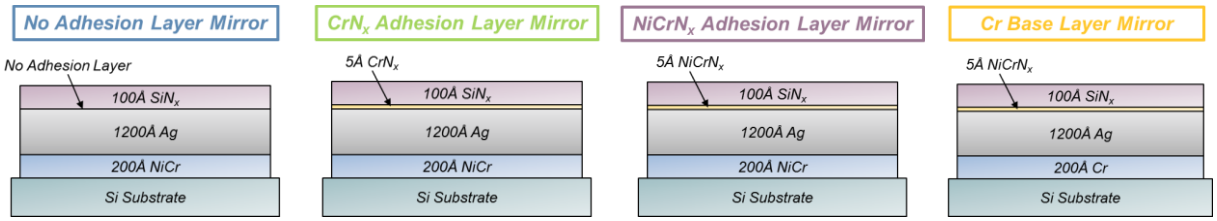

Figure 68. Protected silver mirror designs deposited for this study: No adhesion layer mirror, CrN_x adhesion layer mirror, $NiCrN_x$ adhesion layer mirror, and Cr base layer mirror.

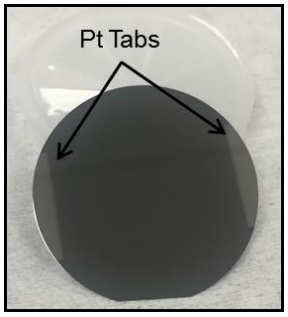

Figure 69. Platinum tabs deposited on Si substrates before deposition of the mirror coatings.

Bare silver mirror coatings consisted of an unprotected Ag layer with no adhesion or protection layers above the silver, as shown in Figure 70. These coatings were used for both coulometric reductions and galvanic corrosion testing. The NiCr base layer was required for adhesion to the substrate and did not affect the electrochemical results.

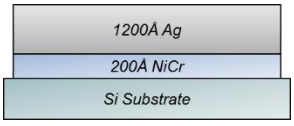

Figure 70. Bare silver mirror coatings deposited for this study.

In addition, single layers of the other mirror materials were deposited for galvanic corrosion testing: NiCr, $NiCrN_x$, Cr, CrN_x, and SiN_x. The single layer coatings were nominally 1000Å thick to reduce the likelihood of pinholes that could extend through the entire layer to the substrate below.

7.2.2 Accelerated Environmental Exposure

Durability and corrosion behavior of the mirrors were evaluated by MFG exposure and Cl_2 FG exposure, as described in Chapter 5. To observe changes in coating morphology throughout MFG exposure, degradation of the mirror surface was imaged under bright field and dark field conditions. Corrosion features were also imaged at higher magnification under DIC mode.

After MFG exposure, specific corrosion features were cross-sectioned for detailed observation and elemental analysis of the layered structure. Specimens were prepared by the FIB lift-out method, as described in Chapter 3. Cross-sectional imaging was performed on a ThermoFisher Titan Themis transmission electron microscope at 300kV in scanning transmission mode (S/TEM). Elemental analyses in this instrument were performed with an integrated Bruker energy dispersive x-ray spectroscopy (EDS) system using four silicon drift detectors situated in the sample chamber. High angle annular dark field mode (HAADF) was used to collect Z-contrast images, where higher-Z material appears brighter. Annular dark field mode (ADF) was used to collect images that include crystallographic orientation contrast.

7.2.3 Coulometric Reduction

Coulometric reduction was used to quantify the amount and identify the type of corrosion products found on the mirrors following MFG and single FG exposures. A constant cathodic current was applied to a corroded sample in an electrolytically conductive solution to reduce the metal ions in the corrosion products back to their elemental form [12, 106]. Each compound has a characteristic voltage where this reduction occurs that is related to the thermodynamics (i.e. the reversible potential) and the electrochemical kinetics. The reduction potential plateaus allow the

corrosion products to be identified. At constant current, the total charge passed, Q, during the reduction is proportional to the mass transformed, m. This allows determination of the amount of corrosion product by Faraday's Law of Electrolysis.

$$m = \frac{QM}{nF} \tag{3}$$

where M is the molar mass, n is the valency change (i.e. the number of electrons transferred per ion), and F is Faraday's constant. The mass change can then be used to estimate the film thickness of the corrosion product assuming theoretical film density.

ASTM B825 recommends deaerated 0.1M potassium chloride (KCl) solution with an Ag/AgCl reference electrode be used for the reductions [106]. However, this solution has been shown to alter the chemistry of the corrosion films on the silver surface as silver oxide can be transformed into silver chloride in the KCl solution, masking corrosion product identification and quantification [12]. An Ag/AgCl reference electrode can also similarly misrepresent the results. Chen et al. [12] has shown that 0.1M sodium sulfate solution adjusted to pH 10 with sodium hydroxide and a mercury/mercurous sulfate reference electrode can be used successfully to differentiate between silver chloride and silver oxide corrosion products.

Coulometric reductions were performed in a standard flat cell (Figure 71) using a Princeton Applied Research 273 potentiostat running CorrWare. The potential at the sample was measured during application of a constant cathodic current density of either -50 µA cm^{-2} or -10 µA cm^{-2}. The working electrode area of the sample was 1 cm^2 and the counter electrode was a 1 in^2 platinum mesh. The reference electrode was either Ag/AgCl or Hg/Hg_2SO_4 (MSE). The electrolyte was either 0.1M KCl or 0.1M Na_2SO_4 adjusted to pH 10 by the drop-wise addition of NaOH. This pH was necessary to decrease the solubility of silver oxide in the Na_2SO_4 electrolyte. The electrolytes were deaerated before reductions for a minimum of one hour by bubbling N_2 through the solutions;

this was required to minimize the amount of dissolved oxygen, which can result in oxygen reduction during measurements. Similarly, an N_2 purge of the flat cell was provided before testing for a minimum of 10 minutes, as well as during reductions.

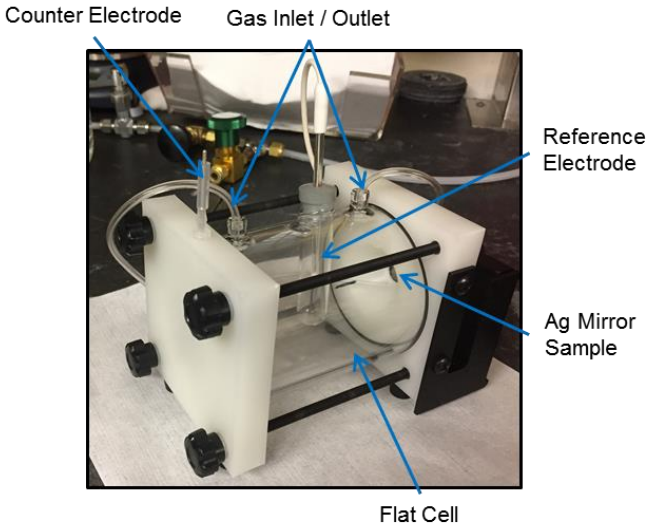

Figure 71. Standard flat cell used for electrochemical testing

Standard coulometric reduction is performed on metallic test samples, as a conductive pathway is required to perform the measurement [106]. By design, the protected silver mirrors in this study have a nonconducting dielectric layer covering the silver layer. As mentioned previously, platinum tabs were deposited beneath the mirror coatings to ensure adequate electrical conductivity to the silver. Electrical connection was made to the Pt tabs by adhesive copper tape. This allowed coulometric reduction to be performed on coated silver films to investigate the corrosion process through pinholes and defects in the dielectric protection layer. Neither the tabs nor the conductive tape was exposed to the electrolyte during the reductions.

In addition to protected silver mirror and bare silver mirror coatings, coulometric reductions were performed on silver foil samples exposed concurrently in the MFG environments.

The silver foil samples were 99.998% purity and approximately 16 × 18 mm in size. Prior to MFG exposure, the foil samples were wet polished with 600 grit SiC paper and then rinsed in methanol.

7.2.4 Galvanic Corrosion

Several electrochemical measurements were performed on the single layer coatings to investigate possible galvanic interactions among the layer materials. The first set of measurements were performed in a standard flat cell in 0.6M NaCl solution with an MSE reference electrode. Polarization curves were measured for single layer coatings of each layer material after monitoring the open-circuit potential (OCP) until it stabilized to ± 1 mV for a minimum of 15 minutes. Cathodic polarization curves were measured by sweeping the potential at 0.1 mV/s from 0.05 V above OCP to 0.3 V below OCP. Anodic polarization curves were measured by sweeping the potential at 0.1 mV/s from 0.05 V below OCP to 0.3 V above OCP.

The galvanic interactions predicted by applying mixed potential theory to the polarization curve measurements were verified by coupling experiments conducted between the silver and each of the materials used for the adhesion and base layers of the mirrors. The coupling experiments were conducted in a modified flat cell in which the counter electrode plate was replaced with a second sample plate, providing a cathode-to-anode area ratio of one. Using an MSE reference electrode, both the coupling potential and current were measured in 0.6M NaCl with the samples connected in zero resistance ammeter (ZRA) mode using a Gamry Reference 600+ potentiostat. The Ag sample was always connected to the working electrode leads; the other material under test was connected to the counter electrode leads. The measurements were performed until the potential stabilized to ±5 mV.

7.3 Results & Discussion

7.3.1 Coulometric Reduction Technique

Figure 72 shows a typical coulometric reduction curve for AgCl on a bare silver mirror coating. AgCl was generated on the bare silver coating by applying a constant anodic current of 0.1 mA/cm^2 in 0.1M KCl for 5 minutes. The reduction was performed at -0.1 mA/cm^2; the duration of the reduction plateau represents a current efficiency of 98%.

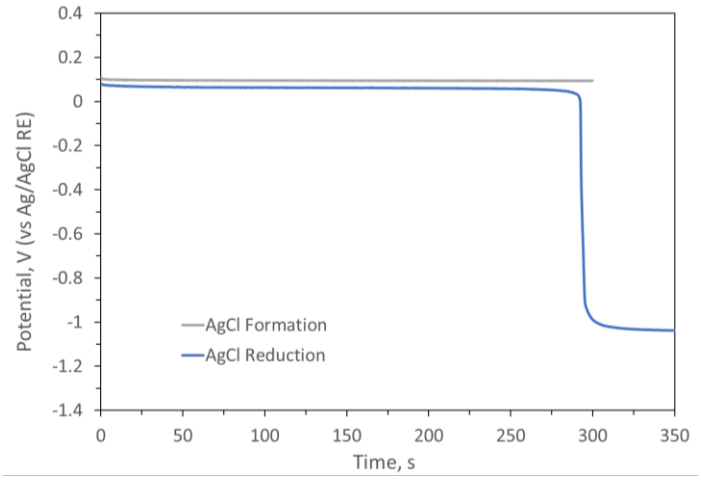

Figure 72. AgCl formation and coulometric reduction on a bare silver mirror coating.

Following successful AgCl formation and reduction on a bare silver coating, a similar test was performed on a no adhesion layer mirror (Figure 73). AgCl was produced via coulometric oxidation in 0.1M KCl at 50 µA/cm^2 for 5 minutes, immediately followed by reduction at -50 µA/cm^2. The AgCl formation and reduction were successful, with similar type and number density of features (Figure 73) as the corrosion features observed on these types of silver mirrors following MFG exposure. The corrosion process appears to initiate at local sites and proceeds laterally outward with time with large portions of the mirror remaining intact and unaffected. The reduction follows this localized corrosion process in reverse, indicating that the coulometric reduction technique can be used to assess corrosion through pinholes and defects in the dielectric protection

layer. The two delamination sites suggest that the corrosion reaction, and reverse reduction process, is occurring underneath the intact SiN_x layer. The transformed silver is no longer layered in structure, as it appears to redeposit as small silver crystallites; thus, the reflective properties of the mirror are reduced in the corrosion regions.

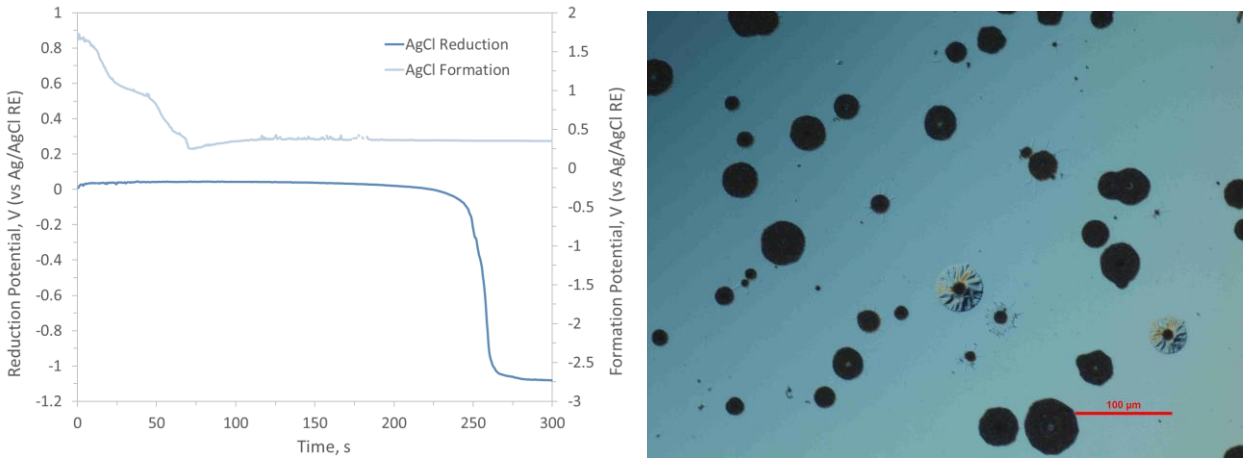

Figure 73. AgCl formation and reduction on a no adhesion layer mirror (left). Optical micrograph of the mirror surface following reduction (right).

As this process is fundamentally different than reduction on a bare metallic silver coating due to the dielectric protection layer, clear differences can be seen in the formation and reduction data. Rather than a constant potential during AgCl formation, the no adhesion layer mirror exhibits a non-linearity at the beginning of the coulometric oxidation. This likely represents the initial time required to push current through the nonconducting dielectric layer to reach the silver and is likely why the reduction plateau exhibits less than 100% current efficiency. Regardless, these data show that this technique can be successfully applied to protected silver mirrors.

For calibration, an AgCl reduction on a bare silver mirror coating in 0.1M Na_2SO_4 is shown in Figure 74. AgCl was produced via coulometric oxidation in 0.1M KCl at 50 µA/cm^2 for 60 seconds, corresponding to a formation charge of 3.0×10^{-3} C cm^{-2}. Coulometric reduction was then performed in 0.1M Na_2SO_4 at -50 µA/cm^2. During reduction, a potential plateau was observed at

-0.28 V MSE before the potential dropped to -1.5 V MSE, the potential for water reduction on Ag under these conditions [12, 17]. AgCl has been shown to correspond to a characteristic potential plateau at -0.28 V MSE [12, 17]. The duration of the plateau was 57 seconds, corresponding to a reduction charge of 2.85×10^{-3} C cm^{-2}, which closely matches the charge passed during AgCl formation. This reduction charge corresponds to an AgCl layer thickness of 76Å, assuming theoretical density. The minor plateau at approximately -0.75 V MSE is due to the reduction of dissolved oxygen in the electrolyte, which was the limiting factor for using lower applied current during the reductions.

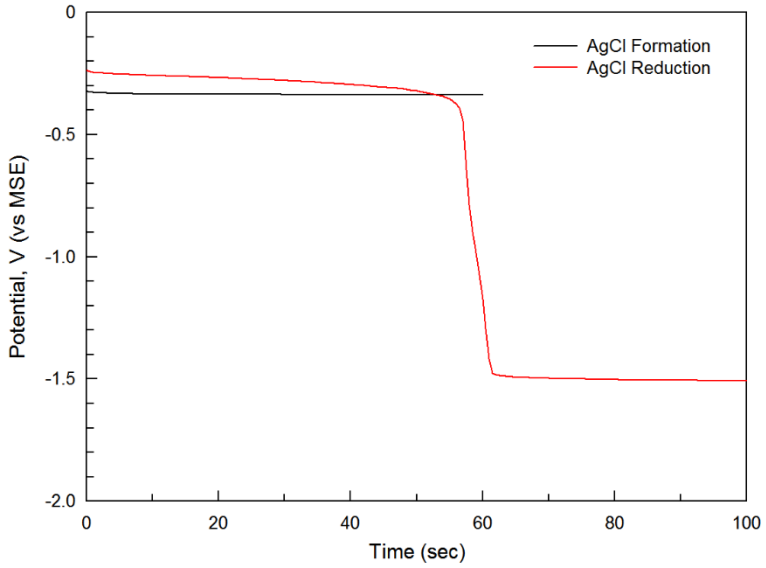

Figure 74. Typical AgCl formation in 0.1M KCl and coulometric reduction in 0.1M Na_2SO_4 on a bare silver mirror coating.

7.3.2 Bare Silver Corrosion Behavior

Bare silver mirrors and silver foil samples were exposed to 10 days of MFG exposure and then subjected to coulometric reduction at -50 µA/cm^2 in 0.1M Na_2SO_4 adjusted to pH 10. After MFG exposure, the silver foil was covered with dark brown corrosion product (Figure 75), while

the bare silver mirror was similarly brown in appearance (Figure 76). The brown color of the corroded surfaces is likely due to silver sulfide.

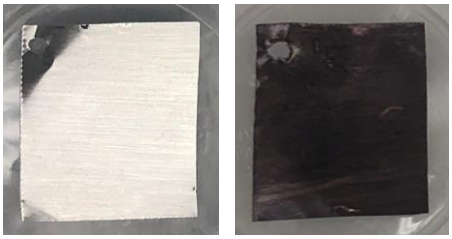

Figure 75. Ag foil sample before (left) and after (right) MFG exposure.

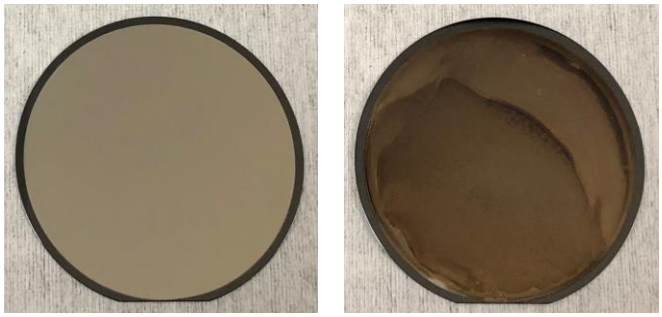

Figure 76. Bare silver mirror coating before (left) and after (right) MFG exposure.

Representative reduction curves are shown in Figure 77. During reductions, potential plateaus were observed at approximately -0.28 V MSE and -1.15 V MSE, corresponding to AgCl and Ag_2S, respectively [12, 17]. During some reductions, small plateaus were observed before the primary AgCl and Ag_2S plateaus. These may be due to differences in crystallography or valence associated with the silver chloride and silver sulfide corrosion products. Different crystal orientations may reduce at different rates. Or, for example, the small plateau near -1.0 V MSE on the silver foil sample may be due to AgS rather than Ag_2S.

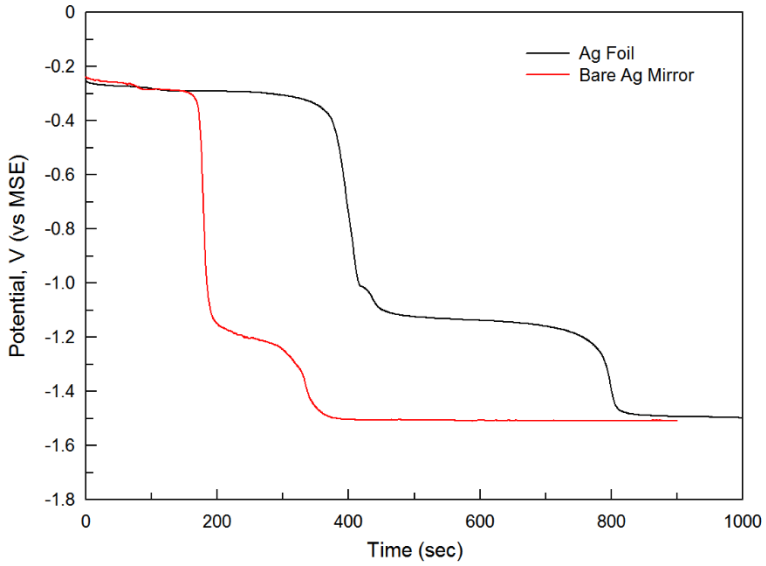

Figure 77. Typical coulometric reduction curves for Ag foil sample and bare Ag mirror coating after MFG exposure.

The durations of both the AgCl and Ag_2S plateaus differed considerably between the silver foil samples and the bare silver mirrors, corresponding to different reduction charges and, thus, different amounts of corrosion products on the surface. This may be due to insufficient cleaning of the silver foil samples prior to MFG exposure, which may have left residual corrosion product on the surface. The differences could also be due to the way the corrosion products develop on the different surfaces, as the microstructure, roughness, and orientation of the foil is very different from the sputtered silver coating.

Reductions on the bare silver mirror coatings represent the upper limit of corrosion product that may develop on protected silver mirrors under the same MFG conditions. In this context, the duration of the silver chloride reduction plateau yields a reduction charge of 9.0×10^{-3} C cm^{-2}, which corresponds to a film thickness of 240Å. The duration of the silver sulfide reduction plateau yields a reduction charge of 7.7×10^{-3} C cm^{-2}, which corresponds to a film thickness of 271Å. These data indicate that chloride and sulfide corrosion chemistries are most important for silver mirror

coatings exposed to the same MFG environments, as no silver oxides, sulfates, or other corrosion products were detected.

Cl_2 and H_2S in the MFG environment potentially participate in the silver corrosion processes through the reactions shown in Equations 4 [13] and 5 [8].

$$Cl_2\ (aq) + 2\ Ag \rightarrow 2\ AgCl \qquad (4)$$

Adsorbed water on the surface dissolves chlorine into the aqueous surface layer, which reacts with the silver to dissolve it and precipitate AgCl upon evaporation [8, 91]. Similarly, the adsorbed water layer dissolves H_2S, which reacts with silver to form Ag_2S [6, 8, 91, 107].

$$2\ Ag + H_2S\ (aq) \rightarrow Ag_2S + H_2\ (g) \qquad (5)$$

Both these reactions highlight the critical role of adsorbed water on the surface, which is a function of relative humidity, in making the ions more readily available to the silver [8, 107]. The contribution of nitrogen dioxide to the corrosion processes on bare silver during MFG exposure is believed to be small [11], though it's possible that NO_2 acts as an oxidant to accelerate Ag_2S or AgCl formation [8].

7.3.3 Effects of Cl_2 on Bare Silver Corrosion Behavior

Bare silver mirrors and silver foil samples were also exposed to 10 days of Cl_2 FG exposure and then subjected to coulometric reduction at -50 $\mu A/cm^2$ in 0.1M Na_2SO_4 adjusted to pH 10. After Cl_2 FG exposure, the silver foil was slightly darkened; the corrosion product was somewhat white in color (Figure 78). The bare silver mirror was still shiny in appearance with areas of white corrosion product around the edge (Figure 79). The white corrosion product is very different than the brown corrosion product observed on the silver surfaces after MFG exposure.

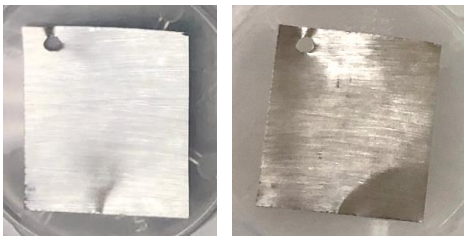

Figure 78. Ag foil sample before (left) and after (right) Cl_2 FG exposure.

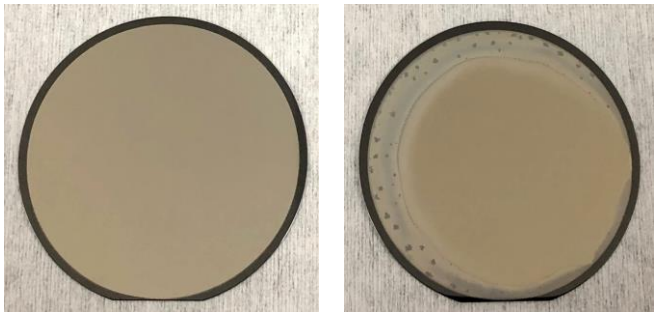

Figure 79. Bare silver mirror coating before (left) and after (right) Cl_2 FG exposure.

Representative reduction curves for reductions performed in the center of the samples are shown in Figure 80. During reductions, potential plateaus were observed at approximately -0.28 V MSE, corresponding to AgCl [12, 17]. Again, the silver foil sample showed substantially more corrosion product on the surface than the center of the bare silver mirror coating.

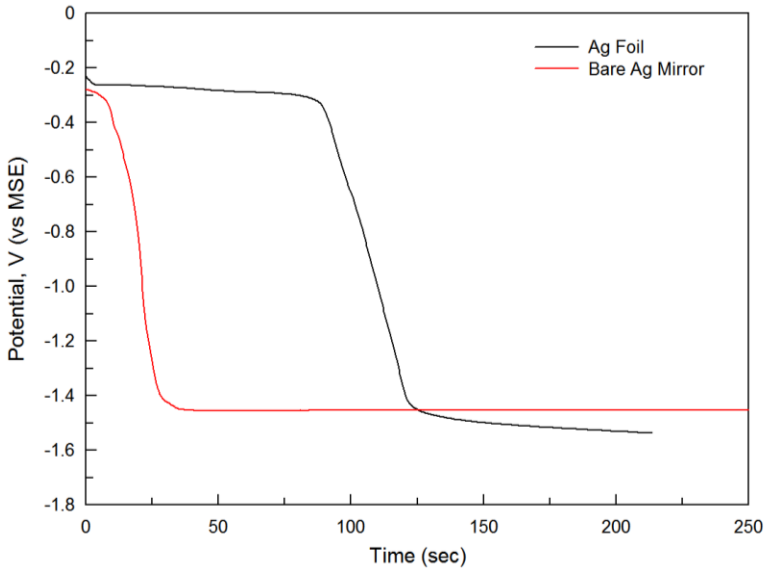

Figure 80. Typical coulometric reduction curves for Ag foil sample and bare Ag mirror coating after Cl_2 FG exposure.

The duration of the AgCl reduction plateau on the bare silver mirror coating corresponds to a reduction charge of 1.0×10^{-3} C cm^{-2}, which represents a film thickness of 27Å. This reduction charge is approximately 11% of the AgCl reduction charge and 6% of the total reduction charge measured on the bare silver mirror coating after MFG exposure. The combination of multiple gaseous pollutants during MFG exposure clearly accelerates silver corrosion compared to the single FG environments; the synergistic effects of Cl_2 and H_2S are believed to cause the significantly accelerated corrosion process. During Cl_2 FG exposure, the AgCl film likely forms relatively uniformly, creating a transport barrier to reactants that slows corrosion as film thickness increases. During MFG exposure, Ag_2S and AgCl form concurrently, with the Ag_2S likely disrupting the AgCl film and resulting in a defective surface film of both silver sulfide and chloride. A defective film allows easier transport of reactants, increasing the corrosion rate and leading to more corrosion product on the surface.

7.3.4 Protected Silver Mirror Corrosion Behavior

Protected silver mirrors were exposed to 10 days of MFG exposure and then subjected to coulometric reduction at -10 μA/cm^2 in 0.1M Na_2SO_4 adjusted to pH 10. Corrosion was apparent on the surfaces of the mirrors following MFG exposure and resulted in reductions in optical properties, as shown in previous chapters. However, corrosion product was not detected on most of the mirrors during coulometric reductions, as shown in Figure 81. Even with the lower applied current density, only the no adhesion layer mirror showed a small reduction plateau at -1.17 V MSE, corresponding to Ag_2S [12, 17]. The duration of this plateau yields a reduction charge of 4.0×10^{-4} C cm^{-2}, which corresponds to a film thickness of 14Å. This small amount of Ag_2S corrosion product may indicate that H_2S is more important than Cl_2 in the corrosion process. However, AgCl may also have been present but was at too low a level to be detected under these experimental conditions. Similarly, the other protected silver mirrors had too little corrosion product to be detected under these reduction conditions. It's possible that AgCl on these mirrors was photo-reduced during or after MFG exposure prior to coulometric reduction [17].

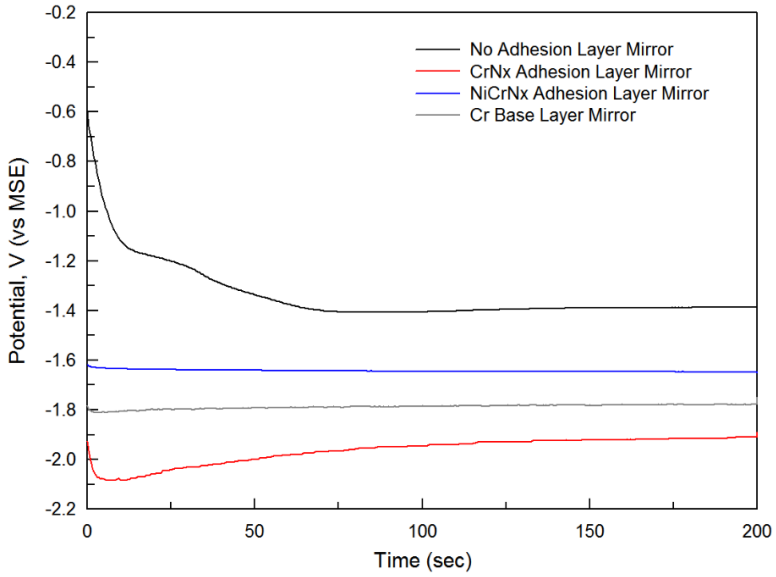

Figure 81. Typical coulometric reduction curves for protected silver mirrors after MFG exposure.

All four designs of protected silver mirrors significantly reduced the amount of corrosion product on the surface compared to bare silver mirrors subjected to MFG exposure. The reduction charge measured on the no adhesion layer mirror was 5% of that measured on the bare silver mirror, providing a quantifiable upper limit to the effectiveness of the protection layer schemes. Corrosion products on the mirrors with adhesion layers were not detectable. At -10 µA/cm^2, a 5 second reduction plateau corresponds to a reduction charge of 1×10^{-4} C cm^{-2} and a film thickness of just 1.3Å. The inability to detect corrosion product via coulometric reduction at these settings indicates that the total amount of corrosion product on the mirrors with adhesion layers is very small; the protection layer schemes reduce corrosion and degradation of the silver layer to less than 1% of that observed on bare silver mirrors.

Protected silver mirrors were also exposed to 10 days of Cl_2 FG exposure and then subjected to coulometric reduction at -10 µA/cm^2 in 0.1M Na_2SO_4 adjusted to pH 10. And again, while corrosion and degradation were apparent on the surfaces of the mirrors following Cl_2 FG

exposure, as shown in previous chapters, corrosion product was not detected on the mirrors during coulometric reductions (Figure 82). While coulometric reduction is very sensitive to small amounts of corrosion products [17], the protected silver mirror designs reduced corrosion to a level that was undetectable by this technique at these settings.

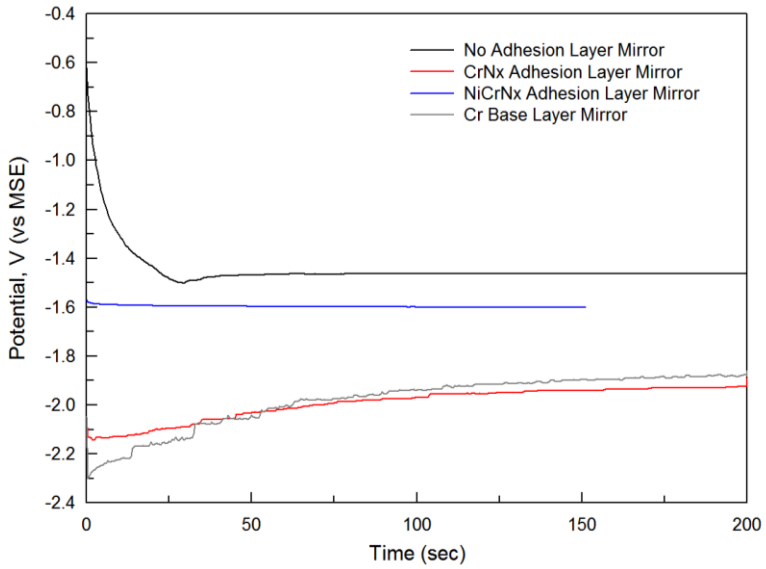

Figure 82. Typical coulometric reduction curves for protected silver mirrors after Cl_2 FG exposure.

7.3.5 Polarization Behavior of Layer Materials

Polarization curves for a bare silver mirror coating in 0.6M NaCl are shown in Figure 83. Potential, *E*, vs. log *i* (current density) plots display the cathodic and anodic reaction kinetics. Conservation of charge requires that all electrons produced in oxidation reactions are consumed in reduction reactions when no external voltage is applied; therefore, the corrosion potential (E_{corr}) is defined where the anodic and cathodic rates are equal, and the applied current density is zero. E_{corr} of the silver coating is -0.5 V MSE.

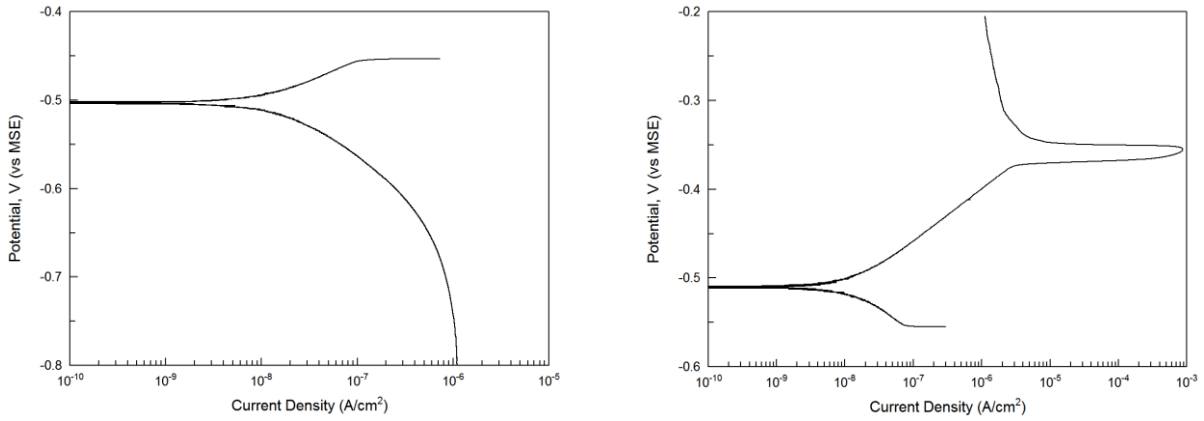

Figure 83. Typical cathodic (left) and anodic (right) polarization curves for Ag.

Polarization curves for NiCr and $NiCrN_x$ single layer coatings in 0.6M NaCl are shown in Figure 84 and Figure 85, respectively. E_{corr} of the NiCr coating is -0.67 V MSE; E_{corr} of the $NiCrN_x$ coating is -0.65 V MSE.

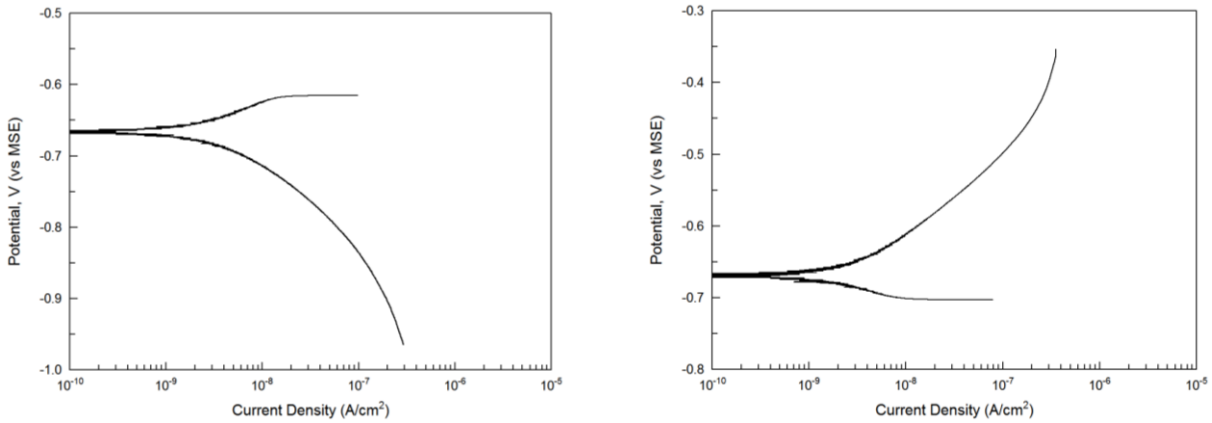

Figure 84. Typical cathodic (left) and anodic (right) polarization curves for NiCr.

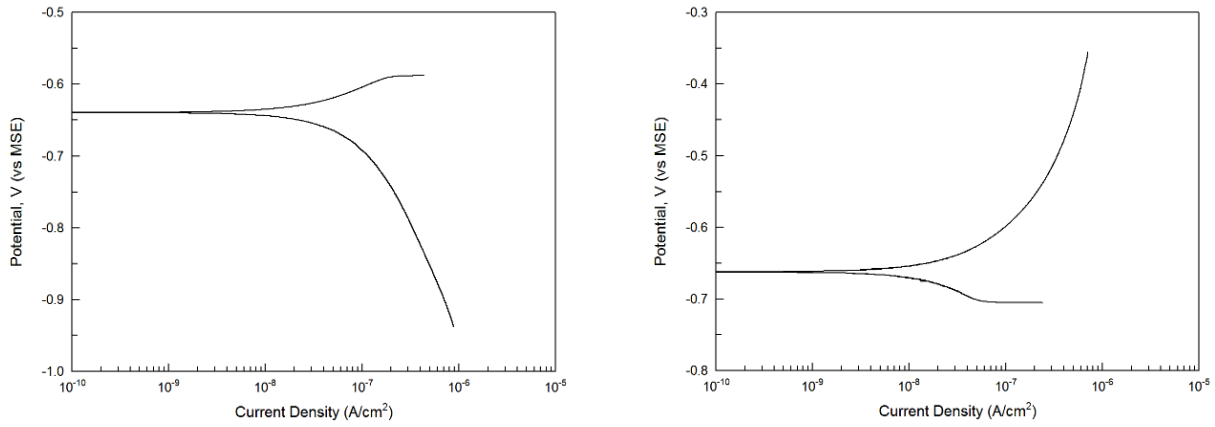

Figure 85. Typical cathodic (left) and anodic (right) polarization curves for $NiCrN_x$.

Polarization curves for a CrN_x single layer coating in 0.6M NaCl are shown in Figure 86. E_{corr} of the CrN_x coating is approximately -0.35 V MSE. Variation in E_{corr} between the cathodic and anodic polarization curves may be due to minor changes in the cathodic reaction that move OCP substantially, as suggested by the flat portion of the anodic curve. The sharp rise of the anodic curve may indicate the CrN_x coating passivates quickly.

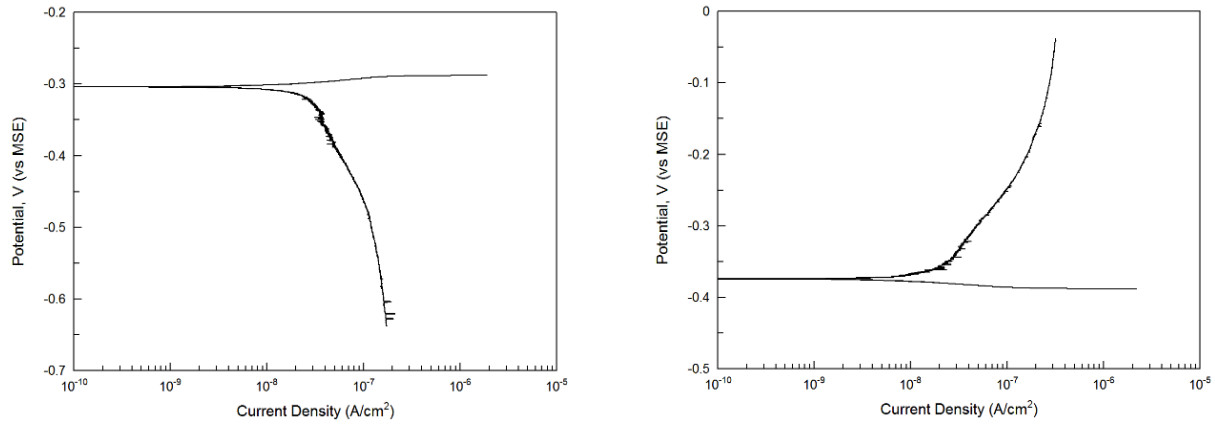

Figure 86. Typical cathodic (left) and anodic (right) polarization curves for CrN_x.

Polarization curves for Cr single layer coatings in 0.6M NaCl are shown in Figure 87. E_{corr} of the Cr coating is approximately -0.55 V MSE. Obtaining repeatable polarization measurements for Cr was difficult as the coatings oxidized quickly once removed from the deposition chamber;

minimizing the time between venting the deposition chamber and performing the polarization measurements was critical. Anodic polarization data for a freshly-deposited Cr coating (approximately 10 minutes from chamber to measurement) is shown; also shown is an anodic curve for a Cr coating that had first been subjected to cathodic polarization, and thus spent one day between chamber and polarization measurement; an anodic curve for a Cr coating that was stored in air for 6 weeks is also shown. The increase of E_{corr} with time between deposition and anodic polarization measurement indicates that the Cr coating quickly forms a protective oxide surface.

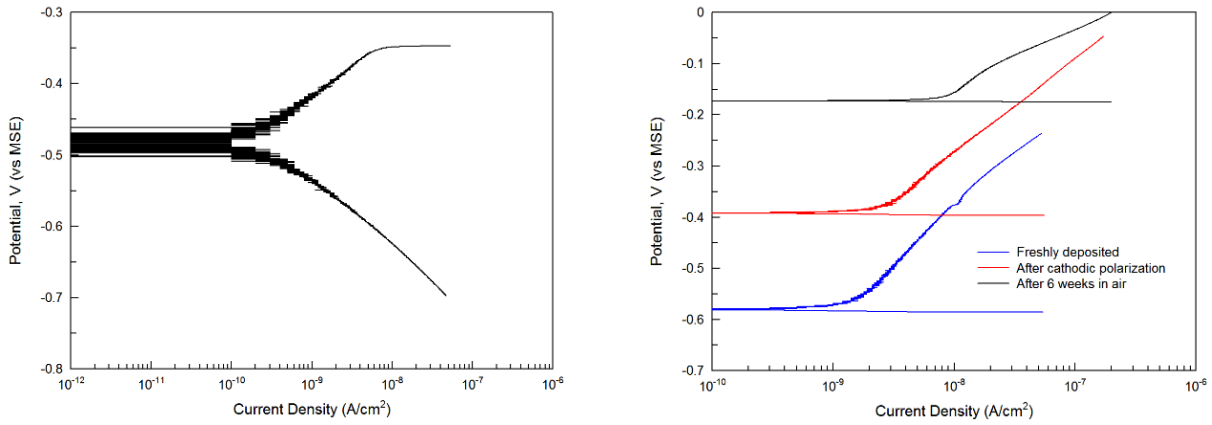

Figure 87. Typical cathodic (left) and anodic (right) polarization curves for Cr.

Polarization curves for a SiN_x single layer coating in 0.6M NaCl are shown in Figure 88. No polarization response is observed, indicating that the SiN_x is not expected to participate in galvanic interactions with the other layer materials.

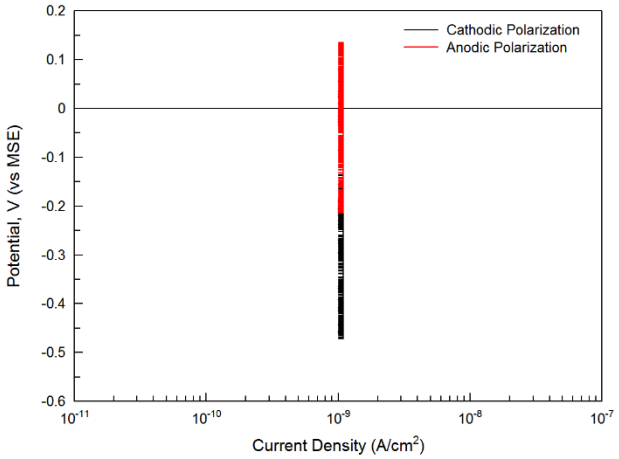

Figure 88. Typical cathodic and anodic polarization curves for SiN_x.

7.3.6 Galvanic Interactions in Layer Materials

The galvanic series derived from the polarization curves presented in the previous section is shown in Table 8. This galvanic series indicates that Ag is more noble than NiCr, $NiCrN_x$, and freshly-deposited Cr. When these materials are coupled with Ag, they could serve as sacrificial anodes to reduce the Ag corrosion rate. However, these materials may not be good sacrificial anodes if they are easily passivated. The variation observed with the Cr polarization measurements suggests that this may occur with Cr layers in the full mirror coating stack, and therefore Cr may not protect Ag. The galvanic series also indicates that CrN_x is more noble than Ag and would not protect the Ag when coupled to it.

Table 8. Galvanic Series for Layers of Protected Silver Mirrors

Single Layer	**E_{corr} (V vs. MSE)**
CrN_x	-0.35
Ag	-0.50
Cr	-0.55
$NiCrN_x$	-0.65
NiCr	-0.67
SiN_x	--

Mixed potential theory indicates that coupled materials will come to the same potential and pass the same magnitude of current during corrosion. Therefore, coupling experiments were conducted between Ag and each of the other layer materials to verify the galvanic series derived from the polarization measurements. Coupling potential and current density for the Ag / NiCr couple is shown in Figure 89, along with overlays of the polarization curves. Similar data is shown for the Ag / $NiCrN_x$ couple in Figure 90. The polarization curves for both couples suggest that both NiCr or $NiCrN_x$ may protect the Ag and reduce its corrosion rate. However, in both coupling experiments, the potential increases to nearly E_{corr} of Ag and the corresponding current density drops into the nanoamp regime. This suggests that the passivation of either NiCr or $NiCrN_x$ prevents these materials from significantly affecting the Ag dissolution rate at a cathode-to-anode area ratio of one.

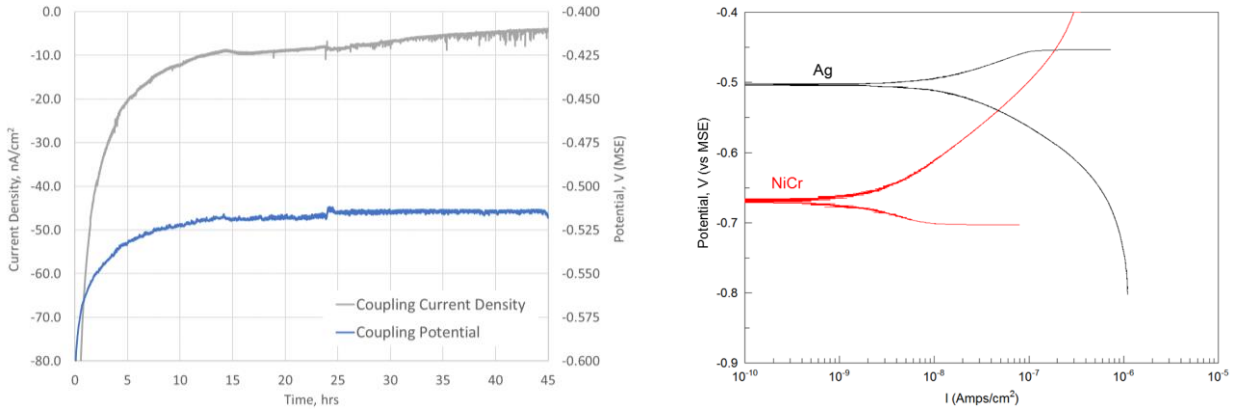

Figure 89. Coupling potential and current density of Ag / NiCr couple (left). Overlay of respective polarization curves (right).

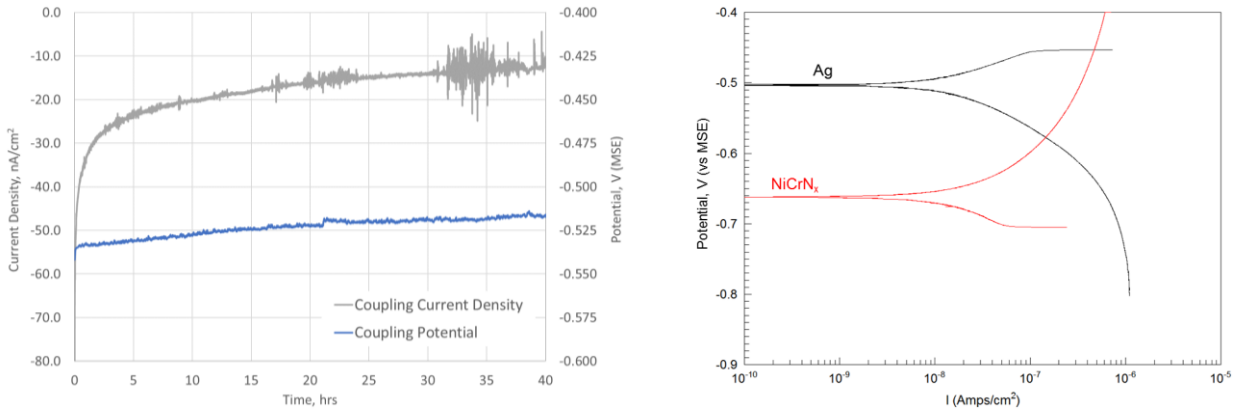

Figure 90. Coupling potential and current density of Ag / $NiCrN_x$ couple (left). Overlay of respective polarization curves (right).

Coupling potential and current density for the Ag / CrN_x couple is shown in Figure 91, along with overlays of the polarization curves. As expected by the galvanic series, the coupling current density is positive, opposite the polarity of the Ag / NiCr and Ag / $NiCrN_x$ couples, indicating that CrN_x is cathodic to Ag. Even so, the coupling potential approaches E_{corr} of Ag and the corresponding current density drops below 10 nA, suggesting that the dissolution of Ag occurs close to E_{corr} of Ag and the dissolution rate is not significantly increased when coupled to CrN_x.

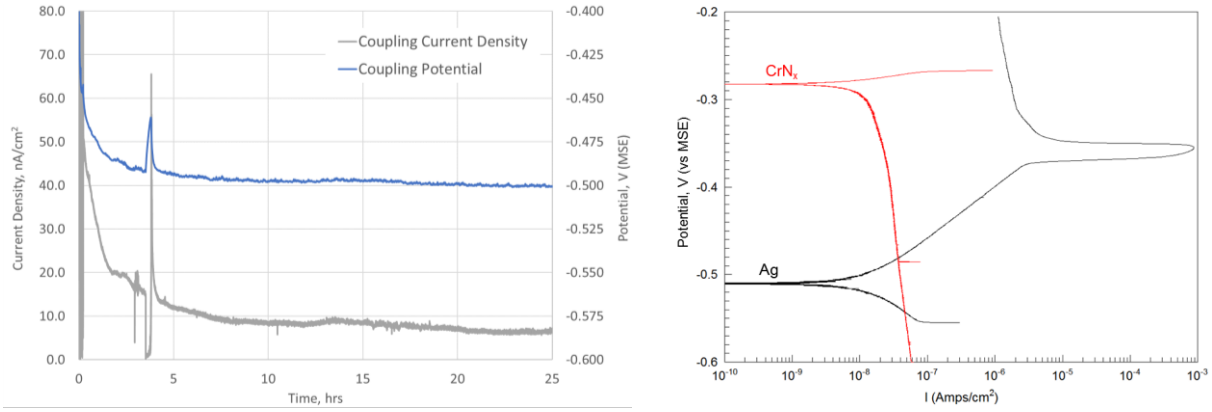

Figure 91. Coupling potential and current density of Ag / CrN_x couple (left). Overlay of respective polarization curves (right).

Finally, coupling potential and current density for the Ag / Cr couple is shown in Figure 92, along with overlays of the polarization curves. Initially, the coupling current density is

negative, corresponding to the freshly-deposited Cr anodic to Ag; however, it appears that Cr passivates upon exposure to the electrolyte, such that Cr becomes cathodic to Ag. This corresponds with the variation observed in the polarization curve measurements and suggests that Cr easily passivates and therefore may not act as a sacrificial anode to Ag.

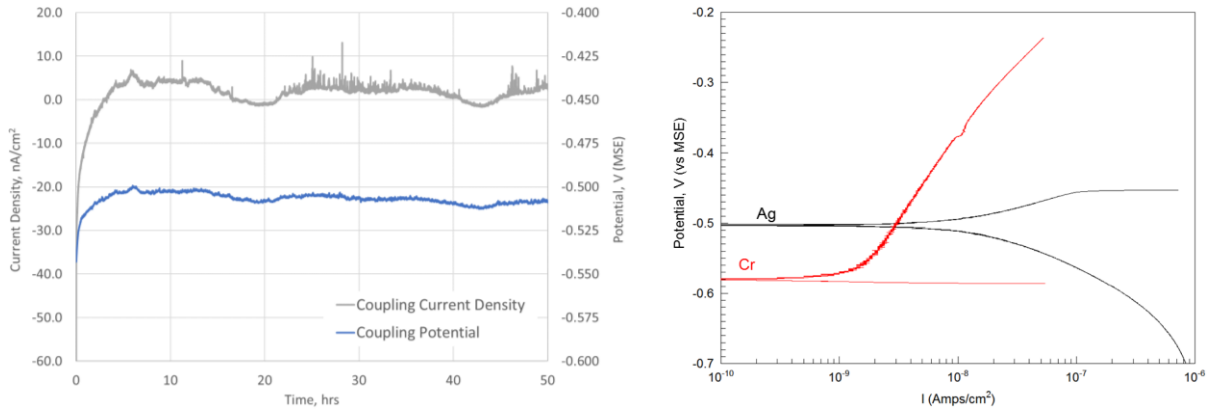

Figure 92. Coupling potential and current density of Ag / Cr couple (left). Overlay of respective polarization curves (right).

7.3.7 Protected Silver Mirror Corrosion Processes and Galvanic Interactions

In previous chapters, it was shown that corrosion features in the protected silver mirrors originate at small defects in the protective dielectric layer and grow laterally along various layer interfaces, only sometimes resulting in significant attack and disruption of the silver layer. The development and growth of the corrosion features is highly dependent on the composition of the layers on either side of the silver. Nickel in both layers adjacent to the silver limits the interfacial corrosion process but results in localized attack of the silver layer itself. In contrast, mirrors with one chromium-based layer adjacent to the silver develop large circular corrosion features at the Ag-Cr interfaces, driven by oxidation, chloridation, and sulfidation at the interface. The galvanic interactions described in the previous section suggest that differences in the electrochemical

behavior between the Ag-Cr and Ag-NiCr interfaces affect the mechanisms of corrosion feature development and growth.

The galvanic interactions predicted by Ag / CrN_x and Ag / Cr coupling measurements suggest that Ag is not protected by either CrN_x, as it is more noble, or Cr, once it passivates. This suggests that in mirrors with one Cr-based layer adjacent to the silver, as the corrosion reaction proceeds along the silver-chromium interface, dissolution of Ag occurs. However, the measured coupling currents were small, and the coupling potentials approached E_{corr} of Ag, such that the Ag dissolution rate is likely not significantly increased by the adjacent Cr or CrN_x.

Circular corrosion regions on the CrN_x adhesion layer mirror during standard MFG exposure are shown in Figure 93. As corrosive species enter the coating through small defects in the SiN_x layer, the CrN_x polarizes the Ag, resulting in Ag dissolution. This dissolution likely leads to reduced adhesion at the Ag–CrN_x-SiN_x interface, which would provide a mechanism for the compressive SiN_x layer to peel away from the Ag layer below. It was previously indicated that adhesion and layer stress may be important for the growth of these circular corrosion regions. The compressive SiN_x layer may contribute to the expansion of the circular corrosion regions through a stress corrosion mechanism. Ag dissolution at the edge of the circular corrosion region reduces adhesion, allowing the stress in the SiN_x layer to propagate a crack at the Ag–CrN_x-SiN_x interface.

To understand the extent to which stress impacts the growth rate of the circular corrosion regions, the penetration rate, *PR*, of Ag dissolution was determined from the measured coupling current density, *i* (less than 10 nA/cm^2), according to Faraday's Law of Electrolysis.

$$PR = \frac{iM}{nF\rho} \qquad (6)$$

where M is the molar mass, n is the valency change (i.e. the number of electrons transferred per ion), F is Faraday's constant, and ρ is the density. A corrosion rate of 10 nA/cm^2 corresponds to

a penetration rate of 1.1×10^{-8} µm/s. Therefore, it would take 300 years for Ag dissolution alone to result in a 100 µm-radius circular corrosion region. Clearly, the circular corrosion regions do not develop entirely due to dissolution of Ag at the interface. The dissolution of even a monolayer of Ag at the interface, combined with stress in the SiN_x layer, may be enough to reduce the interfacial adhesion and increase the growth rate of the circular corrosion regions.

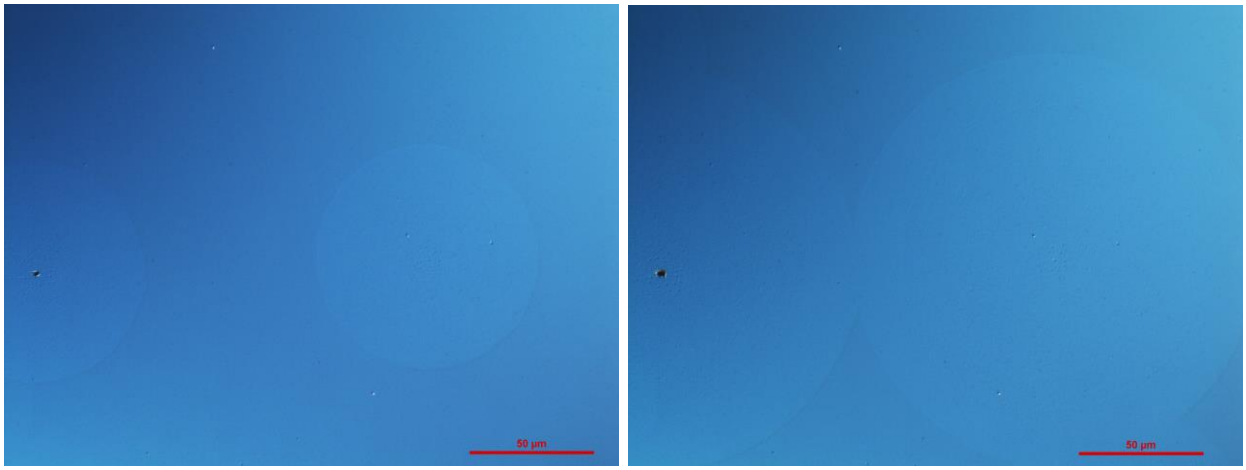

Figure 93. Optical micrographs of circular corrosion regions on the CrN_x adhesion layer mirror after 5 days (left) and 10 days (right) of MFG exposure.

A similar circular corrosion region on the Cr base layer mirror after standard MFG exposure is shown in Figure 94. As the corrosion reaction proceeds along the Cr-Ag interface, Cr may initially be anodic to Ag. However, upon exposure to corrosive species, including moisture, Cr likely passivates, thus becoming cathodic to Ag. As in the CrN_x adhesion layer mirror, this likely results in Ag dissolution, reduced adhesion at the Cr-Ag interface, and the development of the circular corrosion regions. The combination of Ag dissolution and stress in the SiN_x and Cr layers increases the rate of the corrosion process.

The development of the delamination blisters within the circular corrosion regions on the Cr base layer mirror is believed to be related to the Ag dissolution process. When the mirrors are removed from the MFG environment at 2 to 3-day intervals for characterization, the humidity and

temperature decrease considerably. This results in precipitation of corrosion product within the circular corrosion regions. Increased volume associated with the precipitated corrosion product may initiate the SiN_x buckling process that results in the delamination blisters [96].

Figure 94. Optical micrographs of circular corrosion regions on the Cr base layer mirror after 10 days of MFG exposure.

In contrast, the galvanic interactions predicted by Ag / NiCr and Ag / $NiCrN_x$ coupling indicate that NiCr and $NiCrN_x$ will cathodically protect Ag. This suggests that in mirrors with NiCr-based layers adjacent to the silver, corrosive attack of the NiCr or $NiCrN_x$ layers may be enhanced. However, these layers may instead passivate, which would interrupt any sacrificial protection provided to the Ag. To investigate this, a small corrosion nodule, similar to that shown in Figure 95, was cross-sectioned for analysis; these small corrosion nodules, on the order of 5 µm in diameter, provide information on the initial aspects of the corrosion process. In contrast, the cross-sectional data presented in Chapter 3 showed a much larger corrosion nodule of 40 µm in diameter, which was much further along in the corrosion process. This larger nodule was too extensively corroded to ascertain which corrosion processes occur first.

Figure 95. Optical micrographs of a corrosion nodule on the $NiCrN_x$ adhesion layer mirror after 10 days of MFG exposure.

An SEM micrograph of a small corrosion nodule is shown in Figure 96. The characteristic central silver agglomerate is apparent, surrounded by a small circular corrosion region. The two lobes of dark material are corrosion product. The white line in Figure 96 marks the location of the FIB cross-section, an SEM micrograph of which is shown in Figure 97; this image was taken during the FIB thinning and preparation process. The contrast in the micrographs indicates that the silver layer is largely intact and that the characteristic silver agglomerate is starting to form below the intact Ag layer. The material below the Ag layer contains corrosion product with numerous voids. To the right of the Ag agglomerate, the Ag layer appears disrupted and this may be the entry point for corrosive species, as well as the exit point for the corrosion product that appears to the right on top of the coating.

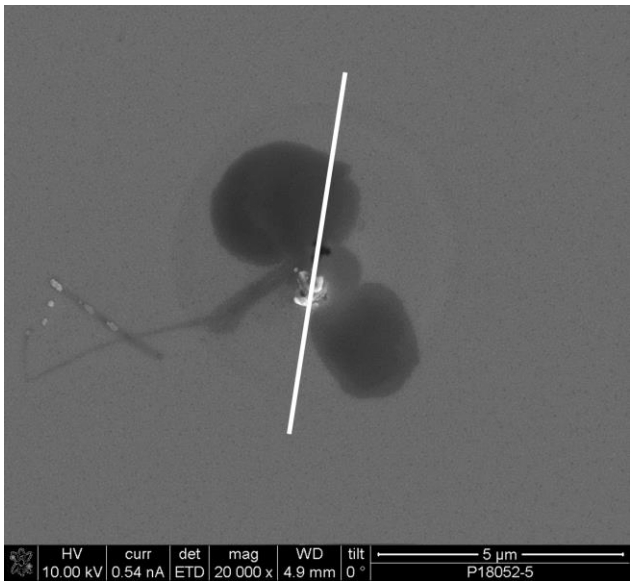

Figure 96. SEM micrographs during FIB preparation of a corrosion feature on the $NiCrN_x$ adhesion layer mirror after MFG exposure. The white line marks the location of the TEM cross-section.

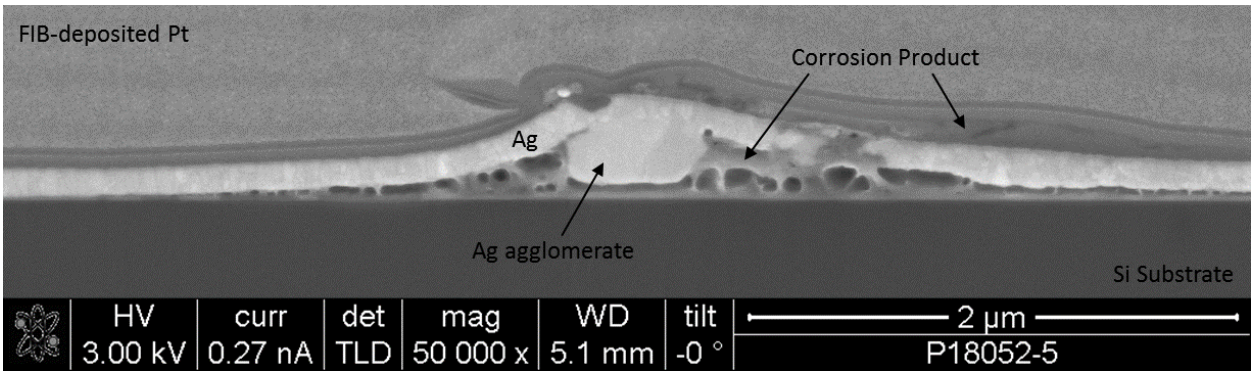

Figure 97. SEM micrographs during FIB preparation of a corrosion feature on the $NiCrN_x$ adhesion layer mirror after MFG exposure.

During FIB preparation of the cross-section, thinning required that additional material be removed, resulting in the final TEM cross-section shown in Figure 98. This image corresponds with the SEM micrograph shown in Figure 97, but represents a different vertical slice of the corrosion feature. Again, the Ag layer is mostly intact, with several large Ag agglomerates apparent, indicating that attack of the Ag has begun. The NiCr base layer is also somewhat intact, though regions of depletion are apparent. EDS maps of the cross-section are provided in Figure

99. These maps indicate that the network of corrosion product below the Ag layer contains nickel, chromium, oxygen, and chlorine. Whereas, the corrosion product on top of the intact SiN_x layer is largely nickel, oxygen, and chlorine; no significant chromium was detected above the SiN_x. The regions of depletion in the NiCr base layer correspond to nickel depletion and chromium enrichment. Notably, the Ag layer does not show substantial corrosion product, even though it has been attacked, as redistribution and transport of the Ag is apparent, including some sulfide corrosion product above the coating.

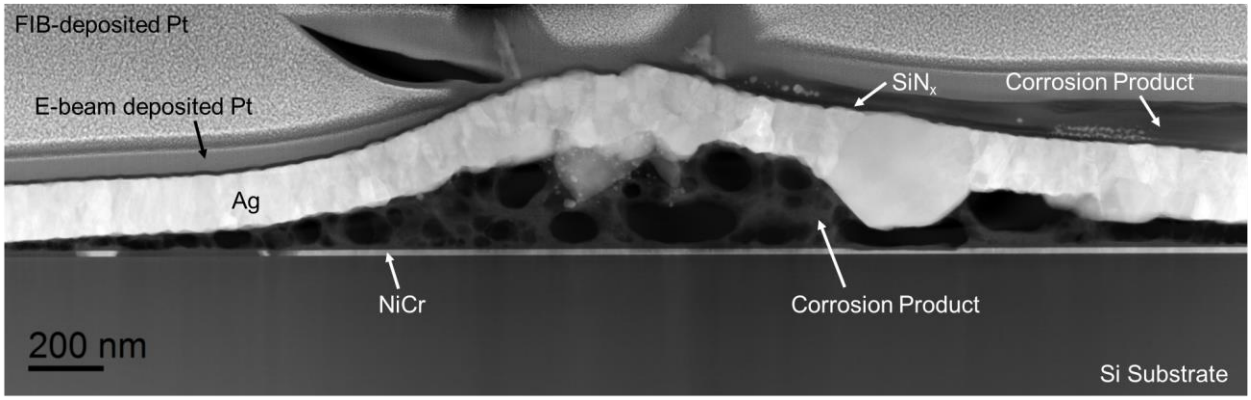

Figure 98. ADF image of cross-section of small corrosion feature on $NiCrN_x$ adhesion layer mirror.

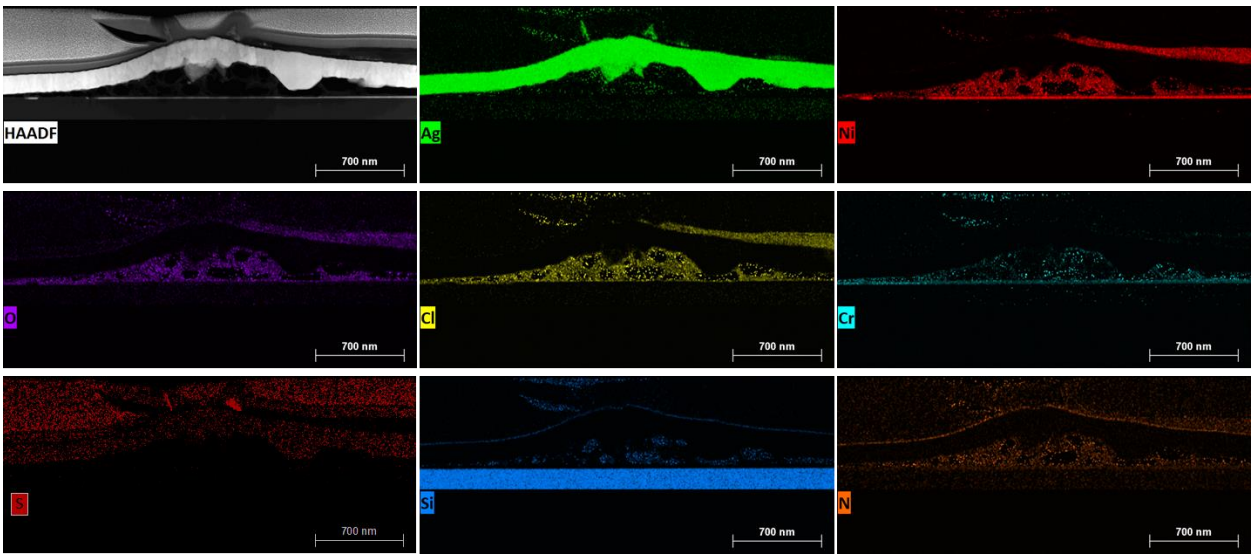

Figure 99. EDS maps of Ag, Ni, O, Cl, Cr, S, Si, and N in the corrosion feature.

These data suggest that the NiCr base layer is substantially corroded before extensive attack of the Ag layer occurs. The nickel in the NiCr layer appears to more readily mobilize under the influence of the moisture, dissolved chlorine, and other corrosive species that enter the coating during MFG exposure. The chromium is also attacked, though less extensively. It's possible that nickel chlorides and oxides drive the initial corrosion process. This may explain why the $NiCrN_x$ adhesion layer mirror experienced extensive corrosion during the Cl_2 FG exposure, as shown in Chapter 5.

Overall, these data are consistent with the galvanic coupling results that indicated that NiCr and $NiCrN_x$ act as cathodic protection to the silver. The fact that the Ag layer is also attacked is not inconsistent with this behavior. A material can be cathodically protected as the cathode in a galvanic couple and still be corroded to some extent. Any decrease in the natural Ag corrosion rate due to coupling with NiCr or $NiCrN_x$ would be dependent on the cathode to anode area ratio, which is possibly very different in the actual mirror coatings than it was in the coupling experiments (1:1).

As corrosive species enter the coating through defects in the SiN_x layer, the $NiCrN_x$ adhesion layer is likely attacked, as is the top of the silver layer. The dynamics and kinetics of this process are not entirely clear from these data; it's possible that the $NiCrN_x$ is exhausted or passivated, or that the nickel-silver interaction improves adhesion to prevent stress corrosion cracking at the Ag–$NiCrN_x$-SiN_x interface. It's also possible that attack of the Ag through the thickness of the layer may occur quickly enough to compete with lateral penetration of the corrosion reaction at the Ag–$NiCrN_x$-SiN_x interface. Regardless, once the corrosive species reach the NiCr base layer, a larger amount of NiCr is available to protect the Ag layer, which it appears to readily do, as suggested by the TEM and EDS data.

7.4 Conclusions

Multiple electrochemical techniques were applied to protected silver mirror coatings to investigate the controlling factors in the mirror corrosion processes. Coulometric reduction was utilized to identify and quantify the corrosion products on the silver mirrors following accelerated environmental exposure. While this technique is very sensitive to a small amount of corrosion product, corrosion could not be detected on any of the protected silver mirrors that included adhesion layers. Only a small amount, equivalent of 14Å, of silver sulfide was detected on the no adhesion layer mirror following MFG exposure. These data demonstrate just how durable these Gemini-style protected silver mirrors are. The small amount of corrosion products on these mirrors is much less than what corrosion scientists are typically concerned with. However, even with less than 1.3Å of corrosion product (the limit of detection in the current experiment), the corrosion processes are enough to degrade optical performance in these mirrors. Ensuring long-term durability of silver mirrors, therefore, requires preventing extremely small quantities of corrosion.

Bare silver mirrors and silver foil samples were also subjected to coulometric reduction following accelerated environmental exposure to further investigate the active corrosion mechanisms in these mirrors. The reductions showed that chloride and sulfide corrosion chemistries are most important for these mirrors during MFG exposures, as no oxides or sulfates were detected. Cl_2 and H_2S are believed to dissolve in the adsorbed water layer on the surface of the mirrors and react with the silver to produce AgCl and Ag_2S. While silver sulfide is the most common form of tarnish generally observed on silver surfaces [8], the susceptibility of silver to chloridation in the MFG environment is a significant concern for these mirrors.

Galvanic interactions among the layers of the protected silver mirror coatings were investigated by polarization curve measurements and verified by galvanic coupling measurements. The resulting galvanic series indicated that NiCr, $NiCrN_x$, and freshly-deposited Cr are less noble than Ag, and therefore available to provide cathodic protection to the Ag. However, the coupling experiments showed that these materials may easily passivate, making them less available to provide protection. On the other hand, CrN_x was found to be more noble than Ag, and therefore not available to protect the Ag to begin with.

These galvanic interactions suggest that differences in the electrochemical behavior of the Ag-Cr and Ag-NiCr interfaces in the protected silver mirrors affect the mechanisms of corrosion feature development and growth. In CrN_x adhesion layer mirrors and Cr base layer mirrors, the more noble CrN_x and the easily-passivated Cr layers do not protect the Ag. Therefore, Ag dissolution occurs at the interface, reducing adhesion, and allowing stress in the coatings to propagate cracks at the interface, leading to the characteristic circular corrosion regions. The growth rate of the circular corrosion regions is significantly quicker than what would be expected from Ag dissolution alone. In $NiCrN_x$ adhesion layer mirrors, NiCr and $NiCrN_x$ appear to provide cathodic protection to the silver as nickel is readily mobilized under the influence of moisture, dissolved chlorine, and other corrosive species. While the dynamics and kinetics of the nickel-silver interaction at the Ag–$NiCrN_x$-SiN_x interface are not entirely clear, the $NiCrN_x$ adhesion layer prevents substantial attack at the interface. The dissolution of silver through the thickness of the layer thus occurs quickly enough to compete with any lateral penetration of the corrosion reaction. Once corrosive species reach the NiCr base layer, a larger amount of nickel is available to protect the silver, which it appears to readily do. Though, ultimately, the silver is attacked as well, leading to the characteristic corrosion nodules.

The dynamics and kinetics of the corrosion process in these mirrors are a combination of multiple factors largely controlled by the composition of the layers adjacent to the silver. As these layers are passivated or consumed, Ag dissolution occurs throughout the corrosion process. Reduced adhesion and stress are, therefore, believed to play a significant role. However, the electrochemical behavior of the layers on either side of the silver layer substantially controls the corrosion process.

Chapter 8. Conclusions

The mechanisms of corrosion and degradation in Gemini-style protected silver mirrors has been shown to depend largely on the composition of the layers on either side of the silver layer. The corrosion process originates at small defects in the dielectric protection layers and proceeds into the coating structure, laterally along various layer interfaces, and only sometimes results in significant layer disruption and silver corrosion. The morphology of the corrosion features, the extent of layer disruption, and the corresponding degradation in optical properties, varies significantly based on the layers adjacent to the silver layer. While the adhesion layer influences the initial corrosion behavior, the base layer below the silver also significantly affects the ensuing corrosion process and corrosion feature development and growth.

Accelerated environmental exposure of various protected silver mirror designs was used to investigate the underlying causes of corrosion and degradation in these mirrors. Mixed flowing gas exposure provided an accelerated testing environment to simulate the kinetics and degradation mechanisms of long-term air exposure. A variety of characterization techniques were utilized to investigate the optical properties, corrosion feature structure, and chemical composition of the exposed mirrors. Mirrors with various adhesion and base layer compositions, as well as mirrors with a variety of stress and nanostructural changes were evaluated. Electrochemical corrosion behavior was also investigated through the development of multiple electrochemical techniques to assess how the different layers contribute to the corrosion processes that occur.

Mirrors with no adhesion layer were shown to develop large circular corrosion regions along the silver-dielectric interface, leading to delamination of the protective SiN_x from the silver. Limited attack of the silver layer kept the layered structure of the mirror largely preserved. Similar corrosion behavior was observed on the CrN_x adhesion layer mirror, which developed similar large

circular corrosion regions. Though delamination of the SiN_x did not occur in these mirrors, rather limited attack of the silver layer resulted in a small amount of silver voiding and subsurface silver transport. The interfacial degradation and the attack of the silver layer itself are two competing processes that influence the development and growth of the corrosion features.

On the $NiCrN_x$ adhesion layer mirror, much smaller corrosion nodules formed that were significantly more disruptive to the layered structure of the coating as the silver layer was directly attacked. The $NiCrN_x$ adhesion layer prevented interfacial degradation along the silver-dielectric interface, enabling attack of the silver and eventually of the silver-base layer interface. In the $NiCrN_x$ adhesion layer mirror, this resulted in limited attack at the lower silver interface but extensive attack of the silver. In the Cr base layer mirror, this resulted in limited attack of the silver, but large circular corrosion regions formed along the lower Ag-Cr interface. The corrosion and dissolution that occurred along this interface reduced adhesion and resulted in the development of delamination blisters. The differences in corrosion feature morphology are a direct result of the roles the upper and lower silver interfaces play in the corrosion processes.

Corrosive species were shown to enter the coating through small defects in the dielectric protection layer. Initial corrosion feature development occurred at pre-existing coating spit defects in the SiN_x layer, as the thickness of the protective layer was inadequate below spits deposited early in the deposition process. This allows moisture that has adsorbed on to the mirror surface to enter the coating structure. The adsorbed water layer dissolves corrosive species that then enter and react with the layers of the coating. The development and growth of the resulting corrosion features depends on the interaction of the layer materials with these dissolved reactants. The corrosion process is, at least in part, a defect-mediated process, with porosity and defects controlling initial corrosion feature development.

Once the corrosive species enter the coating layers, dissolution and corrosion occurs. The compositions of the adhesion layer and the base layer influence the degradation process. In the CrN_x adhesion layer mirror, the growth of the large circular corrosion regions did not disrupt the layered structure of the silver, thereby preserving the optical properties of the mirror. Whereas in the Cr base layer mirror the development of delamination blisters within the circular corrosion regions that developed along the Ag-Cr interface reduced the optical performance of this mirror. The difference in properties occurs due to the different vertical location of the chromium-based layer within the layered structure of the mirror coating. The development of the circular corrosion regions in both these mirrors was shown to be related to the oxidation and chloridation of the silver and chromium at the Ag-Cr interfaces. The thermodynamic stability of the chromium corrosion products is a possible driving force for the corrosion reaction to proceed preferentially along these interfaces.

The role of the environmental variables in the corrosion behavior of these mirrors was further investigated by single flowing gas exposures and salt fog exposures. It was shown that the chlorine component of the MFG environment has a significant influence on the corrosion processes that occur. In the CrN_x adhesion layer mirror and the Cr base layer mirror, mirrors with one Cr-based layer adjacent to the silver, a small level of residual chlorine in the environment resulted in the development of the circular corrosion regions. This was observed during all the accelerated testing as well as during long-term laboratory storage. Therefore, adsorbed moisture on the surface is believed to provide transport of corrosive species, including dissolved chlorine, to enable dissolution of silver and chromium at the Ag-Cr interfaces; this reduces adhesion and allows stress-induced corrosion processes to create the circular corrosion regions. In the CrN_x adhesion layer mirror, reduced adhesion led to the removal of the protective overcoat of SiN_x when the mirrors

were washed, exposing the silver directly to corrosive species. While a CrN_x adhesion layer may provide a benefit in terms of reflectance due to the absence of the absorptive nickel in the adhesion layer, the poor durability associated with reduced adhesion offsets this benefit in optical performance.

In the $NiCrN_x$ adhesion layer mirror, increased chlorine concentration was found to significantly increase the extent of corrosion, with more and larger corrosion nodules forming. This is associated with the susceptibility of both nickel and silver to corrosive attack by Cl_2 and moisture. A small amount of chlorine in the environment may significantly influence the durability of these mirrors. Ultimately, understanding the testing environment and its interactions with the silver mirror designs is critical to appropriately applying accelerated testing.

The role of stress in the durability and corrosion behavior of these mirrors was also assessed by reducing stress in the highest stress layers of the mirror coatings. A significant reduction in SiN_x stress was realized with an increase in sputtering pressure, whereas reducing the target bias power did not reduce stress in this layer. However, neither of these process changes resulted in improved durability as more extensive corrosion was observed in $NiCrN_x$ adhesion layer mirrors with these SiN_x layers. SiN_x layer quality, in terms of the number of spit defects and the density of the layer, was found to be more important in determining the extent of corrosion. Similarly, reduced Cr stress was realized by changing to a floating substrate condition; this also did not significantly improve durability. However, a small improvement in scatter was observed in Cr base layer mirrors with reduced stress Cr base layers, and is associated with reduced delamination blisters. These blisters form due to reduced adhesion at the Ag-Cr interface which allows buckling of the coating to occur. Reducing stress in the layers, therefore, is believed to play an important role in the development of corrosion features along the interfaces.

However, within the range of stresses studies, reducing stress in the SiN_x and Cr base layers did not significantly reduce the extent of corrosion in various mirrors. Furthermore, reduced stress in the coatings did not change the corrosion feature morphology. In all $NiCrN_x$ adhesion layer mirrors, regardless of the stress state or layer quality of the SiN_x layer, characteristic corrosion nodules formed. Similarly, in all Cr base layer mirrors, regardless of the stress state or layer quality of the Cr or SiN_x layers, characteristic circular corrosion regions formed. While stress may play a role in the extent of corrosion and the corrosion kinetics, the composition of the layers on either side of the silver have a larger influence on the mechanisms of corrosion feature development and growth.

The final portion of this work focused on the development and application of several electrochemical techniques to investigate the controlling factors in the mirror corrosion processes including the active corrosion mechanisms. While coulometric reduction was successfully applied to these silver mirrors, no corrosion product was detected on protected silver mirrors with various adhesion layers that were subjected to accelerated environmental exposure. These protection layer schemes reduced corrosion on the mirrors to less than 1.3Å of equivalent thickness of corrosion product. However, even at these levels, degradation in optical properties occurs, indicating that ensuring long-term silver mirror durability requires preventing a very small amount of corrosion.

The coulometric reduction of bare silver mirrors and silver foil samples indicated that silver sulfide and silver chloride chemistries are most important for these mirrors following accelerated environmental exposure. Cl_2 and H_2S are believed to dissolve in the adsorbed water layer on the surface of the mirrors and react with the silver to produce AgCl and Ag_2S. As correlation between accelerated testing and long-duration exposure in the lab was shown in at least one silver mirror design, the importance of both chlorine and sulfur chemistries cannot be overlooked. This is not

necessarily correlated with bare silver corrosion behavior which has generally found silver sulfide to be the most common corrosion product observed. The layers adjacent to the silver may affect the corrosion behavior related to chlorine chemistries, even at very low chlorine concentrations.

Galvanic interactions among the layers of the mirror coatings was also investigated through polarization measurements verified by galvanic coupling experiments. It was found that NiCr, $NiCrN_x$, and freshly-deposited Cr are less noble than Ag, and therefore available to provide cathodic protection to silver. However, the coupling experiments showed that these materials may easily passivate, making them less available to provide protection. On the other hand, CrN_x was found to be more noble than Ag, and therefore not available to protect the Ag to begin with. These galvanic interactions suggest that differences in the electrochemical behavior of the Ag-Cr and Ag-NiCr interfaces in the protected silver mirrors affect the mechanisms of corrosion feature development and growth. Once the corrosive species enter the coating layers, dissolution and corrosion occurs. The compositions of the adhesion layer and the base layer influence the ensuing corrosion process.

As corrosive species enter the coatings through defects in the SiN_x layer, the electrochemical behavior of the adhesion layer first influences the progression of the corrosive attack in the mirrors. In the no adhesion layer mirror, the dissolution of the silver occurs directly as no adhesion layer is there to affect this process. As silver dissolution proceeds, adhesion at the silver-dielectric interface is reduced. Compressive stress in the SiN_x layer is relieved through the growth of the circular corrosion regions and the development of delamination blisters. In the CrN_x adhesion layer mirror, the more noble CrN_x does not protect the Ag, resulting in dissolution of Ag, reduced adhesion at the Ag–CrN_x-SiN_x interface, and the growth of the circular corrosion regions. The lateral growth of the circular corrosion regions is driven by the oxidation, chloridation, and

sulfidation of silver and chromium in combination with stress. Meanwhile, the dissolution of the silver also progresses into the depth of the coating.

In the Cr base layer mirror, once the silver attack extends to the silver-base layer interface, similar development and growth of the circular corrosion regions occurs. The Cr base layer is easily passivated, making it no longer available to protect the silver. Therefore, Ag and Cr dissolution occurs at the Ag-Cr interface, reducing adhesion, and allowing stress in the coating to propagate cracks at the interface, leading to the large circular corrosion regions. The growth rate of the circular corrosion regions is significantly faster than what would be expected from Ag dissolution alone.

In the $NiCrN_x$ adhesion layer mirror, as corrosive species enter the coating, the $NiCrN_x$ likely provides cathodic protection to the silver initially. However, the dissolution of silver into the depth of the coating ultimately occurs. While silver could be cathodically protected and still corrode some, the dynamics and kinetics of this process are not entirely clear; it's possible that the $NiCrN_x$ is consumed or passivated, or that the nickel-silver interaction improves adhesion to prevent stress corrosion cracking at the Ag–$NiCrN_x$-SiN_x interface. It's also possible that attack of the Ag through the thickness of the layer may occur quickly enough to compete with lateral penetration of the corrosion reaction at the Ag–$NiCrN_x$-SiN_x interface. Regardless, once the corrosive species reach the NiCr base layer, a larger amount of NiCr is available to protect the Ag layer, which it appears to readily do. This creates the corrosion nodules and limits the extent of interfacial corrosion processes in this mirror.

Ultimately, the layers adjacent to the silver influence the dynamics and kinetics of the corrosion processes that occur in these protected silver mirrors. As various layers are passivated or consumed, adhesion, stress, and silver dissolution influence the corrosion behavior. These

factors control the development and growth of corrosion features, impacting the optical properties and the long-term durability of the mirrors. While the layers on either side of the silver layer have long been considered necessary, the mechanisms by which they improve mirror durability were not well understood. This work moves us closer toward understanding the environmental durability and corrosion behavior of protected silver mirrors. The electrochemical behavior, interfacial adhesion, layer stress, and coating porosity all must be considered in the development of more durable silver mirror designs.

References

[1] M. Boccas, T. Vucina, C. Araya, E. Vera and C. Ahhee, "Protected-silver coatings for the 8-m Gemini telescope mirrors," *Thin Solid Films,* vol. 502, pp. 275-280, 2006.

[2] D.-Y. Song, R. W. Sprague, H. A. Macleod and M. R. Jacobson, "Progess in the development of a durable silver-based high-reflectance coating for astronomical telescopes," *Appl. Optics,* vol. 24, no. 8, pp. 1164-1170, 1985.

[3] H. Ford, P. Feldman, D. Golimowski, Z. Tsvetanov, F. Bartko, J. Crocker, P. Bely, R. Brown, C. Burrows, M. Clampin, G. Hartig, M. Postman, M. Rafal, W. Sparks, R. White, T. Broadhurst, G. Illingworth, T. Kelly, B. Woodruff, E. Cheng, R. Kimble, C. Krebs, S. Neff, M. Lesser and G. Miley, "The advanced camera for the Hubble Space Telescope," in *Proc. SPIE vol. 2807*, pp. 184-186, 1996.

[4] D. A. Sheikh, "Improved silver mirror coating for ground and space-based astronomy," in *Proc. SPIE 9912,* Advances in Optical and Mechanical Technologies for Telescopes and Instrumentation II, 991239, 2016.

[5] G. Hass, J. B. Heaney, H. Herzig, J. F. Osantowski and J. J. Tirolo, "Reflectance and durability of Ag mirrors coated with thin layers of Al2O3 plus reactively sputtered silicon oxide," *Appl. Optics,* vol. 14, no. 11, pp. 2639-2644, 1975.

[6] H. E. Bennett, R. L. Peck, D. K. Burge and J. M. Bennett, "Formation and growth of tarnish on evaporated silver films," *J. Appl. Phys.,* vol. 40, no. 8, pp. 3351-3360, 1969.

[7] G. Hass, "Reflectance and preparation of front-surface mirrors for use at various angles of incidence from the ultraviolet to the far infrared," *J. Optic. Soc. Am.,* vol. 72, no. 1, pp. 27-39, 1982.

[8] T. E. Graedel, "Corrosion mechanisms of silver exposed to the atmosphere," *J. Electrochem. Soc.,* vol. 139, no. 7, pp. 1963-1970, 1992.

[9] D. K. Burge, H. E. Bennett and E. J. Ashley, "Effect of atmospheric exposure on the infrared reflectance of silvered mirrors with and without protective coatings," *Appl. Optics,* vol. 12, no. 1, pp. 42-47, 1973.

[10] S. F. Pellicori, "Scattering defects in silver mirror coatings," *Appl. Optics,* vol. 19, no. 18, pp. 3096-3098, 1980.

[11] D. W. Rice, P. Peterson, E. B. Rigby, P. B. P. Phipps, R. J. Cappell and R. Tremoureux, "Atmospheric corrosion of copper and silver," *J. Electrochem. Soc.*, vol. 128, no. 2, pp. 275-284, 1981.

[12] Z. Y. Chen, D. Liang, G. Ma, G. S. Frankel, H. C. Allen and R. G. Kelly, "Influence of UV irradiation and ozone on atmospheric corrosion of bare silver," *Corros. Eng. Sci. & Tech.*, vol. 45, no. 2, pp. 169-180, 2010.

[13] D. Liang, H. C. Allen, G. S. Frankel, Z. Y. Chen, R. G. Kelly, Y. Wu and B. E. Wyslouzil, "Effects of Sodium Chloride Particles, Ozone, UV, and Relative Humidity on Atmospheric Corrosion of Silver," *J. Electrochem. Soc.*, vol. 157, no. 4, pp. C146-C156, 2010.

[14] J. Farmer, N. Thomas, W. Siekhaus, H. Gregg, A. Erlandson, C. Marshall, E. Honea, S. Payne, T. Parham and L. Chase, *Atmospheric tarnishing of silver-plated laser mirrors*, United States, 1997. doi:10.2172/574529.

[15] S. Schwinde, M. Schurmann, P. J. Jobst, N. Kaiser and A. Tunnermann, "Description of particle induced damage on protected silver coatings," *Appl. Optics*, vol. 54, no. 16, pp. 4966-4971, 2015.

[16] W. H. Abbott, "The development and performance characteristics of mixed flowing gas test environment," *IEEE Trans. Compon., Hybrids, Manuf. Technol.*, vol. 11, no. 1, pp. 22-35, 1988.

[17] H. Lin, G. S. Frankel and W. H. Abbott, "Analysis of Ag corrosion products," *J. Electrochem. Soc.*, vol. 160, no. 8, pp. C345-C355, 2013.

[18] N. Thomas, J. Wolfe and J. Farmer, "Protected silver coating for astronomical mirrors," in *Proc. SPIE 3352*, Advanced Technology Optical/IR Telescopes VI, 580-586, 1998.

[19] T. Vucina, M. Boccas, C. Araya and C. Ahhee, "Gemini's protected silver coatings: First two years in operation," in *Proc. SPIE 6273*, Optomechanical Technologies for Astronomy, 62730W, 2006.

[20] N. Thomas and J. Wolfe, "UV-shifted durable silver coating for astronomical mirrors," in *Proc. SPIE 4003*, Optical Design, Materials, Fabrication, and Maintenance, pp. 312-323, 2000.

[21] A. C. Phillips, D. M. Fryauf, N. P. Kobayashi, B. DuPraw, S. Cheleden, C. Ratliff, M. J. Bolte and D. Cowley, "Update on UCO's advanced coating lab development of silver-based mirror coatings," in *Proc. SPIE 9912*, Advances in Optical and Mechanical Technologies for Telescopes and Instrumentation, 99122G, 2016.

[22] D. M. Fryauf, J. J. Diaz Leon, A. C. Phillips and N. P. Kobayashi, "Effect of intermediate layers on atomic layer deposition-aluminum oxide protected silver mirrors," *J. Astron. Telesc. Instrum. Syst.,* vol. 3, no. 3, 2017.

[23] S. Schwinde, M. Shurmann, N. Kaiser and A. Tunnerman, "Investigation of SiO2-Al2O3 nanolaminates for protection of silver reflectors," *Appl. Optics,* vol. 56, no. 4, pp. C41-C46, 2017.

[24] J. D. Barrie, P. D. Fuqua, K. A. Folgner and C.-T. Chu, "Control of stress in protected silver mirrors prepared by plasma beam sputtering," *Appl. Optics,* vol. 50, no. 9, pp. C135-C140, 2011.

[25] E. Limam, V. Maurice, A. Seyeux, S. Zanna, L. H. Klein, G. Chauveau, C. Grezes-Besset, I. Savin de Larclause and P. Marcus, "Role of SiC substrate surface on local tarnishing of deposited silver mirror stacks," *Appl. Surf. Sci.,* vol. 436, pp. 1147-1156, 2018.

[26] H. N. Adams, "Protective coating for surfaces of silver and mirror fabrication". U.S. Patent 3,687,713, 29 August 1972.

[27] T. Schneider and P. Stupik, "A UV-enhanced protected silver coating for the Gemini telescopes," in *Proc. SPIE 10700,* Ground-based and Airborne Telescopes VII, 1070048, 2018.

[28] A. C. Phillips, D. M. Fryhauf and N. P. Kobayashi, "Progress and new techniques for protected-silver coatings," in *Proc. SPIE vol. 9151,* Advances in Optical and Mechanical Technologies for Telescopes and Instrumentation, 91511B, 2014.

[29] A. C. Phillips, J. S. Miller, M. Bolte, B. DuPraw, M. Radovan and D. Cowley, "Progress in UCO's search for silver-based telescope mirror coatings," in *Proc. SPIE 8450,* 84502G-1, 2012.

[30] F. Anjum, D. M. Fryauf, R. Ahmad, A. C. Phillips and N. P. Kobayashi, "Improving silver mirrors with aluminum oxynitride protection layers: variation in refractive index with controlled oxygen content by radiofrequency magentron sputtering," *J. Astron. Telescopes, Instr. Systems,* vol. 4, no. 4, p. 044004, 2018.

[31] C. T. Chu, P. D. Fuqua and J. D. Barrie, "Corrosion characterization of durable silver coatings by electrochemical impedance spectroscopy and accelerated environmental testing," *Appl. Optics,* vol. 45, no. 7, pp. 1583-1593, March 2006.

[32] J. D. Wolfe, R. E. Laird, C. K. Carniglia and J. P. Lehan, "Durable silver-based antireflection coatings and enhanced mirrors," in *Technical Digest, Topical Meeting on Optical Interference Coatings,* Optical Society of America, 1995.

[33] D. A. Sheikh, S. J. Connell and R. S. Dummer, "Durable silver coating for Kepler Space Telescope primary mirror," in *Proc. SPIE vol. 7010*, Space Telescopes and Instrumentation, 70104E, 2008.

[34] D. M. Fryauf, J. J. Diaz Leon, A. C. Phillips and N. P. Kobayashi, "Silver film surface modification by ion bombardment decreases surface plasmon resonance absorption," *Appl. Mater. & Interfaces*, vol. 9, pp. 15841-15847, 2017.

[35] J. L. Stanford and H. E. Bennett, "Enhancement of Surface Plasma Resonance Absorption in Mirrors by Overcoating with Dielectrics," *Appl. Optics*, vol. 8, pp. 2556-2557, 1969.

[36] A. J. Braundmeier and E. T. Arakawa, "Effect of surface roughness on surface plasmon resonance absorption," *J. Phys. Chem. Solids*, vol. 35, no. 4, pp. 517-520, 1974.

[37] P. J. Jobst, O. Stenzel, M. Schurmann, N. Modsching, S. Yulin, S. Wilbrandt, D. Gabler, N. Kaiser and A. Tunnerman, "Optical properties of unprotected and protected sputtered silver films: surface morphology vs. UV/VIS reflectance," *Adv. Opt. Techn.* , vol. 3, no. 1, pp. 91-102, 2014.

[38] A. Sytchkova, S. Schwinde, M. L. Protopapa, M. Palmisano, A. Piegari, M. Schurmann and N. Kaiser, "Optical characterisation of silver mirrors with transparent overcoats," in *Proc. SPIE 10691*, 106910N, 2018.

[39] J. D. Wolfe and N. L. Thomas, "Durable silver coating for mirrors". U.S. Patent 6078425, 20 June 2000.

[40] M. Schurmann, S. Schwinde, P. J. Jobst, O. Stenzel, S. Wilbrandt, A. V. Szeghalmi, A. Bingel, P. Munzert and N. Kaiser, "High-reflective coatings for ground and space based applications," in *Proc. SPIE 10563*, 105630M-2, 2014.

[41] D. M. Fryhauf, A. C. Phillips and N. P. Kobayashi, "Corrosion barriers for silver-based telescope mirrors: comparative study of plasma-enhanced atomic layer deposition and reactive evaporation of aluminum oxide," *J. Astron. Inst. Sys.*, vol. 1, no. 4, 2015.

[42] T. Schneider, T. Vucina, C. Ah Hee, C. Araya and C. Moreno, "The Gemini Observatory protected silver coating: ten years in operation," in *Proc. SPIE 9906*, Ground-based and Airborne Telescopes VI, 990632, 2016.

[43] M. R. Jacobson, R. C. Kneale, F. C. Gillett, K. Raybould, J. M. Filhaber, C. Carnigilia, R. Laird, D. Kitchens, R. Shimshock and D. C. Booth, "Development of silver coating options for the Gemini 8-M telescopes project," in *Proc. SPIE 3352*, 1998.

[44] K. A. Folgner, *"Environmental durability of silver mirrors with nanostructured protective coatings"*, MS Thesis ,University of California Los Angeles, 2016.

[45] M. Boccas, T. Vucina, C. Araya, E. Vera and C. Ahhee, "Coating the 8-m Gemini telescopes with protected silver," in *Proc. SPIE 5494*, 2004.

[46] J. Wolfe, "Control of Stress-Corrosion Cracking in Thin Film Designs," in *Soc. of Vacuum Coaters*, 26th Annual Tech. Conf. Proc., 498-503, 1993.

[47] P. D. Fuqua and J. D. Barrie, "Optical properties and corrosion resistance of durable silver coatings," in *Mat. Res. Soc. Symp. Proc. vol. 555*, pp. 85-90, 1999.

[48] Y. Ben Amor, E. M. Sutter, H. Takenouti, M. E. Orazem and B. Tribollet, "Interpretation of electrochemical impedance for corrosion of a coated silver film in terms of a pore-in-pore model," *J. Electrochem. Soc.*, vol. 161, no. 14, pp. C573-C579, 2014.

[49] S. Schwinde, M. Schurmann, R. Schlegel, J. Kinast, R. J. Dorn, J. L. Lizon, S. Tordo and N. Kaiser, "Protected silver coatings for reflectors," *CEAS Space Journal*, 2019.

[50] X. Xu, B. Li, W. He, C. Wang and M. Wei, "NiCrNx interlayer thickness dependence of spectral performance and environmental durability of protected silver mirrors," *Optical Eng.*, vol. 57, no. 4, pp. 045101-1, 2018.

[51] S. Schwinde, M. Schurmann, N. Kaiser and A. Tunnerman, "Protected and enhanced silver for mirrors: damage mechanisms and how to prevent them," in *Proc. SPIE 9627*, 96271R, 2015.

[52] E. Limam, V. Maurice, A. Seyeux, S. Zanna, L. H. Klein, G. Chauveau, C. Grezes-Besset, I. Savin de Larclause and P. Marcus, "Local degradation mechanisms by tarnishing of protected silver mirror layers studied by combined surface analysis," *J. Phys. Chem. B*, vol. 122, no. 2, pp. 578-586, 2018.

[53] K. L. Mittal, "Adhesion measurement of thin films," *Electrocomponent Science & Technology*, vol. 3, no. 1, pp. 21-42, 1976.

[54] R. H. Dauskardt, M. Lane, Q. Ma and N. Krishna, "Adhesion and debonding of multi-layer thin film structures," *Eng. Fracture Mech.*, vol. 61, no. 1, pp. 141-162, 1998.

[55] J. Wolfe, D. Sanders, S. Bryan and N. Thomas, "Deposition of durable wide-band silver mirror coatings using long-throw, low-pressure, DC-pulsed magnetron sputtering," in *Proc. SPIE 4842*, Specialized Optical Developments in Astronomy, 343-351, 2003.

[56] *Military Specification (MIL)-C-48497A, Coating, Single or Multilayer, Interference: Durability Requirements for*, DOD, 8 September 1980.

[57] *ASTM B905-00 Standard Test Methods for Assessing the Adhesion of Metallic and Inorganic Coatings by the Mechanized Tape Test,* West Conshohocken, PA: ASTM International, 2016.

[58] G. Abadias, "Stress in thin films and coatings: Current status, challenges, and prospects," *J. Vacuum Sci. Techn. A,* vol. 36, p. 020801, 2018.

[59] N. Valette, G. Chauveau, C. Grezes-Beret, V. Costes, L. Savin de Larclause, K. Gase and F. Lemarquis, "PACA2M magnetron sputtering silver coating: a solution for very big mirror dimensions," in *Proc. SPIE 10563*, 1056308, 2014.

[60] A. Lalo, G. Ravel, M. Ignat, B. Cousin and M. Swain, "Ageing under mechanical stress: first experiments for a silver based multilayer mirror," in *Proc. SPIE 10568*, 105681Y, 2004.

[61] A. C. Phillips, J. Miller, W. Brown, D. Hilyard, B. DuPraw, V. Wallace and D. Cowley, "Progress toward high-performance reflective and anti-reflection coatings for astronomical optics," in *Proc. SPIE 7018*, 70185A-1, 2008.

[62] J. D. Wolfe, "Durable silver mirror with ultra-violet thru far infra-red reflection". U.S. Patent 7,838,134, 23 November 2010.

[63] M. J. Thwaites, "High density plasmas". U.S. Patent 6,463,873, 15 October 2002.

[64] P. J. Kelly and R. D. Arnell, "Magnetron sputtering: a review of recent developments and applications," *Vacuum,* vol. 56, no. 3, pp. 159-170, 2000.

[65] D. L. Smith, Thin Film Deposition: Principles & Practice, Boston: McGraw-Hill, Inc., 1995.

[66] X. Xu, W. He, C. Wang, M. Wei and B. Li, "SiNx thickness dependence of spectral properties and durability of protected-silver mirrors," *Surf. Coat. Tech.*, vol. 324, pp. 175-181, 2017.

[67] C.-T. Chu, D. R. Alaan, J. D. Barrie and P. D. Fuqua, "Correlation of long-duration and accelerated testing of protected silver mirrors," *submitted for publication.*

[68] C.-T. Chu, D. R. Alaan and D. P. Taylor, "Accelerated atmospheric corrosion testing of electroplated gold mirror coatings," in *Proc. SPIE 7786,* Current Developments in Lens Design and Optical Engineering XI and Advances in Thin Film Coatings VI, 2010.

[69] C.-T. Chu, C. J. Panetta and D. R. Alaan, "Mixed-flowing-gas testing of gold mirror coatings," in *Optical Interference Coatings,* OSA Technical Digest (Optical Society of America), 2010.

[70] C.-T. Chu, P. D. Chaffee, C. J. Panetta and J. D. Barrie, "Mixed flowing gas testing of silver mirror coatings," in *Optical Interference Coatings*, OSA Technical Digest (Optical Society of America), 2007.

[71] *ASTM B827-05 Standard Practice for Conducting Mixed Flowing Gas (MFG) Environmental Tests,* West Conshohocken, PA: ASTM International, 2014.

[72] *ASTM B845-97 Standard Guide for Mixed Flowing Gas (MFG) Tests for Electrical Contacts,* West Conshohocken, PA: ASTM International, 2018.

[73] L. A. Giannuzzi and F. A. Stevie, "A review of focused ion beam milling techniques for TEM specimen preparation," *Micron,* vol. 30, no. 3, pp. 197-204, 1999.

[74] K. A. Folgner, C.-T. Chu, Z. R. Lingley, H. I. Kim, J.-M. Yang and J. D. Barrie, "Environmental durability of protected silver mirrors prepared by plasma beam sputtering," *Appl. Opt.,* vol. 56, no. 4, pp. C75-C86, 2017.

[75] P. Waters and A. A. Volinsky, "Stress and moisture effects on thin film buckling delamination," *Exp. Mech.,* vol. 47, pp. 163-170, 2007.

[76] A. G. Evans and J. W. Hutchinson, "On the mechanics of delamination and spalling in compressed films," *Int. J. Solids Structures,* vol. 20, no. 5, pp. 455-466, 1984.

[77] J. W. Hutchinson and Z. Suo, "Mixed mode cracking in layered materials," *Adv. Appl. Mech.,* vol. 29, pp. 63-191, 1992.

[78] D. M. Fryauf, A. C. Phillips and N. P. Kobayashi, "Moisture barrier and chemical corrosion protection of silver-based telescope mirrors using aluminium oxide by plasma-enhanced atomic layer deposition," in *Proc. SPIE 8820*, 88200Y-1, 2013.

[79] K. A. Folgner, C.-T. Chu, S. D. Sitzman, S. C. Stuart, Z. R. Lingley and J. D. Barrie, "Effects of adhesion layer composition on the environmental durability of protected silver mirrors," in *Proc. SPIE 10691*, Advances in Optical Thin Films VI, 106910X, 2018.

[80] D. D. Wagman, W. H. Evans, V. B. Parker, I. Halow, S. M. Bailey and R. H. Schumm, "Selected values of chemical thermodynamic properties," National Bureau of Standards Technical Note 270-4, 1969.

[81] *ASTM B810-01a Standard Test Method for Calibration of Atmospheric Corrosion Test Chambers by Change in Mass of Copper Coupons,* West Conshohocken, PA: ASTM International, 2017.

[82] *ASTM B117-16 Standard Practice for Operating Salt Spray (Fog) Apparatus,* West Conshohocken, PA: ASTM International, 2016.

[83] J. F. Dante and R. G. Kelly, "The Evolution of the Adsorbed Solution Layer during Atmospheric Corrosion and Its Effects on the Corrosion Rate of Copper," *J. Electrochem. Soc.*, vol. 140, no. 7, pp. 1890-1897, 1993.

[84] B.-D. Yan, S. L. Meilink, G. W. Warren and P. Wynblatt, "Water adsorption and Surface Conductivity Measurements on a-Alumina Substrates," *IEEE Trans. Comp. Hybrids Manufact. Techn.*, Vols. CHMT-10, no. 2, pp. 247-251, 1987.

[85] M. Tencer and J. S. Moss, "Humidity Management of Outdoor Electronic Equipment: Methods, Pitfalls, and Recommendations," *IEEE Trans. Comp. Packag. Techn.*, vol. 25, no. 1, pp. 66-72, 2002.

[86] R. Schubert, "A Second Generation Accelerated Atmospheric Corrosion Chamber," in *Degradation of Metals in the Atmosphere*, D. a. Lee, Ed., Warrington, PA, ASTM International , 1986, pp. 374-384.

[87] H. Lin and G. S. Frankel, "Accelerated Atmospheric Corrosion Testing of Ag," *Corrosion*, vol. 69, no. 11, pp. 1060-1072, 2013.

[88] Y. Wan, E. N. Macha and R. G. Kelly, "Modification of ASTM B117 Salt Spray Corrosion Test and Its Correlation to Field Measurements of Silver Corrosion," *Corrosion*, vol. 68, no. 3, 2012.

[89] V. Guilbaud-Massereau, A. Celerier and J. Machet, "Study and improvement of the adhesion of chromium thin films deposited by magnetron sputtering," *Thin Solid Films*, vol. 258, no. 1-2, pp. 185-193, 1995.

[90] J. H. Kim and K. W. Chung, "Microstructure and properties of silicon nitride thin films deposited by reactive bias magnetron sputtering," *J. Appl. Phys.*, vol. 83, pp. 5831-5839, 1998.

[91] M. Watanabe, S. Shinozaki, E. Toyoda, K. Asakura, T. Ichino, N. Kuwaki, Y. Higashi and T. Tanaka, "Corrosion products formed on silver after one-month exposure to urban atmospheres," *Corrosion*, vol. 62, no. 3, pp. 243-250, 2004.

[92] D. W. Rice, P. B. P. Phipps and R. Tremoureux, "Atmospheric corrosion of nickel," *J. Electrochem. Soc.*, vol. 127, no. 3, pp. 563-268, 1980.

[93] D. W. Rice, W. Kinsolving and J. J. Laskowski, "Indoor corrosion of metals," *J. Electrochem. Soc.*, vol. 127, no. 4, pp. 891-901, 1980.

[94] H. Windischmann, "Intrinsic stress in sputter-deposited thin films," *Critical Reviews in Solid State and Material Sciences*, vol. 17, no. 6, pp. 547-596, 1992.

[95] H. Windischmann, "Intrinsic stress in sputtered thin films," *J. Vac. Sci. Technol. A,* vol. 9, no. 4, pp. 2431-2436, 1991.

[96] M.-W. Moon, J.-W. Chung, K.-R. Lee, K. H. Oh, R. Wang and A. G. Evans, "An experimental study of the influence of imperfections on the buckling of compressed thin films," *Acta Materialia,* vol. 50, no. 5, pp. 1219-1227, 2002.

[97] S. Schmidt, T. Hanninen, J. Wissting, L. Hultman, N. Goebbels, A. Santana, M. Tobler and H. Hogberb, "SiNx coatings deposited by reactive high power impulse magnetron sputtering: Process parameters influencing the residual coating stress," *J. Appl. Phys.,* vol. 121, p. 171904, 2017.

[98] W. D. Nix and B. M. Clemens, "Crystallite coalesence: A mechanism for intrinsic tensile stresses in thin films," *J. Materials Research,* vol. 14, no. 8, pp. 3467-3473, 1999.

[99] R. H. Jones and R. E. Ricker, "Mechanisms of Stress-Corrosion Cracking," in *Stress-Corrosion Cracking: Materials Performance and Evaluation, Second Edition,* R. H. Jones, Ed., ASM International, 2017, pp. 1-40.

[100] K.-N. Tu and A. M. Gusak, Kinetics in Nanoscale Materials, Hoboken, New Jersey: John Wiley & Sons, Inc., 2014.

[101] G. C. A. M. Janssen, M. M. Abdalla, F. van Keulen, B. R. Pujada and B. van Venrooy, "Celebrating the 100th anniversary of the Stoney equation for film stress: Developments from polycrystalline steel strips to single crystal silicon wafers," *Thin Solid Films,* vol. 517, pp. 1858-1867, 2009.

[102] G. G. Stoney and C. A. Parsons, "The tension of metallic films deposited by electrolysis," *Proc. Royal Soc. London A,* vol. 82, 1909.

[103] R. Koch, "Stress in evaporated and sputtered thin films - A comparison," *Surface & Coatings Technology,* vol. 204, pp. 1973-1982, 2010.

[104] R. G. Kelly, J. R. Scully, D. W. Shoesmith and R. G. Buchheit, Electrochemical Techniques in Corrosion Science and Engineering, New York: Marcel Dekker, Inc., 2003.

[105] Y. Fukuda, T. Fukushima, A. Sulaiman, I. Musalam, L. C. Yap, L. Chotimongkol, S. Judabong, A. Potjanart, O. Keowkangwal, K. Yoshihasa and M. Tosa, "Indoor corrosion of copper and silver exposed in Japan and ASEAN countries," *J. Electrochem. Soc.,* vol. 138, no. 5, pp. 1238-1243, 1991.

[106] *ASTM B825 Standard Test Method for Coulometric Reduction of Surface Films on Metallic Test Samples,* West Conshohocken, PA: ASTM International, 2013.

[107] T. E. Graedel, J. P. Franey, G. J. Gualtieri, G. W. Kammlott and D. L. Malm, "On the mechanism of silver and copper sulfidation by atmospheric H2S and OCS," *Corrosion Science,* vol. 25, no. 12, pp. 1163-1180, 1985.